The Hong Kong Polytechnic University

Department of Applied Physics

Modeling the Dielectric Behaviors of Perovskites: Ferroelectrics and Incipient Ferroelectrics

HAIYAO DENG

A thesis submitted in partial fulfillment of the requirements
for the degree of Doctor of Philosophy

December 2011

Certificate of originality

I hereby declare that this theis is my own work and that, to the best of my knowledge and belief, it reproduces no material previously published or written, nor material that has been accepted for the award of any other degree of diploma, except where due acknowledgement has been made in the text.

(sign here)

_____

Haiyao Deng

_____

Abstract

This dissertation is devoted to an atomistic understanding of the dielectric properties of oxide perovskites. I shall concentrate on the long-known barium titanate (BTO) and strontium titanate (STO), although other related materials will also be discussed.

The BTO is known as a ferroelectric, which undergoes a series of polar structural phase transitions as temperature goes down. In the work presented here, the focus is placed on the tetragonal-cubic transition that occurs about $410K$. A lot of theoretical work have been invested to clarify the transition mechanism, which pertains basically to the behaviors of the static dielectric constant and hence to the lowest frequency phonon mode. Those work were largely based on First-priciples computations or models whose origin need be revealed. Despite their usefulness, they shed little light upon the modes other than the lowest frequency one and their inter-relations. This situation may be partly due to the difficulty in establishing an atomistic model that is amenable to intuitive analysis. In this dissertation, I try to fill this gap and show how such a model can actually be achieved. In doing so, insights into other problems are obtained.

A central issue concerns the identity of the observed peaks in the imaginary part of the dielectric function. The assignment of these peaks are accomplished by comparison with the said model. Accordingly, the peaks around $180cm^{-1}$ and $510cm^{-1}$ are considered to correspond to O vibrations along and normal to the Ti-O-Ti bonds, respectively. The perceived anistropy is found to arise from the strong Ti-O covalent bonding. All remaining

peaks are considered to correspond to Ti motions. These motions are highly anharmonic. As a result, these peaks are prone to temperature changes and spectrual weight transfer has to happen between them. Based on the model, one can explain (1) the huge ratio $\frac{\epsilon_a}{\epsilon_c}$ and (2) the polar chain formation in the cubic phase.

STO, on the contrary, is only an incipient ferroelectric. The model is equally applicable to this compound. The O vibrations are found at similar but slightly shifted frequencies. Such shifts are comprehensible by this model. In this compound, a key issue relates to the correlations between a zone boundary mode and a zone center mode. Both display softening behaviors. However, the softening with the latter is incomplete. The physics behind this incompleteness has been a matter for debate. In this dissertation, it is attributed to the inter-relations between these two modes. I explore this idea from both a vibronic and a phenomenological point of view. A fingerprint is found.

Ferroelectricity can be induced in STO by replacing O^{16} with O^{18}. The isotope effect is remarkable: the transition temperature can be as high as $24K$. Different views have appeared to explain the effects. Based on the aforementioned model, I put forth a different idea, which states that, the main effects of the isotope substitution are to suppress the Ti zero-point fluctuations. This is signified by a decrease in the Ti tunneling frequency.

In addition, I discuss the implications for cuprate superconductors.

Acknowledgements

This thesis is based on the work I did in the past three years under the supervision of my advisors, Dr. Haitao Huang and Dr. Chi Hang Lam. Most results of the work have been published in Ref.[1, 2, 3, 4, 5, 6, 7, 8, 9], except those presented in chapter 2 and some in chapter 3 and 4. Ref.[1, 6] are not used here. I'm greatly indebted to my advisors. I also wish to express my deep gratitudes to my collegues Kaige Hu (City University of Hong Kong) and Cho Tung Yip.

For the sake of illustrations, I have replicated a number of figures from other publications in chapter 1 and one in chapter 2. They are acknowledged as follows:

- FIG.1.2, after [17], ©1964 The Americal Physical Society
- FIG.1.3, after [22], ©1966 Elsevier Ltd
- FIG.1.4, after [18], ©1994 The Americal Physical Society
- FIG.1.5, after [19], ©2008 The Americal Physical Society
- FIG.1.6, panel (a) after [37], ©2006 Taylor& Francis Group; and (b) after [38], ©1976 The Americal Physical Society
- FIG.1.7, after [41], ©International Union of Crystallography
- FIG.1.8 and FIG.1.9, after [47]

- FIG.1.10, after [48], ©1995 The Americal Physical Society
- FIG.1.11, after [49], ©1980 The Americal Physical Society
- FIG.1.12 and FIG.1.13, after [50], ©1980 The Institute Of Physics
- FIG.1.14, after [51], ©1982 The Americal Physical Society
- FIG.1.15, after [53], ©1983 The Americal Physical Society
- FIG.1.16, after [54], ©2008 The Americal Physical Society
- FIG.1.17, (a) after [56], ©1962 The Americal Physical Society (b) and (c) after [55], ©1967 Elsevier Ltd
- FIG.1.18, after [58], ©1978 The Americal Physical Society
- FIG.1.19 and FIG.1.20, after [60], ©2008 The Americal Physical Society
- FIG.**??**, after [66], ©1975 The Americal Physical Society
- FIG.1.21, after [68], ©1993 The Americal Physical Society
- FIG.1.22, after [76], ©2009 The Institute Of Physics
- FIG.1.23, after [75], ©2000 EDP Sciences
- FIG.1.24, after [85], ©2006 The Americal Physical Society
- FIG.2.1, after [19], ©2008 The Americal Physical Society
- FIG.4.5, after [137], ©1995 The Americal Physical Society

In addition, Table 2.1 is taken from Bussmann et al.[117](©EDP Sciences). FIG.4.6 is the result of a collaboration with Kaige Hu, where the raw data of $\epsilon(0)$ were taken from Ref.[71] for STO, Ref.[124] for $KTaO_3$ and Ref.[125] for $CaTiO_3$.

Table of Contents

List of Tables

List of Figures

Chapter 1

INTRODUCTION

1.1 Preamble

In this thesis, I try to convey a unified, clear and tractable atomistic picture for understanding the lattice dynamics of perovskites and their variants. My focus will be on properties that are governed by the dielectric function. The obtained picture is applied to two well known compounds, barium titanate ($BaTiO_3$ or BTO) and strontium titanate ($SrTiO_3$ or STO). The experimental data of them are rich but perplexing and uneasy sometimes. It is just these uneasy aspects that motivate my work recorded in the present thesis. Therefore, it is paramount to explain these facts in the first place, which is the task of this introduction chapter. I will begin with a description of the crystal structrue and then move to talk about the electronic structure. Appreciation of these structures are essential in reaching the physical picture. Thereafter, I briefly review the basics of lattice dynamics and mention some preliminary concepts and often used models (a detailed discussion will, however, be postponed to the next chapter). I also discuss how to experimentally investigate the lattice dynamics. Then I turn to introducing structural phase transitions in terms of correlation functions. Basic machineries are then discussed. I proceed to reivew

the phenomenological aspects of both BTO and STO. These are accompanied by critical remarks, in order to reveal the gap of understanding.

1.2 Crystal Structures

A pure perovskite compound has a general formula as ABX_3, with A and B being metal elements while X often being (and hereafter restricted to) oxygen. A variety of choices can be adopted by A and B. In the present thesis, I shall be largely referring to $BaTiO_3$ (BTO) and $SrTiO_3$ (STO), although our discussions are actually very general. Despite their seemingly simple chemical formulations, incredibly rich phenomena on both the atomistic and electronic scale have been found in these substances[10, 12, 71, 151]. Properties relate to structure. A perovskite compound can usually befall in a bunch of crystal structures, depending on ambient conditions such as pressure and temperature[10]. However, every structure can be somewhat deemed as slight deviations from a parent one: the ideal cubic structure, whose unit cell is depicted in FIG.1.1 and the postitions of each site are listed in TABLE 1.1. In this unit cell, the A atoms occupy the corners of a cube, the B atom takes up the center and the O's are placed at the face centers surrounding the B atom, thus making the so-called BO_6 cluster. Another way to draw the unit cell is to reverse the positions of A and B while at the same time positing the O atoms at the edge centers. It is useful to note that an O atom in this structure is also caged by two B atoms and four A atoms.

The geometrically ideal structure is not neccesarily the physically stable one. A crude way to quantify the stability is via the so-called tolerance factor t, which is defined as[14]

$$t = \frac{t_{AO} + 1}{\sqrt{2}(t_{BO} + 1)} \tag{1.1}$$

where $t_{BO} = \frac{r_B}{r_O}$ and $t_{AO} = \frac{r_A}{r_O}$, with $r_{O,A,B}$ being the radii of corresponding ions. Although

being empirical and ambiguious in determination of the radii, it can often serve as a preliminary indicator of stability. For example, from the numbers given by Shannon[15], the value of t for STO is around 1.02, quite close to that for the ideal cubic structure (in which case $t = 1$). This implies STO in the vicinity of criticality and its properties sensitive to changes in external parameters, as analyzed by Itoh et al[16]. When replacing Sr with Ba, the unit cell becomes bigger and the Ti ion can not be in good touch with all O ions. The way out is to have Ti ions off-center shifted so as to touch some of the O ions, thus resulting in polarization.

The mass ratio of BO_3 to A seems also an interesting quantity. Denote the mass of the former and the latter by m_1 and m_2, respectively. Take $ATiO_3$ for instance. It was found that, polar structural instability appears only for $m_2 > 100$. Since $m_1 \approx 95.9$, this finding suggests the instability condition $m_2/m_1 > 1$[16].

Table 1.1: Atomistic positions in a perovskite unit cell

Site	Location	Coordinates
A cation	(2a)	(0,0,0)
B cation	(2a)	(1/2,1/2,1/2)
O(apical)	(6b)	(1/2,1/2,0)
O(planar)	(6b)	(1/2,0,1/2);(0,1/2,1/2)

1.3 Electronic Structure

The relevant electronic orbitals (which are those close to the Fermi level) on B sites are of d-wave symmetry while those on the A sites are of s-wave symmetry and those on the O sites are of p-wave symmetry (see Ref.[17, 19] and FIG.1.2-1.4 for details). The five d-orbitals fall in two multiplets due to crystal field, the triplet $t_{2g} = \{d_{xy}, d_{yz}, d_{zx}\}$ and the doublet $e_g = \{d_{x^2-y^2}, d_{3z^2}\}$. Strong covalent bonds of σ-type are expected to form between the $Bd_{x^2-y^2}$ and the planar Op's and between the Bd_{3z^2} and the apical Op's. Such bonds

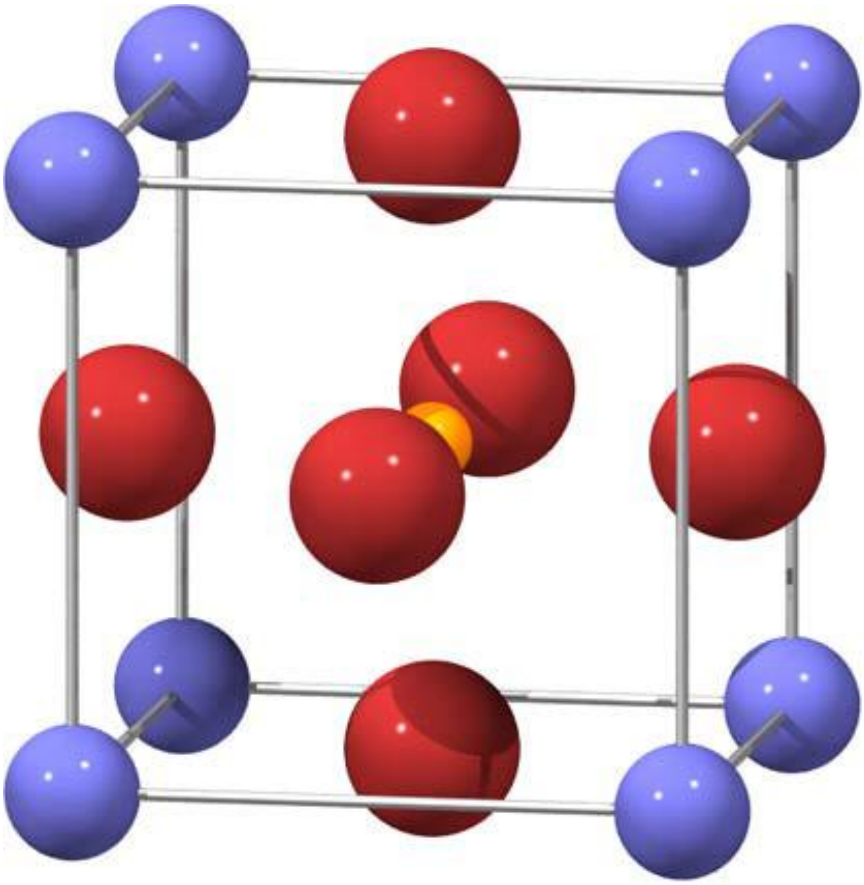

Figure 1.1: Unit cell of ideal perovskite structure. The Ti, O and A ions are represented by the yellow, red and blue spheres respectively.

may play important role in perovskite structure formation, especially in the formation of the BO_6 octehedra, which is perfect for this bonding if all e_g orbitals are empty. On the contrary, in compounds where d_{3z^2} is filled, for example in high-Tc superconductors[151], a degraded structure happens that can simply be regarded as obtained by stacking BO_2 layers.

First-principles computations have been done on $ATiO_3$ and other compounds[19, 20]. The charge density map obtained for BT and ST from such computations shows that the charges about the Ti ions and O ions are linked into a net, suggesting covalent bonding between these ions (see FIG.1.5). On the other hand, the charges around the Ba or Sr ions are nearly spherically distributed and detached from the Ti-O charge net, suggesting that these ions can be taken as simple charges. Roughly, to have an intuition about the crystal formation energy, one may think these perovskite compounds are formed like this: *strong covalent Ti-O bonding makes the linked TiO_6 skeleton, which is further corroborated by adding Ba or Sr ions via ionic bonding.*

For $PbTiO_3$, the situation is a little different: the Pb sites have lone electron pairs, which can be shared with partially filled O sites. This is reflected in the charge density map as well[19]. Such lone pairs can have important effects on the crystal structure, which however is beyond the scope of this thesis[21].

Throughout this thesis, the configuration denoted by $As^0Bd^0Op^6$ will be used as the reference for considering electronic excitations.

1.4 Lattice Dynamics: An Overview

1.4.1 Rigid Ion Model

In this model, every ion is treated as a rigid sphere with certain charges[23]. They are assumed to interact with one another via a potential energy. Let us write down the

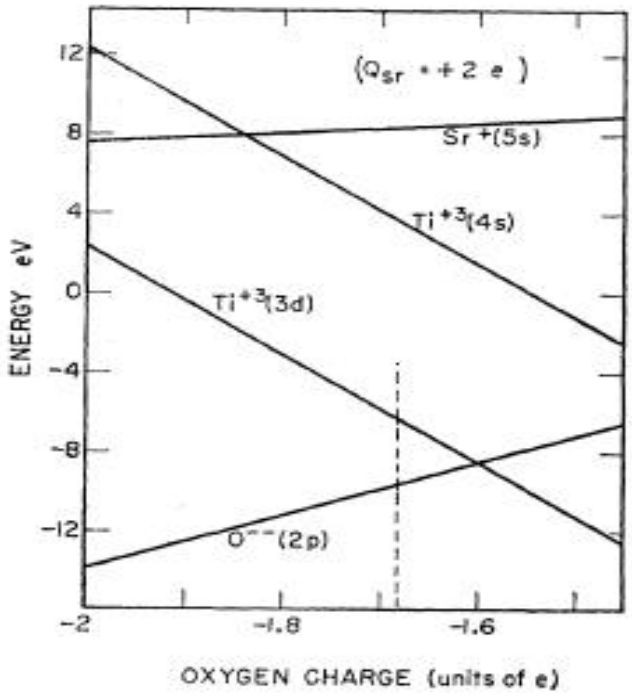

Figure 1.2: Atomic level structure of perovskites. Reproduced with permission from[17]

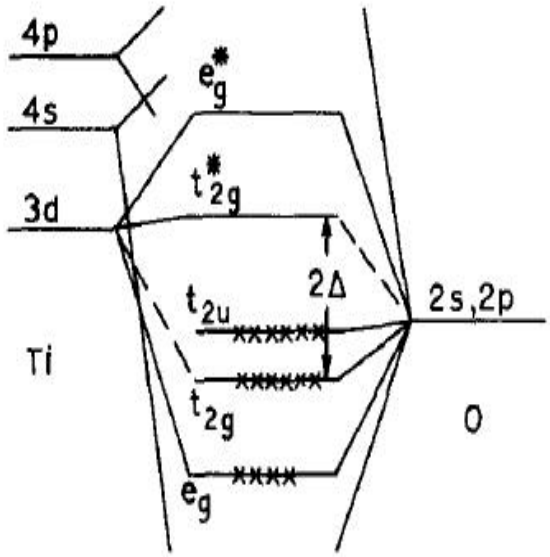

Figure 1.3: Bonding in perovskites. Reproduced with permission from[22]

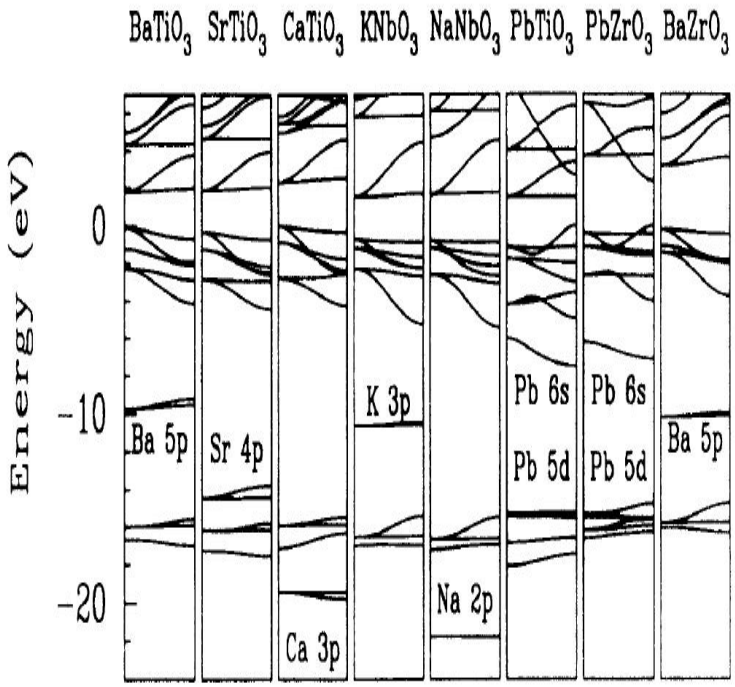

Figure 1.4: Band structure of perovskites from Γ to X. Reproduced with permission from[18]

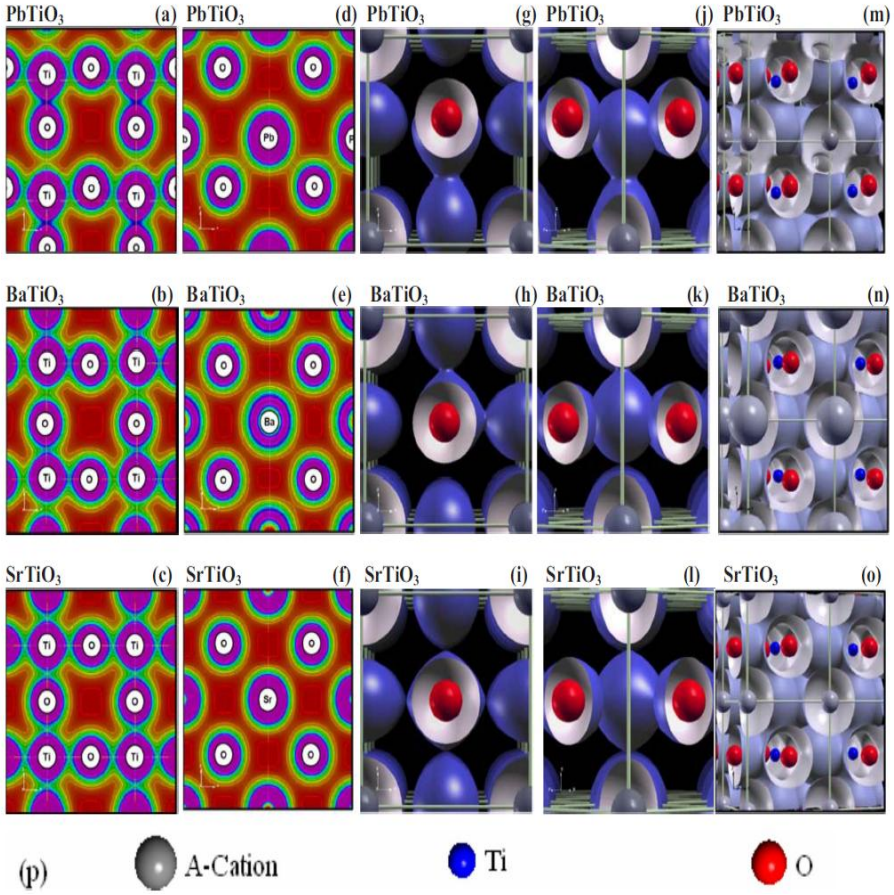

Figure 1.5: Electronic density map. Reproduced with permission from[19]

displacement vector of the κ-type ion belonging to the l-th unit cell as $\vec{u}_{l\kappa} = \vec{r}_{l\kappa} - \vec{R}_{l\kappa}$, where $\vec{R}_{l\kappa}$ labels the corresponding ideal cubic structure site and $\vec{r}_{l\kappa}$ the instantaneous position of that ion. The potential energy can then be written as $V(\{\vec{u}_{l\kappa}\})$. Assuming that these displacements are minute in comparison with the lattice constants and that the potential reaches its minimum (at least local) at vanising displacements, the equations of motion for the ions can be solved through harmonic approximation. In this case, one ends up with a system of normal modes each labelled by a wavevector $\vec{q}$ and a branch tag j with frequency $\omega_{\vec{q}j}$. One can write[24]

$$\vec{u}_{l\kappa} = \sum_{j\vec{q}} (NM_\kappa)^{-1/2} \vec{e}(\kappa, j\vec{q}) Q(j\vec{q}) e^{i\vec{q}\cdot\vec{R}_{l\kappa}}, \tag{1.2}$$

with N being the number of unit cells of the crystal, M_κ the mass of the κ atom while $\vec{e}(\kappa, j\vec{q})$ being the normalized eigenvector and $Q(j\vec{q})$ the canonical coordinates. Since $\vec{u}_{l\kappa}$ is real, one must have $Q^*(j, \vec{q}) = Q(j, -\vec{q})$. In terms of these variables, the Hamiltonian in the harmonic approximation can be couched as

$$H_2 = \frac{1}{2} \sum_{j\vec{q}} [\dot{Q}(j, \vec{q}) \dot{Q}(j, -\vec{q}) + \omega^2(j\vec{q}) Q(j, \vec{q}) Q(j, -\vec{q})] \tag{1.3}$$

The system will be stable if all $\omega(j\vec{q})$ are positive, as assumed by the harmonic approximation. Further, under this approximation, all these frequencies will be simply constants and have no dependence on temperature.

1.4.2 Core-Shell Model

The rigid ion model presumes that each ion can be regarded as a rigid entity. However, in reality, ions, in particular anions, can be polarized relatively easily. In anions, the outermost shell electrons are usually loosely attached. To take into account this aspect,

the shell model was forwarded[25, 26, 27], whose basic idea is to divide an ion into a core and a shell. The core consists of the rigid part of the ion: the nuclei plus the inner-shell electrons. The shell represents the outermost-shell electrons as a whole, namely the valence electrons. An interaction is introduced between these two components. Denote the displacement of the core by $\vec{u}_{l\kappa}$ and that of the shell by $\vec{w}_{l\kappa}$. The interaction is then written as $U(\{\vec{u}_{l\kappa}\},\{\vec{w}_{l\kappa}\})$. There are also interactions between the shells, $U'(\{\vec{w}_{l\kappa}\})$ and between the cores $V'(\{\vec{u}_{l\kappa}\})$. Applying Newton's law, one then obtains a set of coupled equations.

$$M_\kappa \ddot{\vec{u}}_{l\kappa} = -[\frac{\partial}{\partial \vec{u}_{l\kappa}}(U+V')] \tag{1.4}$$

$$M'_\kappa \ddot{\vec{w}}_{l\kappa} = -[\frac{\partial}{\partial \vec{w}_{l\kappa}}(U+U')] = 0 \tag{1.5}$$

where M'_κ stands for the effective mass of the κ shell. In the adiabatic limit, one postulates $M'_\kappa = 0$ and hence obtains the second equation in the second line, which amounts to the requirement that $\vec{w}_{l\kappa}$ instaneously minimize the potentials $U+U'$ involving the shell variables.

Eq.(1.5) can be formally solved to get $\vec{w}$ in terms of $\vec{u}$, which governs how the ion is deformed. This is then substituted into eq.(1.4) to obtain a closed set of equations involving only the cores. One can write

$$V(\{\vec{u}_{l\kappa}\}) = V' + U[\{\vec{u}\},\{\vec{w}_{l\kappa}(\{\vec{u}_{l\kappa}\})\}]$$

analogous to the potential used in the rigid ion model. One sees that, the effect of deformation on the motions of cores in the adiabatic limit is to simply alter the potential in which the cores find themselves, $V' \rightharpoonup V$. The eigen frequencies $\omega_{j\vec{q}}$ can then be found with V under harmonic approximation.

Usually, one assumes a linear relation between $\vec{u}$ and $\vec{w}$, that is, $\vec{u}_{l\kappa} = \sum_{l'\kappa'} Z(l\kappa, l'\kappa')\vec{w}_{l'\kappa'}$, with Z being a proper matrix. As simple as it is, this linear relation appeared inadequate in describing some aspects of perovskites, as emphasized in the work of Migoni et al.[28]. Therefore, non-linear relations have appeared in studying the lattice dynamics of these compounds[28, 29].

1.4.3 Spin Model

Occasionally, the above simple phonon picture may not be the best starting point in describing lattice dynamics. In fact, there will be interactions among these normal modes and interactions with other degrees of freedom of the system. In the best case, such interactions may be taken into account by adding a self-energy to $\omega(j\vec{q})$[30], namely, they will be renormalized to be $\tilde{\omega}^2(j\vec{q}) = \omega^2(j\vec{q}) + \Delta(j\vec{q})$, where $\Delta(j\vec{q})$ denotes the self-energy. This quantity is generally complex, $\Delta(j\vec{q}) = \Delta'(j\vec{q}) + i\Delta''(j\vec{q})$ and is a function of temperature. Now that after renormalization the normal mode depends on time as $Q(j\vec{q}) \propto \exp(i\tilde{\omega}(j\vec{q})t)$, one sees that the imaginary part of $\Delta(j\vec{q})$ gives rise to damping of the $j\vec{q}$ mode while its real part makes a correction and directly shifts the frequecy from $\omega(j\vec{q})$ to $\sqrt{\omega^2(j\vec{q}) + \Delta'(j\vec{q})}$. In particular, if the correction is negative, the frequency will decrease (i.e., soften). Moreover, if as a function of temperature or other knobs one or several of the renormalized frequencies soften all the way down crossing zero, the system will be destablized and structural phase transitions will be in store[31].

Worsely, the harmonic approximation may fail in the presence of significant anharmonicity, for example when the potetial energy is a maximum surrounded by a set of local minima in vicinity for vanishing $\vec{u}_{l\kappa}$[22]. In such case, some of the $\omega(j\vec{q})$ will turn out to be imaginary, indicating the instability of the ideal structure. Nevertheless, as we will discuss in later chapters, the phonon concept may still apply under certain conditions. When these conditions are not met, the situation becomes intricate and novel phenomena can

occur. Under these circumstances, it turns out more suitable to start with a pseudospin description[10], in which one relates the displacement vector to spin-type variable, $\vec{u}_{l\kappa} = u_0 S_{l\kappa}$. The specifics of S depend on how many local minima exist. Often, not all degrees of freedom are better off with spin characters. Some remain as simple phonons. And usually, there are interactions between the spins and phonons, leading to the so-called spin-phonon model[32, 33, 34, 88, 36].

1.4.4 The Sources of Effective Inter-ion Interactions

As indicated by the shell model, the effective potential energy V for the cores contains two portions: the direct interaction energy V' and that due to interactions with the shells. Since the cores have small radii and can hardly get into touch with one another, their direct interactions should mainly stem from the electrostatic forces, which vanishes to the first order by virtue of symmetry and gives rise to the dipolar energy up to the second order in dispalcements. Thus, one can write

$$V' = \sum_{l\kappa, l'\kappa'} \frac{z_{l\kappa} z_{l'\kappa'}}{2|\vec{R}_{l\kappa,l'\kappa'}|^5} [3(\vec{u}_{l\kappa,l'\kappa'} \cdot \vec{R}_{l\kappa,l'\kappa'})^2 - |\vec{u}_{l\kappa,l'\kappa'}|^2 |\vec{R}_{l\kappa,l'\kappa'}|^2] \tag{1.6}$$

where the summation is taken over pairs and $z_{l\kappa}$ denotes the effective charge carried by the core $l\kappa$ in response to point charges, and $\vec{u}_{l\kappa,l'\kappa'} = \vec{u}_{l\kappa} - \vec{u}_{l'\kappa'}$ as well as $\vec{R}_{l\kappa,l'\kappa'} = \vec{R}_{l\kappa} - \vec{R}_{l'\kappa'}$. As regards the interactions of cores with the shells, we expect two types in nature. One is due to Pauli's exclusion principle, which prohibits two electrons to occupy the same state. This means that when the core carries its electrons getting close to the shell, it will feel a strong repulsion as a result of the rise in electronic density and hence in kinetic energy. This repulsion is short range and serves to confine the cores[23]. In the present thesis we

model it by a quartic axial on-site potential, i.e.,

$$\gamma_{\rho,l\kappa} u^4_{\rho,l\kappa}$$

where $\rho = x, y, z$ and $u_{\rho,l\kappa}$ stands for the $\rho-$th component of $\vec{u}_{l\kappa}$. Obviously, in the shell model this term should be lumped into V'.

The other type arises from the conventional electron-phonon interactions. It is just this part that is taken as the ion deformation energy $U[\{\vec{u}_{l\kappa}\}, \vec{w}(\{\vec{u}_{l\kappa}\})]$ in the shell model. To evaluate it, one usually resorts to the adiabatic approximation, observing that the frequency associated with the motions of electrons is much higher than that with the cores due to their small mass ratio. In next chapter we shall propose a way to calculate this term in the specific case of perovskite compounds. Such calculations shall prove important in identifying the character of dielectric responses.

1.4.5 Symmetry Analysis

Suppose the elementary lattice excitations can be well-described as phonons. For any perovskite, there are in total 15 phonon branches, out of which three are acoustic and the rest are optic. It is useful to classify the zone-center optical branches by irreducible representations of the underlying symmetry group. For ideal cubic structure, these branches fall in two categories with $3T_{1u}$ and T_{2u} symmetry, respectively. Each is a triplet with repective frequency. Crystal distortions lower the symmetry and these triplets have to be split (see FIG.1.6). In particular, under tetragonal deformation (in which case the symmetry group becomes C_{4v}), each T_{1u} splits into an E plus an A_1 while T_{2u} into an E plus a B_1. The symmetry properties play important part in scattering experiments and are regardeless of dynamic details. Throughout our thesis, the T_{2u} and its decendents ($E + B_1$) zone center modes receive little attention for the reason that, they are either optically inactive or their

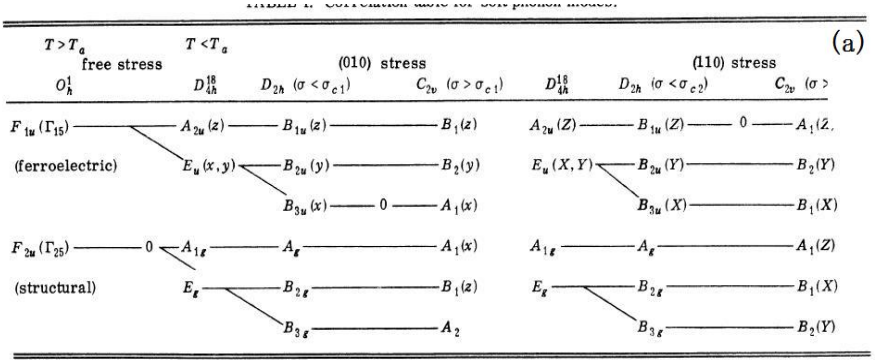

(b)

Rhombohedral $P_S \parallel (111)$ $C_{3v}^5(R3_{xyz}m_{\bar{x}y})$		Orthorhombic $P_S \parallel (110)$ $C_{2v}^{14}(C2_{xy}m_{\bar{x}y}m_z)$		Tetragonal $P_S \parallel (001)$ $C_{4v}^1(P4_zm_xm_{xy})$		Cubic $P_S = 0$ $O_h^1(Pm\bar{3}m)$
$3A_1$	IR: $E \parallel P_S$ R active	$3A_1$	IR: $E \parallel P_S$ R active	$3A_1$	IR: $E \parallel P_S$ R active	$3F_{1u}$ IR active, E arbitr.
3E	IR: $E \perp P_S$ R active	$3B_1$	IR: $E \parallel (011)$ R active	3E	IR: $E \perp P_S$ R active	R inactive
		$3B_2$	IR: $E \parallel (101)$ R active			
$1A_2$	Silent	$1A_2$	IR inactive R active	$1B_1$	IR inactive R active	$1F_{2u}$
1E	IR: $E \perp P_S$ R active	$1B_1$	IR: $E \parallel (011)$ R active	1E	IR: $E \perp P_S$ R active	Silent
		$1B_2$	IR: $E \parallel (101)$ R active			
7 (IR + R)		12 (IR + R)		7 (IR + R) + 1R		3 IR

Figure 1.6: Symmetry analysis. Reproduced with permission from[37, 38]

signals are extremely weak[37, 38].

1.5 Experimental Probes

There is a wide spectrum of techniques to probe lattice vibrations. In the present thesis, we are mainly concerned with the long wavelength (zone center) polar variables of the lattice. The fundamental quantity is the dielectric function, which is often studied by optical methods (infrared reflectivity and Raman-Stokes scattering) and diffuse X-ray scattering, in addition to direct capacitance measurement. Neutron scattering is often used in determining the phonon spectrum, but will not be described here.

1.5.1 Capacitance Measurement

This is the direct way to measure the dielectric function. One just fills the substance to be measured in a plate capacitor and connects the whole in a circuit driven by a votage, $U(t)$, which may be alternating at frequency ω. Let the impedance be $Z(\omega)$ and the capacitance at $\omega = 0$ be C_0. Now let the polarization induced by the voltage across the capacitor be $P(t)$. Assuming the electric field $E(t)$ inside the material is uniform, one then has $E(t) = U(t)/D$, where D is the spacing between the capacitor plates. Within linear response theory, one relates $P(t)$ to $E(t)$ as $P(t) = \int_{-\infty}^{t} \chi(t-t')E(t')dt'$, with $\chi(t-t')$ being the susceptibility function. The current $I(t)$ can now be obtained via a generic relation $I(t) = S\dot{P}(t)$, where S is the plate area. After Fourier transform, one finds $\chi(\omega) = \frac{i}{Z(\omega)\omega} \cdot \frac{D}{S}$. The susceptibility function can be utilized to find the dielectric function: $\epsilon(\omega) = \epsilon_\infty + 4\pi\chi(\omega)$.

1.5.2 IR Reflectivity

In the IR method, one measures the reflectance, R, of a beam of light impinging upon a crystal. Suppose the light ray propagates in the $[1,0,0]$ direction. The electric field it carries is therefore in the perpendicular direction, let's say, $[0,0,1]$. The reflectance is related to the $33-$component of the cystal's dielectric tensor, ϵ_c, which is a function of temperature (T) and the light frequency ω. Let the light ray travel along $[0,0,1]$ and the ϵ_a will be involved. One has

$$R_{a,c}(\omega) = |\frac{\sqrt{\epsilon_{a,c}(\omega)} - 1}{\sqrt{\epsilon_{a,c}(\omega)} + 1}|^2 \tag{1.7}$$

At $\omega = 0$, $\epsilon_{a,c}$ should be real. In general they are complex, $\epsilon_{a,c} = \epsilon'_{a,c} + i\epsilon''_{a,c}$. Due to analyticity, Kramers-Kronig relation holds between their real and imaginary parts. Usually, the dielectric function has two contributions respectively from the lattice and the

valence electrons. As long as ω is not high, the contribution from the latter (denoted by ϵ_∞) can be neglected. Actually, in many compounds, $\epsilon_\infty \sim 5$. In short, from reflectivity one can infer the dielectric function, which contains clean information about lattice dynamics.

1.5.3 Raman Scattering

In Raman-Stokes scattering, a photon with frequency ω_i is absorbed and then emitted at a different frequency ω_f by the crystal. The coupling responsible for such events is embodied as $-\sum_{\alpha\beta} \hat{E}_\alpha \hat{P}_{\alpha\beta} \hat{E}_\beta$, with $\hat{P}_{\alpha\beta}$ being the $\alpha\beta$-component of the susceptibility tensor operator and $\hat{E}$ is the electric field operator. The Raman intensity per unit solid angle is evaluated as

$$I = I_0 \sum_{i,f} \rho_i \sum_{\alpha\beta} |\langle f|\hat{P}_{\alpha\beta}|i\rangle e_i^\alpha e_f^\beta|^2 \bar{\delta}(\hbar\Omega + \varepsilon_f - \varepsilon_i) \tag{1.8}$$

where $\vec{e}_{i,f}$ is the orientation vector in which the electric field of the incident and the scattered wave is polarized and all subscripts take values from $\{x, y, z\}$. In addition, $|i\rangle$ ($|f\rangle$) is the initial (final) state of the crystal with energy ε_i (ε_f) and Ω the frequency change of the light. Here we use $\bar{\delta}$ to denote the Dirac function. Thermal effects are taken care of by the Boltzman factor ρ_i. Up to the second-order perturbation, one can express $\hat{P}_{\alpha\beta}$ as follows,

$$(\hat{P}_{\alpha\beta})_{fi} = \frac{1}{\hbar} \sum_r \left(\frac{\langle f|\mu_\alpha|r\rangle\langle r|\mu_\beta|i\rangle}{(\varepsilon_r - \varepsilon_i)/\hbar - \omega_i - i\Gamma_r} + \frac{\langle f|\mu_\beta|r\rangle\langle r|\mu_\alpha|i\rangle}{(\varepsilon_r - \varepsilon_f)/\hbar - \omega_i + i\Gamma_r} \right) \tag{1.9}$$

Here $\vec{\mu} = \sum_{l\kappa} z_{l\kappa} \vec{u}_{l\kappa}$ denotes the dipole operator. For cubic or tetragonal structure, the susceptibility tensor operator must be diagonal, $\hat{P}_{\alpha\gamma} \propto \bar{\delta}_{\alpha\gamma}$. Using fluctuation-dissipation theorem, the above formula (for Stokes component) may be reduced to[39]

$$I_{a,c} = \tilde{I}_0 [n(\Omega) + 1] \epsilon''_{a,c}(\Omega) \tag{1.10}$$

under proper circumstances. Here $n(\Omega) = \frac{1}{\exp(\frac{\hbar\Omega}{k_B T})-1}$ is the Bose-Einstein population factor.

Selection rules are expected to exist because of crystal symmetry. They are implicit in the matrix element $\langle i|\hat{P}_{\alpha\gamma}|f\rangle$. To be Raman active, they should not all vanish. Details about these rules for cubic and tetragonal structure have been summarized in FIG.1.6 and in Ref.[84], within harmonic approximation.

1.5.4 Diffuse X-ray Scattering

X-ray is with such a high frequency that the lattice can always be regarded as nearly static and such a short wavelength that the atomistic structure can be uncovered. The usual way to deal with this subject is embodied in the following formula that relates the scattering intensity per unit solid angle to the direction change of the ray,

$$\begin{aligned} I &= |\sum_{l\kappa} f(\kappa\vec{Q}) \exp(i\vec{Q}\cdot\vec{r}_{l\kappa})|^2 \\ f(\kappa\vec{Q}) &= f_0(\kappa)\exp(-W_{\kappa\vec{Q}}) \end{aligned} \tag{1.11}$$

where $f_0(\kappa)$ is the atomic scattering factor and $W_{\kappa\vec{Q}}$ is the Debye-Waller factor for the κ-type atom. Approximating $\vec{r}_{l\kappa}$ with $\vec{R}_{l\kappa} \equiv \vec{R}_l + \vec{R}_\kappa$ and using that $|\sum_l \exp(i\vec{Q}\cdot\vec{R}_l)|^2 \approx N v_{BZ} \sum_{\vec{G}} \bar{\delta}(\vec{Q}-\vec{G})$, where $\vec{G}$ denotes the reciprocal vectors, one can rewrite the above as

$$\begin{aligned} I &= N v_{BZ} \sum_{\vec{G}} |F_0(\vec{G})|^2 \bar{\delta}(\vec{Q}-\vec{G}) \\ F_0(\vec{Q}) &= \sum_\kappa f_0(\kappa)\exp(i\vec{Q}\cdot\vec{R}_\kappa), \text{ which is the structure factor} \end{aligned} \tag{1.12}$$

This is no more than the formula for Bragg scattering.

Allowing the atoms to deviate from the crystallogrphic positions, one writes $\vec{r} = \vec{R}_l + \vec{R}_\kappa + \vec{u}_{l\kappa}$. To the first order in $\vec{u}_{l\kappa}$, one has for the scattering amplitude an additional term

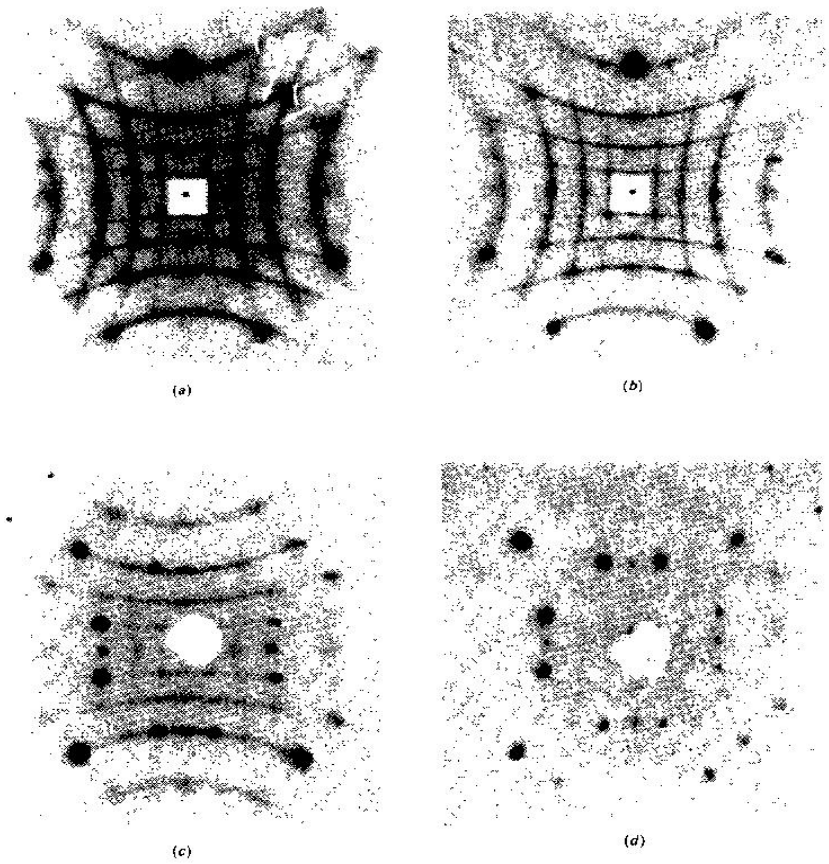

Figure 1.7: Diffuse x-ray scattering pattern. Reproduced with permission from[41]

that reads

$$i\sum_{l\kappa} f(\kappa\vec{Q})\exp(i\vec{Q}\cdot\vec{r}_{l\kappa})\vec{Q}\cdot\vec{u}_{l\kappa} \tag{1.13}$$

Imagine that $\vec{u}_{l\kappa} = \vec{U}_{\vec{q}\kappa}\exp(i\vec{q}\cdot\vec{R}_{l\kappa})$, which leads to a correction to the Bragg scattering

$$I' = Nv_{BZ}\sum_{\vec{G}}|F'(\vec{G},\vec{q})|^2\bar{\delta}(\vec{Q}+\vec{q}-\vec{G}) \tag{1.14}$$

Here F' is not written explicitly. We see that new intensive areas should appear around Bragg peaks (e.g., FIG.1.7), hence the name diffuse scattering[30].

1.5.5 Resonance Methods

These methods are powerful in expoliting the local environment of some ion. Often used include electron paramagnetic resonance (EPR)[42] and nuclear magnetic resonance (NMR)[43]. The strategy is to investiagte the spectra of a local spin attached to certain ion. Such spin can be the nuclear spin or the spin of some unpaired electron belonging to the ion. As far as perovskites are concerned, these methods have been mainly employed at the Ti site, which carries a nuclear spin of 5/2 or 7/2 depending on which Ti isotope is spoken of. This spin can take on a few values. In the presence of a magnetic field B along z-direction, these values come with different energies that rely on both the B and the local environment. By studying radiation absorption, the energy structure and hence the local environment can be unveiled. EPR goes with analogous procedures except that the nuclear spin replaced by an electron spin which can be brought about through elemental substitution. These methods are limited in temporal resolution ($\sim 10^{-8}s$). The X-ray absorption fine structure spectrscopy (XANS) provides a fast probe which can go to the scale of $10^{-15}s$[44]. In this method, instead of spin's levels, the atomic levels themselves are directly used.

1.6 Mechanism of Structural Phase Transitions

Let's introduce the spatial correlation function as follows

$$C_{\alpha\beta}(\vec{R}_{l\kappa} - \vec{R}_{l'\kappa'}) = \langle u^{\alpha}_{l\kappa} u^{\beta}_{l'\kappa'} \rangle \tag{1.15}$$

which is related to the static susceptibility as $\chi^0_{\alpha\beta} = (k_B T)^{-1} C_{\alpha\beta}$ (a form of fluctuation-dissipation theorem). Here the $\langle ... \rangle$ dictates the thermodynamic average. In high symmetry phases one usually has $\langle \vec{u}_{l\kappa} \rangle = 0$, as assumed in the above expression. This function

measures the response of the crystal at $\vec{R}_{l\kappa}$ to a stimuli at $\vec{R}_{l'\kappa'}$. Structrual phase transition takes place whenever one component of the correlation function does not vanish for infinitely distant unit cells, that is, $C_{\alpha\beta}(|\vec{r}_{l\kappa} - \vec{r}_{l'\kappa'}| \longrightarrow \infty) \neq 0$ for certain $\alpha\beta$. For cubic or tetragonal crystal structures, we expect both C and χ^0 to be diagonal. We here briefly describe some often quoted mechanisms that can lead to such structural instability.

1.6.1 Soft Phonons

Provided the crystal can be taken as a collection of simple harmonic oscillators (after renormalization) as described by Eq.(1.3), the correlation function can be easily obtained. Actually, the response of a particular normal mode to a stimuli turns out to be inversely proportional to its renormalized frequency squared, i.e., $C_{j\vec{q}} \propto \frac{k_B T}{\tilde{\omega}^2(j\vec{q})}$. So the structural transition happens when one of the $\tilde{\omega}^2(j\vec{q})$ vanishes. In the present thesis, we are mainly concerned with the zone center mode, i.e., $\vec{q} = 0$. Hereafter we denote the frequency of the softening mode by ω_s. Let T_c be the transition temperature and we expect $\omega_s^2(T_c) = 0$. For temperatures not much above T_c, we may approximate ω_s^2 around T_c as $\omega_s^2 = A \cdot (T - T_c)$, where A is a parameter. This leads to the Curie-Weiss law, $\chi_0 \sim (T - T_c)^{-1}$. Usually, it's thought that displacive transitions come in this description[30]. As aforementioned, softening behaviors can arise from anharmonicity, interactions with other degrees of freedom such as electrons[30].

1.6.2 Orientational Ordering

This mechanism applies to compounds where the spin description is more appropriate[10]. Let's take a half spin for example. It is described by Pauli matrix, σ^z, which indicates the orientation of the displacement vector. Assume a monatomic basis for the compound. The displacements are then related to them as $u_l = u_0\sigma_l^z$, which couple to each other via $K_{ll'}\sigma_l^z\sigma_{l'}^z$. Within mean-field theory, every spin finds itself coupled to a local molecular

field, $-h\sigma^z$. Its dynamics is provided by thermal agitations. And the response is often encapsulated by Glauber theory. The static susceptibility is then given by $\chi_0 \sim (T - K(0)/k_B)^{-1}$, which also agrees with the Curie-Weiss law with $T_c = K(0)/k_B$. Here $K(0) = \sum_{l'} K_{ll'}$.

1.6.3 Lyddane-Sachs-Teller relationship

This relation has been the most common route to evaluating the dielectric constant $\epsilon(0)$ from optical phonon frequencies. In line with it, the $\epsilon(0)$ is given by[45]

$$\frac{\epsilon(0)}{\epsilon_\infty} = \prod_j \frac{\omega^2(jl)}{\omega^2(jt)} \tag{1.16}$$

where $\omega(jt)$ ($\omega(jl)$) denotes the frequency of the j-th transverse (longitudinal) optical zone center mode. We here give a brief derivation. The polarization of a compound couples to the electric field of a light ray by $-\vec{P} \cdot \vec{E}$. One may decompose the polarization as $\vec{P} = \vec{P}_t + \vec{P}_l$, with $\vec{q} \cdot \vec{P}_t = 0$. Here $\vec{q}$ is the wave vector of the light. Now that $\vec{q} \cdot \vec{E} = 0$, we infer that only $\vec{P}_t$ couples to the light. $\vec{P}_t$ comes from transverse optical modes. Treating these modes as harmonic oscillators, one obtains the dynamic dielectric function as

$$\epsilon(\omega) = \epsilon_\infty + \sum_j \frac{S_j}{\omega_{jt}^2 - \omega^2} \tag{1.17}$$

where S_j is termed the oscillator strength of the j-th mode. Note that ω_{jt} appears as poles of $\epsilon(\omega)$. Now we argue that ω_{jl} must appear as the zeros of $\epsilon(\omega)$. From Maxwell theory, the divergence of the electric displacement vector in a compound free from mobile charges must vanish: $\vec{q} \cdot \vec{D} = 0$, which leads to $\epsilon(\omega)\vec{q} \cdot \vec{E} = 0$. Therefore, for longitudinal mode

$(\vec{q}\cdot\vec{E}\neq 0)$ one must have $\epsilon = 0$. Thus,

$$0 = \epsilon_\infty + \sum_j \frac{S_j}{\omega_{jt}^2 - \omega_{jl}^2} \tag{1.18}$$

which yields the desired relation.

1.6.4 Dynamic Responses

The best way to distinguish between the above mechanisms, apart from direct observations with both spatially and temporarily high resolution spectroscopy, is perhaps to examine the system's dynamic response[46]. The dynamic response function is written as

$$C_{\alpha\beta}(\vec{R}_{l\kappa} - \vec{R}_{l'\kappa'}; t-t') = \Theta(t)\langle u_{l\kappa}^{\alpha}(0)\dot{u}_{l'\kappa'}^{\beta}(t-t')\rangle/(k_B T) \tag{1.19}$$

which is related to the imaginary part of the dynamic susceptibility function as

$$\begin{aligned}\chi_{\alpha\beta}^{''}(\vec{R}_{l\kappa} - \vec{R}_{l'\kappa'};\omega) &= -\frac{1}{k_B T}\int_{-\infty}^{\infty} C_{\alpha\beta}(\vec{R}_{l\kappa} - \vec{R}_{l'\kappa'};t)\exp(i\omega t)\ dt \\ &= \frac{i\omega}{k_B T}\langle u_{l\kappa}^{\alpha}(-\omega)u_{l'\kappa'}^{\beta}(\omega)\rangle \end{aligned} \tag{1.20}$$

In the above, the upper dot dictates a time derivative and $\Theta(t)$ is the step function. The $\chi^{''}$ can be experimentally determined by several methods such as measuring scattering intensity and capacitance, while the real part χ' can be found through Kramers-Kronig relation. The fundamental quantity discussed in the present thesis is the (relative) dynamic dielectric tensor, which can be related to the dynamic susceptibility as

$$\epsilon_{ij}(\omega) = \epsilon_\infty \bar{\delta}_{ij} + 4\pi\chi_{ij}(\omega) \tag{1.21}$$

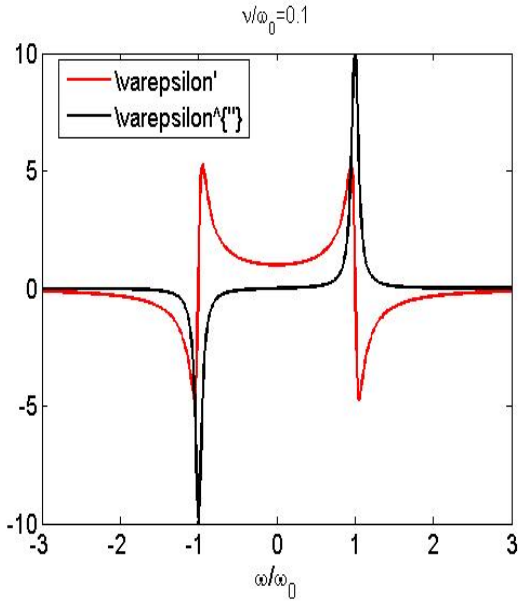

Figure 1.8: The dielectric constant of a damped oscillator. Reproduced from[47]

where ϵ_∞ is a constant that is frequency and temperature independent. In the cubic structure, it reduces to a simple form: $\epsilon_{ij} = \epsilon\bar{\delta}_{ij}$; whereas in the tetragonal structure, it becomes $\epsilon_{ij} = diag[\epsilon_a, \epsilon_a, \epsilon_c]$.

Consider a normal mode with frequency ω_0 in the phonon scheme. It is easy to show that, the $\chi^{''}$ corresponding to this mode bears the following form,

$$\chi^{''}(\omega) = \chi_0 \frac{\omega\Gamma/\omega_0^2}{[(\omega/\omega_0)^2 - 1]^2 + (\omega\Gamma/\omega_0^2)^2} \overset{\Gamma\to 0}{\to} \chi_0[\bar{\delta}(\omega - \omega_0) + \bar{\delta}(\omega + \omega_0)] \tag{1.22}$$

where χ_0 is the static susceptibility and Γ is included to acount for possible dissipation effects (e.g., FIG.1.8). It features two Lorentzian resonance peaks at $\pm\omega_0$, which can be seen in e.g. raman spectra. Approaching transition, these peaks shift toward $0cm^{-1}$.

On the other hand, the dynamic response of a spin activated by a heat bath can be shown to follow the Debye-type manner. In fact, it takes on the following form in the disordered phase

$$\chi(\omega) = \frac{\chi_0}{1 - i\omega\tau}, \quad \chi^{''} = \frac{\chi_0\omega\tau}{1 + \omega^2\tau^2} \tag{1.23}$$

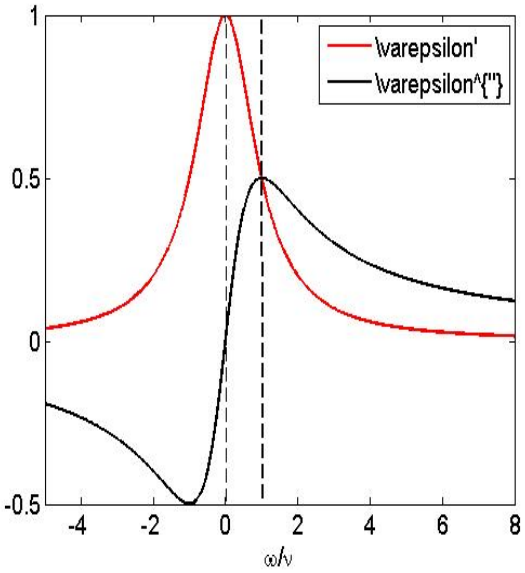

Figure 1.9: The dielectric constant of a relaxation mode. Reproduced from[47]

Here $1/\tau$ is the spin flip rate, whose temperature dependence depends on the microscopic flip regime. Note that, $\chi^{''}$ also displays a peak around $\omega = \tau^{-1}$. But this peak does not fit the Lorentzian shape and is unusually broad (e.g., FIG.1.9). This is sometimes called a relaxation peak, for the reason that χ in this case is in essentially the same form as that for a Brownian particle. Similarly, it also shifts to $0cm^{-1}$ when approaching transition. This implies τ goes to ∞, a phenomena called critical slowing down (the relaxation process takes infinite time).

Despite their apparent discrepancy, there is an intimate relation between the resonance and relaxation regime. This relation is revealed when a harmonic oscillator experiences very large friction. On such occasion with so large Γ, one can neglect the $(\omega/\omega_0)^2$ term in the denominator of eq.(1.22). In this limit, by comparison with eq.(1.23), one finds an effective relaxation time $\tau = \Gamma/\omega_0^2$. Another aspect of this relation can be uncovered by studying a spin in a transverse field, which will coherently flip this spin. Such coherent flip mode behaves in exactly the same way as a simple hamonic oscillator. When in contact with a heat bath, incoherent flip could also happen due to thermal activation.

The competition between these two channels results in a soft frequency that has such a form[30]: $\hbar^2\omega_s^2 = 4E_T[E_T - J(0)\tanh(\frac{E_T}{k_BT})]$, where $E_T/\hbar$ denotes the spin flip rate due to the transverse field.

Because of the demonstrated closeness between these regimes, it is sometimes not easy to identify the ture nature of a critical mode.

1.7 Phenomenology of $BaTiO_3$

Structural phase transitions of this compound are summarized in FIG.1.10. Above around $405K$, it is found in the cubic phase; when cooled below that temperature, it transits to a tetragonal phase. Further cooling brings it to other phases that won't be discussed in the thesis. We are mainly interested in the modes that are optically active in these phases.

1.7.1 Cubic Phase: The Modes of ϵ

In this phase, the dielectric tensor is represented by a simple scalar $\epsilon(\omega, T)$. Extensive experimental studies have been conducted. We mention some typical results here. According to early IR and RS as well as neutron scattering data as displayed in FIG.1.11-FIG.1.16, three modes were usually said to be found in the spectral function[49, 50]. The two with higher frequencies, which will be tagged as TO_2 and TO_4 by convention, were located about $178cm^{-1}$ and $510cm^{-1}$, respectively. The TO_4 was found negligible while the TO_2 with barely discernible temperature dependence in terms of both line widths (which were shown very small) and positions[50]. As regards the lowest frequency mode to be labelled as TO_1, some controversies exist between Raman and Infrared results[50, 51, 52]. Albeit both found significant temperature dependence of this mode, they disagree on whether its frequency vanishes as the cubic-tetragonal transition is approached. According to IR data[50] exhibited in FIG.1.12, this mode levels off around $60cm^{-1}$ as the critical point is

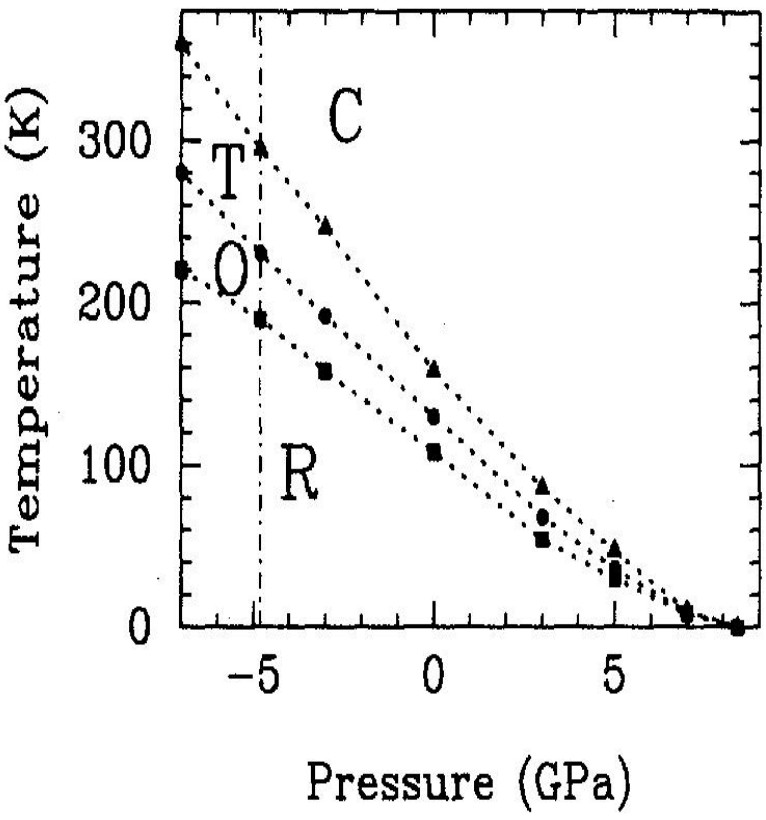

Figure 1.10: Phase diagram of BTO by first principles computation. Reproduced with permission from[48]

reached whereas according to Raman data[51] exhibited in FIG.1.14, it is a genuine soft mode with vanishing frequency. The matter is further complicated by the fact that, this mode when fitted with phonon theory has a very large damping (see FIG.1.13). Actually, it's overdamped. This leads to the one-mode-versus-two-mode dispute[53]. It was argued that, this mode could be a merger of two close modes, one of which (denoted by TO_{1h}) levels off while the other (TO_{1l}) really softens to zero (see FIG.1.15). The two-mode scenario finds support from a latest work[54] based on ab initio calculations combined with effective model construction (see FIG.1.16). Let's see that, *a soft mode seems desirable to explain the discrepancy between the ϵ measured with capacitance technique and that with L-S-T relation*. Another point of worth is that, a feasible spectral weight transfer between TO_{1h} and TO_2 were indicated by the temperature dependence of their oscillator strengths[50]: that of the former decreases as that of the latter increases, in the course of elevating temperature, as shown in FIG.1.12. This transfer was a clue to the coupling between these two modes.

1.7.2 Tetragonal Phase: The Modes of ϵ_a

In this phase, we need two independent functions to characterize the dielectric tensor. We thus in this subsection describe results pertaining to ϵ_a at first, leaving ϵ_c to next subsection. As exhibited in IR and Raman spectra (FIG.1.17), also three modes were supposed to exist[55, 56]. The modes with higher frequencies were found to sit at similar frequencies as that for cubic phase, namely, they are situated about $182cm^{-1}$ (called f_2) and $482cm^{-1}$(called f_4), respectively. The lowest-frequency mode f_1, which was located in between $0cm^{-1}$ and $35cm^{-1}$, was again argued to be overdamped when fitted with phonon theory[56, 58]. It was shown to depend on temperature in an unexpected way (see FIG.1.18): as the cubic-tetragonal critical point is approached (from below), its frequency increases with temperature together with the damping rate[58], standing contrary to the

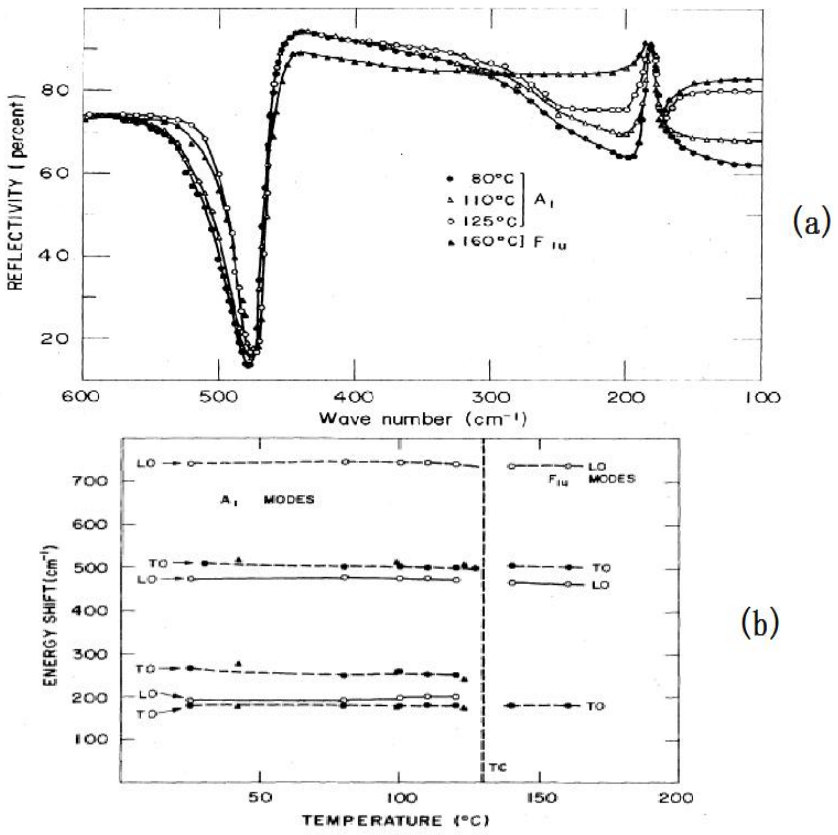

Figure 1.11: Reflection spectra and dielectric modes of BTO. Reproduced with permission from[49]

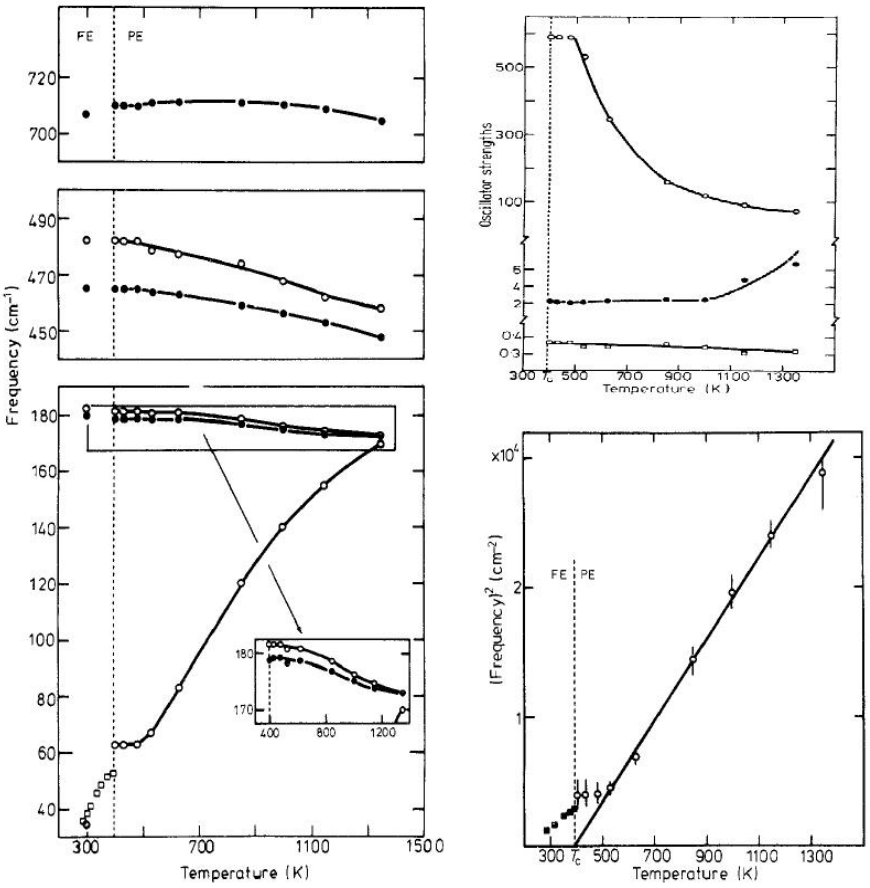

Figure 1.12: Dielectric modes of BTO deduced from reflection spectra. Reproduced with permission from[50]

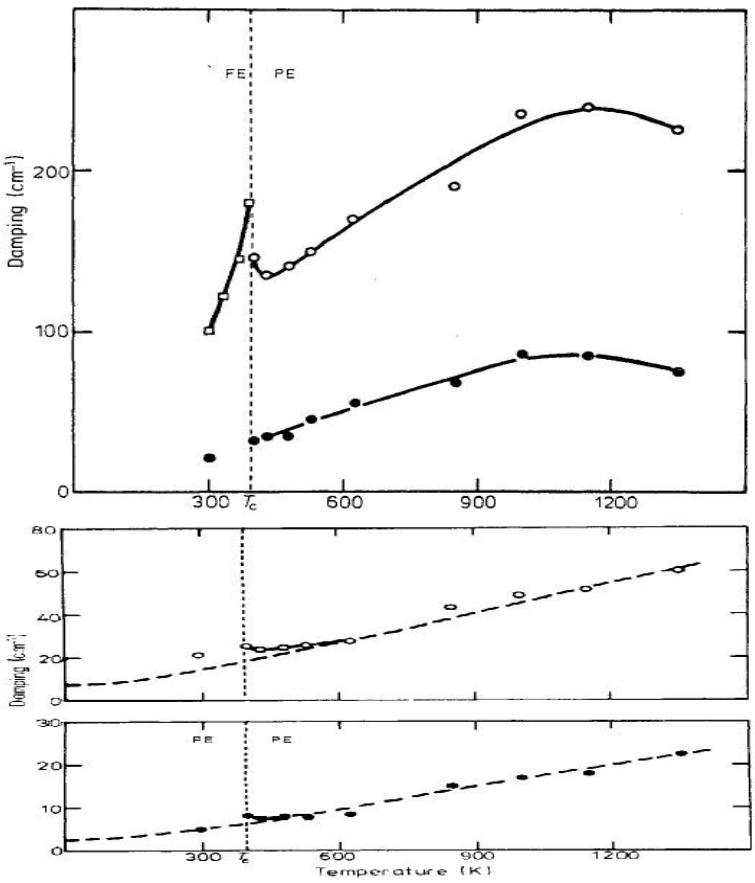

Figure 1.13: Damping rates of dielectric modes of BTO. Reproduced with permission from[50]

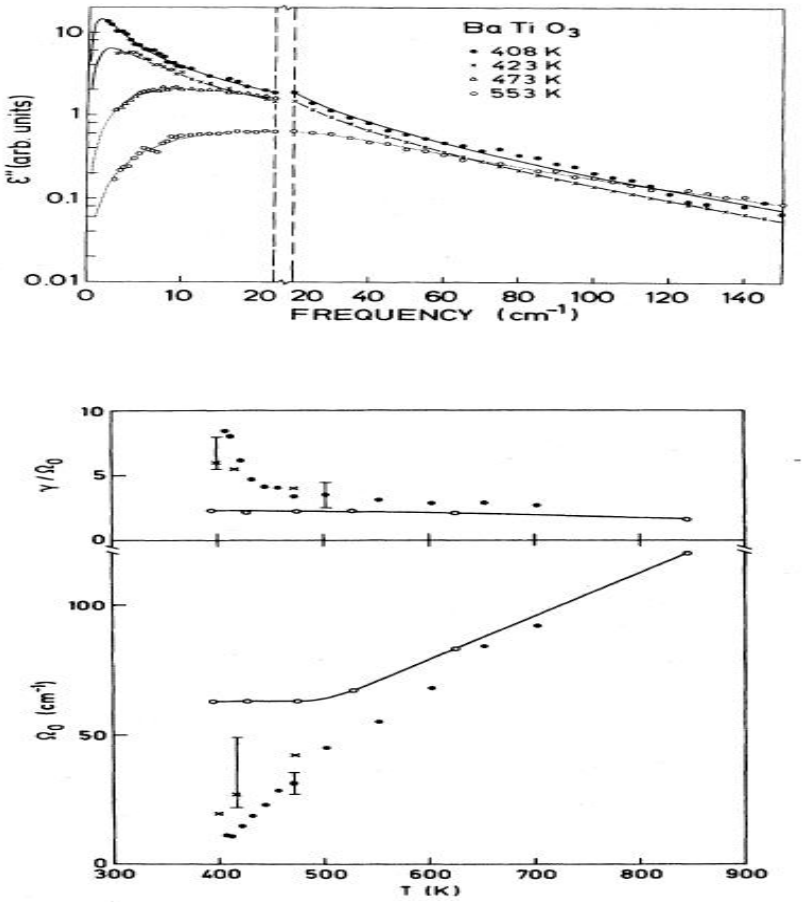

Figure 1.14: Raman spectra and the deduced modes of BTO. Reproduced with permission from[51]

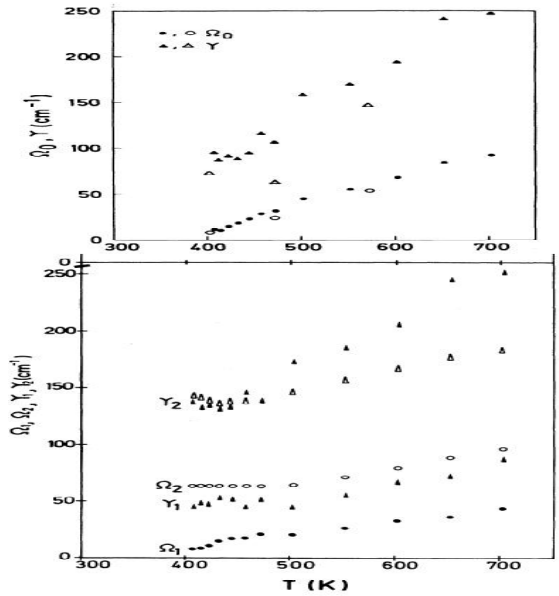

Figure 1.15: One mode vs. Two mode. Reproduced with permission from[53]

behaviors of TO_1, which was shown to be a genuine soft mode. Temperature dependence of all three modes remain to be exploited yet. It is expected that the $f_{2,4}$ modes are likely to bear similar dependence as $TO_{2,4}$.

1.7.3 Tetragonal Phase: The Modes of ϵ_c

Early IR and Raman experiments had disclosed three peaks (see FIG.1.11), which were positioned around $180cm^{-1}$ (LM), $278cm^{-1}$ (SM) and $507cm^{-1}$ (AM), respectively[49, 55, 59]. For historical reasons, they are called the Last, Slater and Axe mode, respectively. All but the SM were shown to have negligible temperature dependence. Both the SM's position and linewidth were found temperature dependent[59]. Moreover, it is this mode, instead of the lower mode (LM), that was found to contribute most among the three to ϵ_c[58]. Not till recently has a fourth mode (DM) been revealed[60]. A basic motivation for seeking this mode is the discrepancy between the static dielectric constant by direct capacitance measurement and that by optic mode parameters (through L-S-T relation)[55]. This long-

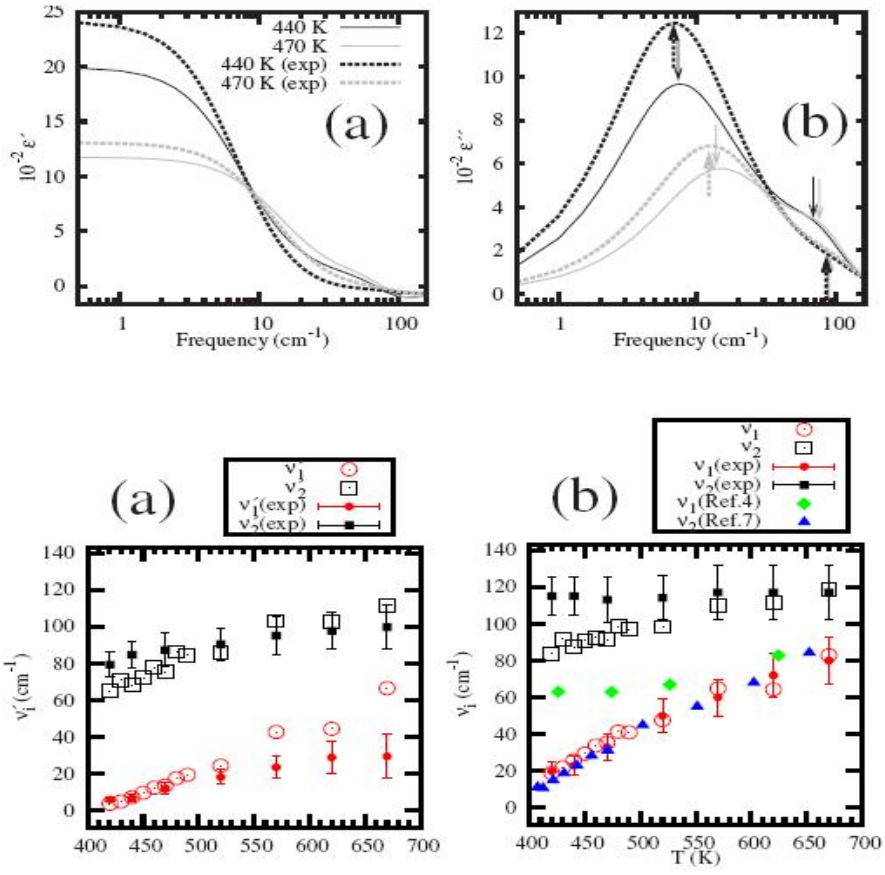

Figure 1.16: Latest result on one-mode-two-mode behaviors of BTO. Reproduced with permission from[54]

	$BaTiO_3$ Ordinary ray	$SrTiO_3$	TiO_2 Ordinary ray	TiO_2 Extraordinary ray
λ_1, ν_1	19.6 μ, 510 cm^{-1}	18.2 μ, 546 cm^{-1}	20.9 μ, 479 cm^{-1}	
γ_1/ν_1	0.057	0.049	0.025	
$4\pi\rho_1$	1.0	1.9	2.0	
λ_2, ν_2	54.7 μ, 183 cm^{-1}	56.3 μ, 178 cm^{-1}	25.9 μ, 386 cm^{-1}	
γ_2/ν_2	0.031	0.034	0.03	
$4\pi\rho_2$	2.0	3.6	2.0	
λ_3, ν_3	296 μ, 33.8 cm^{-1}	114.3 μ, 87.5 cm^{-1}	52.5 μ, 189 cm^{-1}	52.5 μ, 189 cm^{-1}
γ_3/ν_3	2.5	0.3	0.1	
$4\pi\rho_3$	2000	299.3	78.5	

(a)

Raman (Present data)

Transverse A_1	Longitudinal A_1	Transverse E_1
		~5
165	175	
270	465	305
515	720	485

(b)

IR Data

Transverse E_1	Longitudinal E_1
0-34	180
183	460
500	720

(c)

Figure 1.17: The measured E-type modes of BTO. Reproduced with permission from (a): [56] and (b), (c): [55]

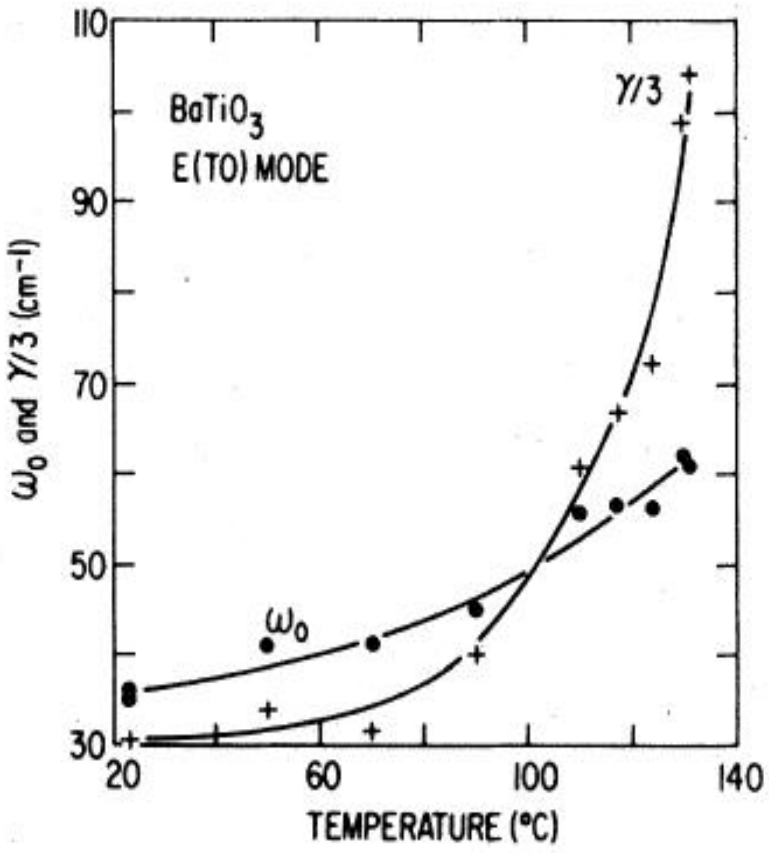

Figure 1.18: Measured temperature dependence of the lowest transverse E mode of BTO (frequency ω_0 and damping rate γ). Reproduced with permission from[58].

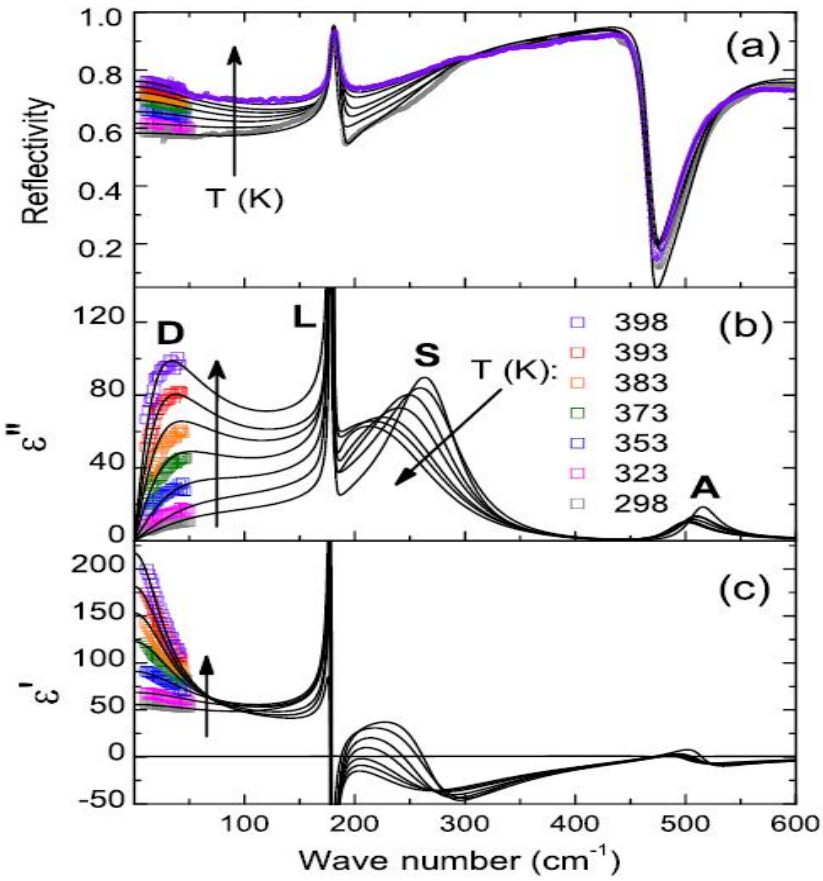

Figure 1.19: The A-type modes of BTO seen in THz spectra. Reproduced with permission from[60].

missing mode was shown to be relaxational in nature (see FIG.1.19 and FIG.1.20). Its relaxation rate, ω_D, as a function of temperature is displayed in FIG1.20. As temperature goes down from T_c, ω_D is seen increasing from about $28cm^{-1}$. Intriguingly, a strong correlation between SM and DM was displayed: the spectral weight of SM flows quickly toward DM as temperature increases toward T_c, and simultaneouly the SM somewhat softens (FIG.1.19).

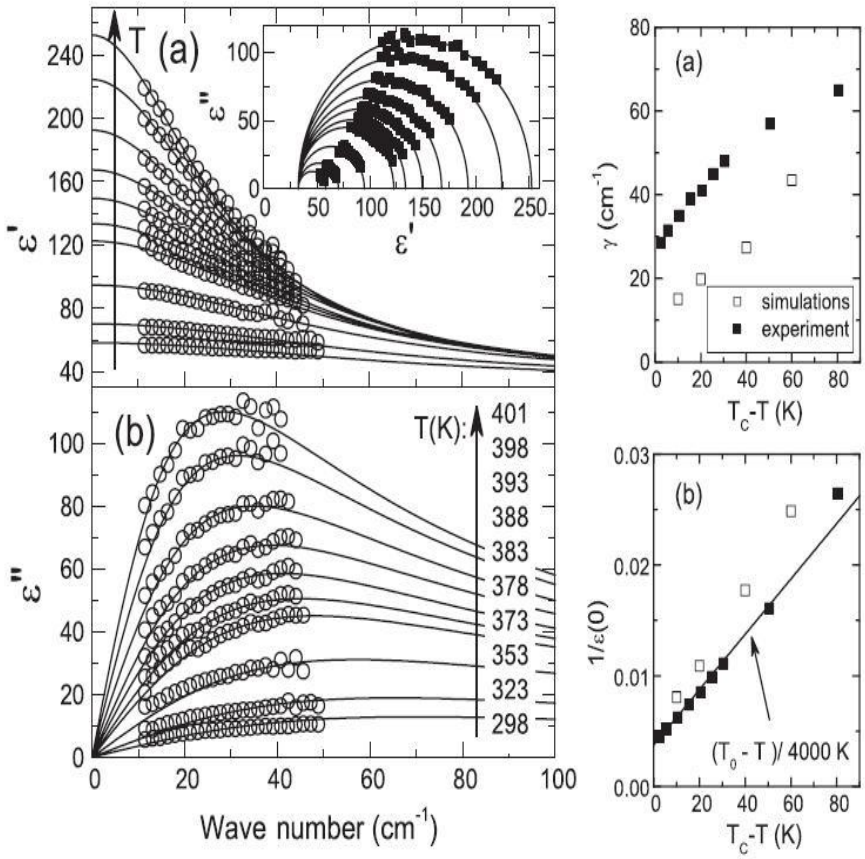

Figure 1.20: The transverse relaxation mode and and its temperature dependence found in tetragonal BTO. Reproduced with permission from[60].

1.7.4 Local Environment of Ti Atoms

There is a long-lasting contest on the character of the structual phase transitions in perovskites. A key ingredient concerns the potential surface in which the Ti atoms move. Is the potential a minimum or a maximum at the crystallographic site? If it's a minimum, the transition should be of displacive type and can be adequately described by phonon softening theory. Otherwise, the Ti atoms will be off-centered and the transition should be of order-disorder type. First principles computations in the 1990s showed that, it is the maximum case[48]. Early diffuse X-ray scattering pointed to the same[41]. Very recently, resonance experiments have been performed to affirm the computations[42, 43, 61]. Experimental difficulty lies in the fact that, the off-center shift is in the order of a few picometers and the Ti flutters among the off-center minima on the time scale of a few nanoseconds. These experiments tell two things: (1) the model by Comes et al (hereafter referred to as 8SM[62, 63, 64]) is largely correct, (2) the Ti fluttering is accompanied by dynamical O cage distortions and (3) such distortions in turn pull the Ti off-center a bit away from the magic directions like $[1, 1, 1]$ but the shift magnitude remains little changed. This angle deviation was found very small (0.1^o) in the cubic phase but rapidly increasing to about 12^o toward the c-axis in the tetragonal phase. These facts have been utilized by Stern to gain insights into the nature of the soft mode and the relaxion mode[65].

1.7.5 Critical Remarks

In view of phonon theory, in cubic phase one expects three T_{1u} type IR active modes[37]. This would exclude the two-mode picture and would identify TO_1 with TO_{1l} (to get the correct $\epsilon(\omega = 0)$). Let's proceed with this thought. Now each T_{1u} should split as $A_1 + E$ when entering the tetragonal phase. An interesting question is, how do they split? Note that, all the modes belonging to this set $\{TO_2, f_2, LM\}$ have close frequencies

around $170cm^{-1}$ while those in $\{TO_4, f_4, AM\}$ have close frequencies around $500cm^{-1}$. At the same time, the three modes in $\{TO_1, f_1, DM\}$ resemble each other in terms of (1) frequency, (2)temperature dependence and (3) line widths as well as (4) the magnitude of osillator strength. This striking comparison naturally suggests that, the TO_1, TO_2 and TO_4 should split into $f_1 + DM$, $f_2 + LM$ and $f_4 + AM$, respectively. A conflict arises in this assignment scheme: the TO_{1h} and the SM cannot find their places, which hints that the harmonic approximation in its simplest form misses something crucial: the strong anharmonicity. Two things seem peculiar with $TO_{2,4}$[49]: (1) the degeneracy within the group corresponding to each of them seems barely lifted by the tetrgonal distortions(2) the longitudinal conterparts of these modes have nearly the same frequencies. Both facts indicate that these modes are likely to be local (like Einstein modes) in character.

There are also other questions that are theoretically interesting. Firstly, what is the nature of TO_{1h} and TO_{1l}? According to Ponomareva et al.[54], the TO_{1l} represents the true soft phonon responsible for the cubic-tetragonal phase transition whereas TO_{1h} signifies a mode that is associated with the motions of a polar cluster. Their analysis shows that, these clusters are formed due to strong short-range correlations along axial directions like $[1, 0, 0]$. But why does the short-range correlations occur along axial directions? Which aspect of the cluster dynamics could give rise to the TO_{1h}? Is the TO_{1l} a relaxation mode or a resonance mode? There is an interesting indication which allows one to link the TO_{1h} with f_1. This indication comes from the observation (see the data by Ponomareva et al.[54] and Burns et al.[58]) that, f_1 has the same frequency (which is about $70cm^{-1}$) as TO_{1h} at around $430K$ and *that temperature dependence shows that f_1 seems a smooth continuation (on the tetragonal side) of the TO_{1h} (on the cubic side)*, as can be seen in e.g. FIG.1.18.

Secondly, where do SM and DM originate? Why do they strongly correlate with each other? The SM seems culpable within the phonon frame, while the DM has not been

exposed until recently[60]. The analysis by Hlinka et al. suggests that, both modes are likely to be attached to the same polar variable (plausibly the Ti atoms). Specifically, they argued that, the DM might be due to dynamic turnover of local dipole between prefered and unpriviliged directions, consistent with the eight-corner model (8CM) forwarded by Comes et al[62]. How about the SM? How is it related to this model? These authors did not give an answer. Although simulations[66, 67, 68] have demonstrated the possibility to have two modes from a single variable (see FIG.1.21), details about the intensity transfer (especially its temperature dependence) and the impacts from the coupling to other modes (LM and AM) have not been understood yet. Further, why is there a significant coupling between the TO_1 and TO_2 but not between TO_1 and TO_4? Due to frequency mismatch? One more interesting question pertains to the very large ratio of ϵ_a to ϵ_c, which was measured to be as large as 30 (see e.g. Z.Li et al.[69]). This ratio increases with decreasing temperature. The reason seems unknown[69]. However, one may find a candidate answer if pursuing the 8CM. In light of this model, in the tetragonal phase, the local dipoles are ordered along c-direction but still random in ab-plane. This means that, polarization fluctuations are stronger in the plane than along the c-direction. Considering the connection between fluctuations and susceptibility as quantified through fluctuation-dissipation theorem (eq.(1.15)), we expect that ϵ_a is much bigger (and even bigger at low temperatures) than ϵ_c. We'll discuss this arguement in more details in later chapters.

1.8 Phenomenology of $SrTiO_3$

Despite similarities to BTO, $SrTiO_3$ does not possess any genuine polar strcutural phase transitions unless modified. Usually it is thought that there are fierce quantum fluctuations in this compound but not in BTO[71, 72], although the origin remains an open question. On the other hand, STO has an interesting non-polar cubic-tetragonal transition taking

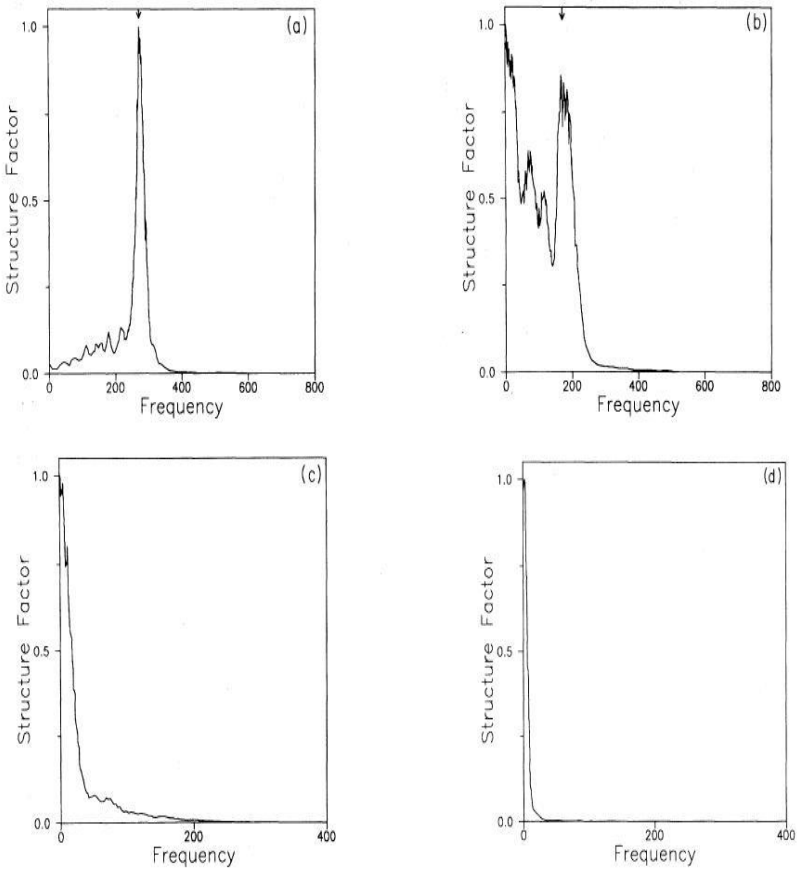

Figure 1.21: Coextence of two modes as predicted in molecular dynamics simulations. Reproduced with permission from[68].

place about $T_a = 105K$, which is due to the condensation of a zone-boundary mode (the R-mode)[73]. It involves the O cage tilting and therefore unit-cell doubling. The tilting angle $\phi = \phi(T)$ was less than 2.2^o and the resulting tetragonal distortion is rather minute, $c/a \sim 1.0005$[74]. This transition is almost of second order because the volume change across the transition is rather small and ϕ does not display a seeable discontinuity. In early times, no anomaly was found in the dielectric function accompanying this transition. However, according to recent studies impacts obviously exist[75].

1.8.1 Quantum Paraelectricity

As said no ferroelectric transitions have been seen in STO. Regardless of this, this compound resembles its ferroelectric counterpart in several aspects. First, the Curie-Weiss law holds at all except extremely low temperatures, $\epsilon^{-1}(0) = A(T - T_0)$[71]. Second, the Curie constant $1/A$ is as large as 10^5, similar to that of most displacive ferroelectrics[71]. Third, a zone-center mode softens at all but extremely low temperatures[26, 76]. However, these ferroelectric-like behaviors get eventually interrupted below about $30K$[71]. The $\epsilon(0)$ and the soft mode were found to saturate below $4K$ at 20000 and $\sim 10cm^{-1}$, respectively[75]. Evidences exist that such stabilization may well be caused by zero-point fluctuations. Hence, STO is often quoted as a quantum paraelectric.

Barret formula is often used to fit $\epsilon(0)$ of quantum paraelectrics. This formula reads[77]

$$\epsilon_B = \frac{C}{\frac{T_1}{2}\coth(\frac{T_1}{2T}) - T_0} \tag{1.24}$$

where T_1 is usually called the quantum temperature while T_0 is the extrapolated Curie temperature and C the Curie constant. At high temperatures ϵ_B reduces to Curie-Weiss law whereas at low temperatures it saturates at $\frac{2C}{T_1 - 2T_0}$. Quantum paraelectricity indicates $T_1 > 2T_0$. When applied to STO, a snag was perceived by Muller et al decades back[71].

It turns out that, ϵ_B could not give a satifactory fit unless an temperature dependent T_1 was assumed. Then T_1 would acquire different values at temperatures above $\sim 30K$ and below $\sim 10K$. The high temperature value T_{1h} was supposed to be a little larger than the low temperature one T_{1l}[78]. Various mechanisms have been put forth to explain this crossover[79], but the issue is still being debated.

We should mention another point in this regime. Muller et al. by EPR experiments found an anomaly at $37K$ in STO, which they interpretted as a tranisition into a coherent quantum state[80]. This finding renewed interest in this material. Viana et al. performed careful dielectric spectroscopy and discovered several features[81]. Notably, they found two peaks in ϵ'' as a function of temperature, one around $10K$ and the other around $80K$. Definitely, these peaks could arise only due to changes in Hamiltonian. What is interesting about these peaks is the remarkable dispersion with frequency, which was not seen at other temperatures. Although these authors attempted to relate these features to the transition claimed as Muller, it is still unclear what is the real nature. On the other hand, Arzel et al. observed sample dependence of this anomaly, who then proposed that the anomaly might be due to motions of dislocations[82].

1.8.2 Dielectric Modes

At all temperatures, three optically active modes (TO_1', TO_2' and TO_4') were observed[56], in consistency with phonon theory (T_{1u} modes). The TO_2' and TO_4' were located around $176cm^{-1}$ and $546cm^{-1}$, respectively. Little temperature dependence has been observed in TO_4' but discernible softening was seen in TO_2'[76], similar to what has been found in BTO (see FIG.1.22). The TO_1' was found with frequency of $87cm^{-1}$ at room temperature and softening all the way down to $\sim 10cm^{-1}$ at very low temperatures[137]. Although damped, the damping rate is less than a half that of its frequency at all temperatures studied[137]. Throughout all temperatures, the mode was found well defined. This is in contrast with the

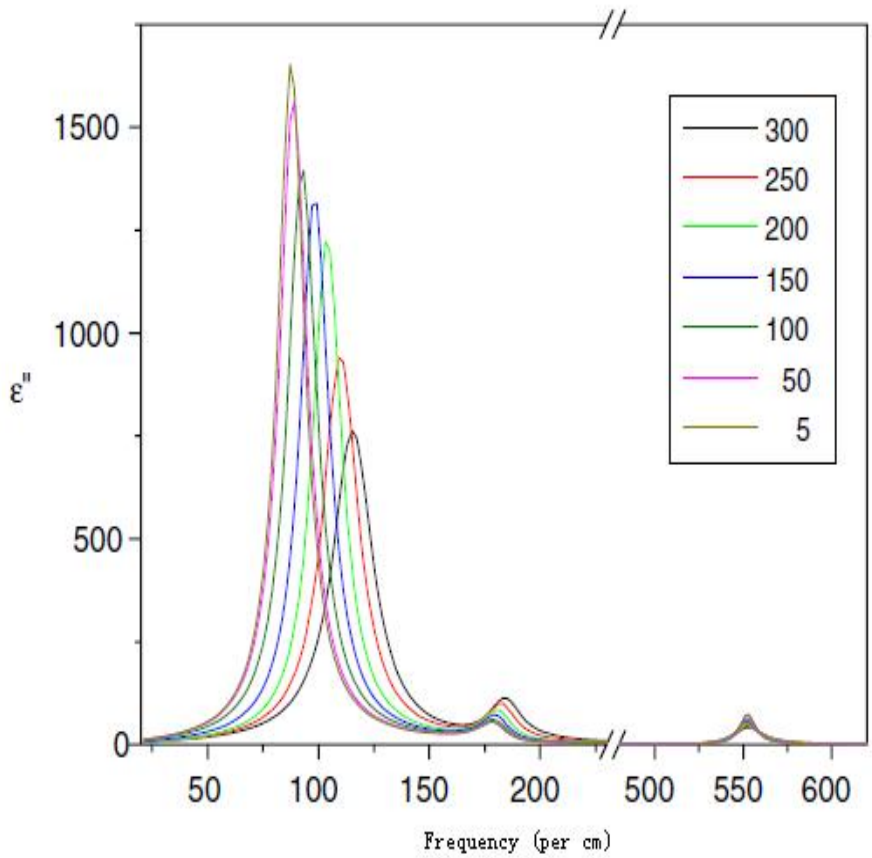

Figure 1.22: The lineshapes of STO (lightly doped) at various temperatures as indicated by the numbers inside the column. Reproduced with permission from[76].

TO_1 in BTO, which was found overdamped at all temperatures and with a much smaller frequency (see e.g.Ref.[56]). Below T_a, according to phonon theory, TO_1' splits into an Eu-type mode f_E' and an A_{2u}-type mode f_A' due to tetragonal deformations[137, 75]. The splitting $f_A' - f_E' > 0$ increases as the system cools down from T_a, above which they merge together, as seen in FIG.1.23. This splitting results in a small anisotropy $\epsilon_a/\epsilon_c \sim 4.2$, which is markedly smaller than for BTO (of 30).

1.8.3 Correlations Between The $105K$ Transition and The Dielectric Static Constant

Although the $105K$ transition is non-polar and the responsible mode is not optically active, they have been demonstrated having subtle impacts on the dielectric response. In the first place, as alreay said, this transition splits the soft mode TO_1' and therefore produces anisotropic dielectric responses. Second, it was found crucial in stabilizing the instigated ferroelectricity[75]. This was convincingly demonstrated by Yamanaka et al., who showed that, the f_E' would vanish around $30K$ were not for the $105K$ transition. Close inspection on the temperature dependences of TO_1' and $f_{A,E}'$ reveals that, the transition not simply splits TO_1' but reduces the softening rate, as can be seen in FIG.1.23. Third, as emphasized by Vogt[137], to obtain a nice fit with Barret's formula, one has to assume temperature dependences of the fitting parameters. Especially, as he found, one may use

$$\omega_1^2(T) = \omega_1^2(T_a)[1 + \alpha\phi^2(T)] \tag{1.25}$$

where ω_1 was introduced by Vogt and roughly amounts to T_1 in ϵ_B and α is a coefficient of about 0.05deg^{-2}. Recently, we have revisited this relation and attempted an interpretation of it. Note that, this form of T_1 is totally different from the form adopted[78, 79].

1.8.4 Isotope Effects: STO18

STO is a quantum paraelectric, but ferroelectricity can be induced by elemental substitution. Here we are mainly interested in O isotope effects. This kind of study was initiated by Itoh et al.[16]. After O^{18} substitution, we write the stoichiometry as $STO_x = STO_{1-x}^{16}O_x^{18}$. Itoh et al. found that $STO_{x>x_c\sim 0.33}$ is a ferroelectric with $T_c \approx 30\text{K}\sqrt{x - x_c}$. When $x = 1$, $T_c \approx 24.5K$ occuring to $STO18 = STO_{x=1}$. This is often cited to vindicate that STO is a quantum paraelectric[16, 83].

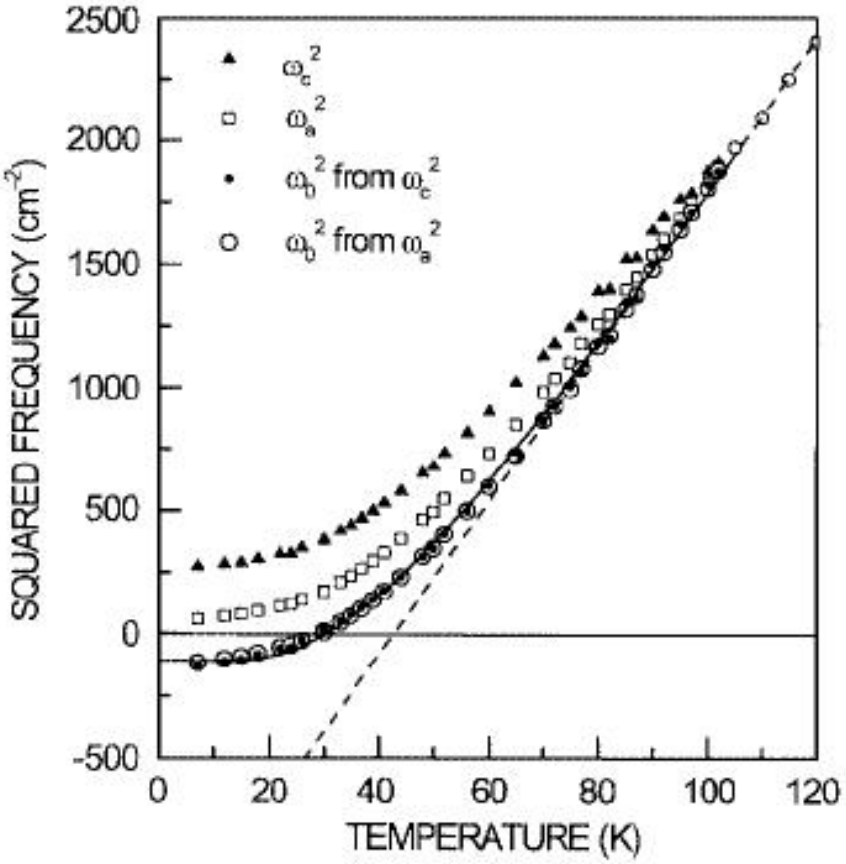

Figure 1.23: STO mode splitting due to the 105K transition. Reproduced with permission from[75].

Since its discovery, many investigations have appeared to clarify the nature of this induced ferroelectric transition in STO18. Some interesting points are summarized here. Firstly, the achieved state below T_c was found with orthohombic symmetry (C_{2v}) and its spontaneuous polarization was argued to point toward the edge centers of the pseudocubic unit cell[84, 85, 86]. Therefore, there is a symmetry change across T_c, from tetragonal to orthohombic. However, this change was found resulting in little volume variations, suggesting a continuous phase transition. Secondly, the TO_2' and TO_4' were discerned around $171cm^{-1}$ and $517cm^{-1}$[85], respectively, below T_c, close to but slightly (%3 and %5, respectively) shifted downward from their positions ($176cm^{-1}$ and $546cm^{-1}$, respectively) in ordinary STO. These two modes are perhaps characteristic of O vibrations. If so, one expects the frequency to be inversely proportional to the square root of the O mass. Thus, the frequency change rate should be about $6\% = \sqrt{\frac{18}{16}} - 1$, indeed compatible with observations. Downward shifts were also noticed in $f'_{A,E}$[84]. This might be due to more efficient coupling with $TO'_{2,4}$. Thirdly, the f'_E mode was found splitting into two modes below T_c while at the same time the f'_A mode transforms into a new mode (almost continuously) as a result of symmetry change[84]. The modes ensuing from f'_E will be labeled as f'_{EA} and f'_{EB}, respectively. Fourthly, both f'_E and f'_A, with the latter all the time lying above the former in frequency, were found softening all the way as the transition is approached from above T_c[84]. One would then take f'_E as the soft mode. This would require the f'_{EA} and f'_{EB} show similar softening behaviors when temperature rises up to T_c, at which point they merge with f'_E, as indeed observed. Nevertheless, the f'_E mode was argued not really responsible for the ferroelectric transition, because the symmetry of this mode does not match the symmetry of the ferroelectric state and its softening was shown incomplete: its frequency gets close to but not reaches zero at T_c[85]. Early Raman spectra on multidomain single crystal $STO18$ exhibits two pronounced peaks (one about $20cm^{-1}$ and the other $10cm^{-1}$) at extremely low temperatures below T_c, whose intensities diminish rapidly

when warmed up[16]. In light of above knowledge, these peaks should simply correspond to the f'_{EA} and f'_{EB}, which can be simultaneously detected in a multidomain sample in which selection rules are not sharp. Fifthly, a quasi-elastic (central) mode of relaxational type was unveiled near T_c, whose intensity was shown to develop rapidly as T_c is approached (FIG.1.24). This mode was suggested to be the direct cause of the transition[85].

The nature of this central mode is still an active topic under debate. In one model it was proposed pertaining to cluster ordering and relaxation[85]. In this scenario, the induced transition is perhaps of percolation type, with the polar cluster size increasing with x and eventually percolating through the whole sample at x_c. Existence of such clusters seem well advocated by both scattering and resonance experiments[86]. Nevertheless, how is the mode related to which kind of cluster motion exactly?

1.8.5 Local Environment of Ti Atoms

The Ti local environment was demonstrated analogous to that in BTO, as shown by similar experiments[61]. Namely, Ti atoms are off-center shifted. The difference is that, the magnitude seems much small ($< 5pm$) in comparison with that of BTO ($\sim 15pm$). Therefore, quantum tunneling must be much stronger in STO. This fact may be the origin of a number of differences between BTO and STO. However, it is unclear on the atomistic scale what is the effect of the $105K$ transition upon the Ti potential surface. There exist abundant facts claiming that the TO'_1 is likely to stem from Ti motions. One therefore has to understand how the TO'_1 splits into f'_A and f'_E and especially why $f'_A > f'_E$. If the 8CM is used, one has to establish the connections between the TO'_1 plus its offsprings ($f'_{A,E}$) and the eigenstates of the 8CM.

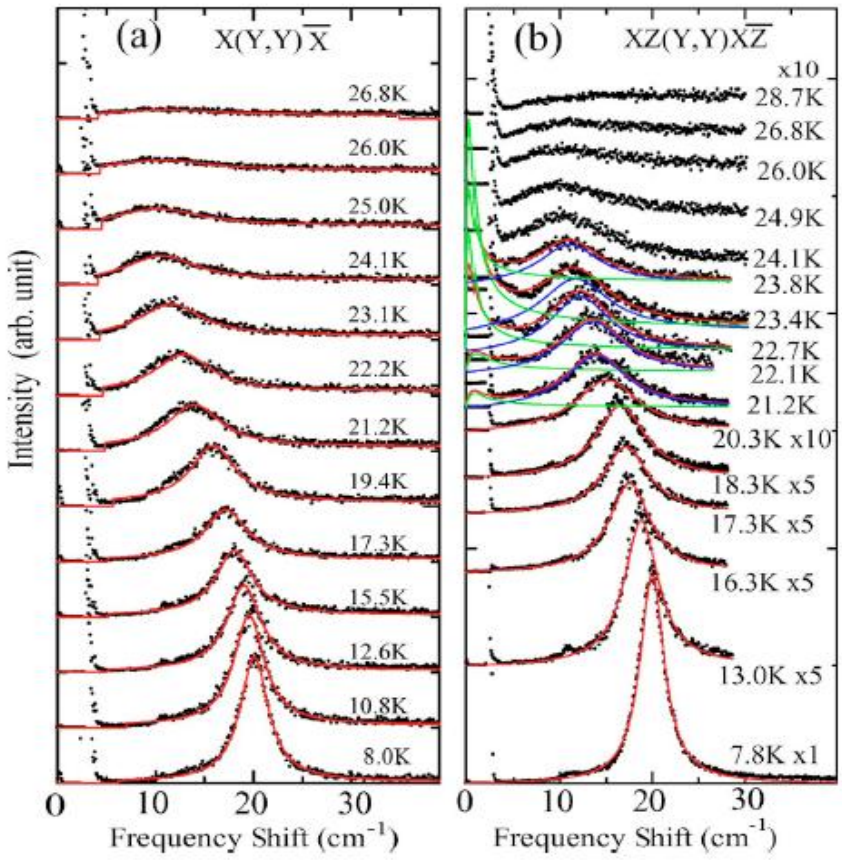

Figure 1.24: The quasi-elastic mode (indicated by the green line) in STO18 near T_c. Reproduced with permission from[85].

1.9 Other Related Materials

Although in the present thesis the discussions are directed explicitly at BTO and STO, they may also be suitable for understanding the lattice dynamics of other perovskite compounds. We mention a few candidates: (1) $KNbO_3$, which behaves in qualitatively the same way as BTO[87]; (2) $KTaO_3$, a compound reminiscent of STO but free from zone boundary structrual instability[137, 88]; (3)compositionally disordered perovskites such as $PbZr_xTi_{1-x}O_3$ and relaxor ferroelectrics[89]; (4) high-Tc superconductors, which can be ragrded as a distant relative of these compounds[151]. These materials will be touched where appropriate.

The thesis is organized as follows. The next chapter is devoted to deriving the model and making comparison with existing ones, followed by applications to BTO and STO in the third and fourth chapter, respectively. The fifth chapter will see some applications to high Tc superconductors. A summary will be given in the final chapter, where future directions will also be mapped.

1.10 Summary of Key Issues

In ending this chapter, we summarize some of the key issues to be discussed in the rest of this thesis. The basic question I am trying to answer is, what are the optically active normal modes of the lattice motions in perovskite ferroelectrics and how are they manifested in the dielectric spectra ? Due to the strong anharmonicity associated with the lattice motions, this question turns out to be very challenging. Specifically, I consider the following issues the most intereting and fundamental from the theoretical point of view:

- What is the nature of the observed peaks situated respectively about $180cm^{-1}$ and $500cm^{-1}$ in ε'' ?

- What is the nature of the cubic-tetragonal transition in BTO ? Why are there two peaks below $150cm^{-1}$ in the cubic phase and what are their nature ?
- What causes the ε_a to be so much bigger than the ε_c in tetragonal BTO ? Why are there four modes in ε_c and only three in ε_a and how are these modes interrelated ?
- How do the modes in cubic BTO evolve into the modes in tetragonal BTO ?
- Where comes the strong anisotropy that is responsible for the formation of stable quasi-one dimensional chains seen in the dis-ordered phase of BTO? How does such anisotropy reflect itself in the dielectric spectra ?
- Why is there strong quantum fluctuations in STO and how do such fluctuations make a difference in the dielectric spectra ?
- What is the physics behind the so-called crossover in the Barret temperature T_1 ?
- How does O isotope replacement induce ferroelectric instability in STO ?
- Are there any correlations between the Ti off-center shift and the O octehedra tilting ? If so, how are they manifested in the dielectric response ?
- On what occasions are the eight-well potential model indispensable ? Why is the double-well potential model inadequate on such occasions ?
- Is there any simple criteria in expressing the competitions between quantum fluctuations and ferroelectric ordering ?

Apart from the listed, one must add this question: what is the nature of the spectral weight transfer that is seen in the dielectric spectra ? This question is evidently relevant in revealing the anharmonic motions of Ti atoms. We shall provide answers (sometimes partial) to these questions in later chapters. The answers will be based on both theoretical and experimental cross-check.

Chapter 2

THEORETICAL FRAME: MODELS AND METHODS

2.1 Single-Body Potential Surfaces

As said in the last chapter, the dielectric response of a compound has two contributions from valence electrons and the ion cores, respectively. The former part (i.e., ϵ_∞) is small and can be taken as a constant in the frequency regime under study. So, we are primarily concerned with the latter part. In this section, we discuss the effective potential surface of the ions (*i.e., the cores*). To this end, we pick up a particular ion, say $l\kappa$, and examine the energy cost of displacing it by $\vec{u}_{l\kappa}$ while holding all other ions. Denote the energy cost by $V_{l\kappa}$. In the following subsections, we discuss this energy for each ion type in $(Ba, Sr)TiO_3$.

2.1.1 V_A

Each A ion coordinates with eight Ti ions and twelve O ions. The contributions to V_A in general come from the interactions with surrounding ions and with valence electrons. We represent these two portions by V_A^{ii} and V_A^{ie}, respectively, so that $V_A = V_A^{ii} + V_A^{ie}$.

First principles computations demonstrated two interesting features about the vibrations of the A ions[19]: (1) extremely weak mixing with the vibrations of Ti and O ions and (2) small band width indicative of Einstein-type phonon. These features are most manifest in the map of partial denisty of phonon states (PDOS, see FIG.2.1), which can be written for any ion $l\kappa$ as $PDOS(\omega|l\kappa) = \sum_{\vec{q}j} |A(l\kappa|\vec{q}j)|^2 \bar{\delta}(\omega_{\vec{q}j} - \omega)$. Here $A(l\kappa|\vec{q}j)$ stands for the probability amplitude of finding the ion $l\kappa$ in mode $\vec{q}j$. The density of states is then given by $DOS(\omega) = \sum_{l\kappa} PDOS(\omega) = \sum_{\vec{q}j} \bar{\delta}(\omega_{\vec{q}j} - \omega)$, implying $\sum_{l\kappa} |A(l\kappa|\vec{q}j)|^2 = 1$. One sees in FIG.2.1 that, $PDOS(Ba|\omega)$ is centered about $\omega = 20cm^{-1}$ with a width of only about $5cm^{-1}$ and in the meanwhile both $PDOS(Ti|\omega)$ and $PDOS(O|\omega)$ identically vanish in that frequency domain. In other words, there is negligible overlap between $PDOS(A|\omega)$ and $PDOS(Ti, O|\omega)$ for any ω, $PDOS(A|\omega) \cdot PDOS(Ti, O|\omega) \sim 0$. In addition, we should note that, the as-described traits are common not only to the cases with $A = Ba, Sr$ but also to that with $A = Pb$, regardless of the fact that Pb has lone electron pairs. For Ba and Sr, the peak frequency are basically the same. For Pb, it is shifted downward. The morphology of $PDOS(A|\omega)$ stands in sharp constrast with $PDOS(Ti, O|\omega)$. All these indicate that, the vibrations of A ions can be treated separately from that of the Ti-O subsystem. Hence, we may explicitly forget about the A ions, assuming that their main effects are to renormalize the Ti-O subsystem. There is another reason for making such approximation: we observe that, the dielectric response of the system comes mainly from the Ti-O subsystem, especially when the structural instability is concerned. In compounds like $PbTiO_3$, this approximation is questionable, since the Pb-sublattice can be another source of instability[21, 90].

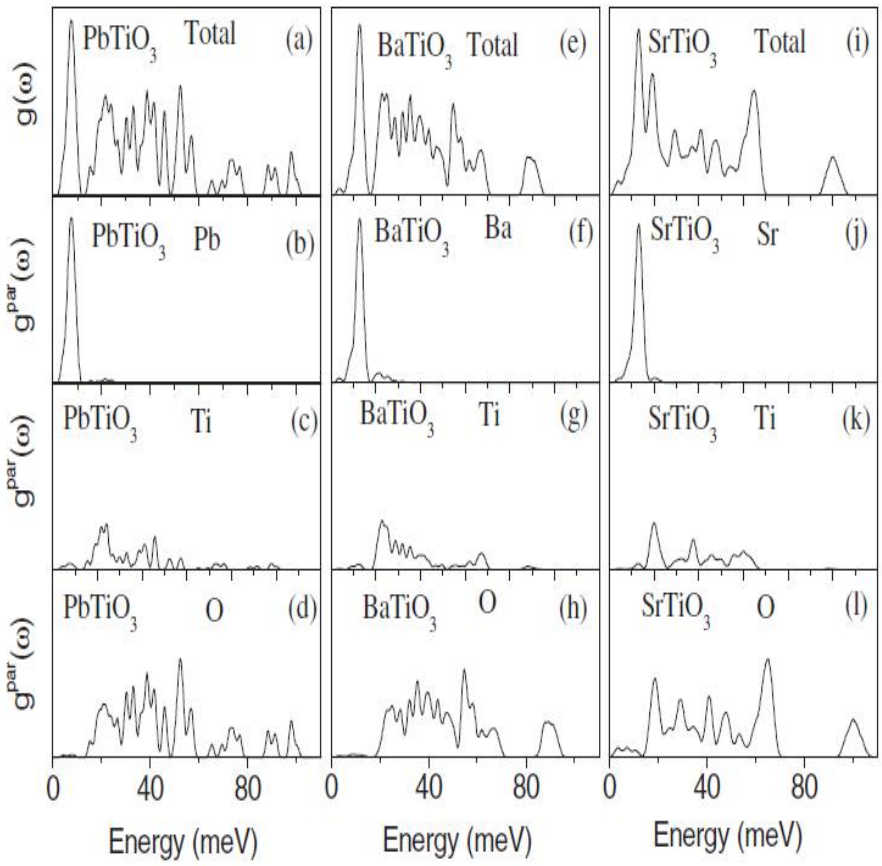

Figure 2.1: Total and partial density of phonon modes for $ATiO_3$ from first principles computations. Reproduced with permission from [19].

2.1.2 V_{Ti}

Contributions From Dipolar Interactions

Every Ti ion coordinates with eight A ions and six O ions. The O ions make an octehedral cage surrounding the Ti ion that is inside the cage. As is clear in PDOS map, the $PDOS(Ti|\omega)$ and $PDOS(O|\omega)$ occur in the same frequency region, alluding to strong couping between these two types of ions. Similar to the case with A ions, one can divide V_{Ti} in two terms, V_{Ti}^{ii} and V_{Ti}^{ie}. The V_{Ti}^{ii} encodes mainly the dipolar interactions with the O ions and the A ions. Ti ions are neither in touch with O ions (*i.e., cores*) nor A ions and hence no Born-Mayer type interactions could exist. For convenience, we can write V_{Ti}^{ii} as

$$\begin{aligned}
V_{Ti}^{ii} &= f_{Ti}(\theta,\varphi)u^2, \quad \vec{u} = u(\sin\theta\cos\varphi, \sin\theta\sin\varphi, \cos\theta) = u\hat{u} \\
f_{Ti}(\theta,\varphi) &= f_{Ti-A}(\theta,\varphi) + f_{Ti-O}(\theta,\varphi) + f_{Ti-Ti}(\theta,\varphi) \\
f_{Ti-A}(\theta,\varphi) &= \frac{z_{Ti}z_A}{2} \sum_{\text{all A sites}} \frac{3(\hat{u}\cdot\hat{R}_{l|A})^2 - 1}{R_{l|A}^3} \\
f_{Ti-O}(\theta,\varphi) &= \frac{z_{Ti}z_O}{2} \sum_{\text{all O sites}} \frac{3(\hat{u}\cdot\hat{R}_{l|O})^2 - 1}{R_{l|O}^3} \\
f_{Ti-Ti}(\theta,\varphi) &= \frac{z_{Ti}^2}{2} \sum_{\text{all Ti sites than the original one}} \frac{3(\hat{u}\cdot\hat{R}_{l|Ti})^2 - 1}{R_{l|Ti}^3} \\
\hat{R}_{l|A,Ti,O} &= \vec{R}_{l|A,Ti,O}/R_{l|A,Ti,O}, \quad R_{l|A,Ti,O} = |\vec{R}_{l|A,Ti,O}|
\end{aligned} \tag{2.1}$$

Here $\vec{u}$ signifies the displacement of the selected Ti ion. At first glance, we would think that V_{Ti}^{ii} generally depends on the direction of $\vec{u}$. However, it is not the case. In general, the second order of the expansion of the Coulombic potential can be written as $\sum_{\rho\rho'} L_{\rho\rho'}u_\rho u_{\rho'}$. Cubic symmetry dictates that $L_{xy,yz,zx} = 0$ and $L_{xx} = L_{yy} = L_{zz}$. By comparison with the dipolar coupling, one must have $f_{Ti}(\theta,\varphi) = Const = K_{Ti|dip}$.

Covalent Bonds

As for V_{Ti}^{ie}, it is convenient to cast this term further in two portions. To elucidate the nature of these portions, we at first consider the valence electrons. As said in chapter 1, strong covalent bonds are expected to exist between the e_g-type d-orbital and the p-orbital. One should note that, the p orbitals can be organized by symmetries. Look at the p_z orbital along the c-axis for example. For any d_{3z^2} orbital at $\vec{R}_{l|Ti}$, there are two p_z orbital at $\vec{R}_{l|O_z}$ and $\vec{R}_{l|O_z} - \vec{e}_c$, respectively, sandwiching that d-orbital. Now instead of $p_{z|l}$, we construct another set of basis orbital which are symmetric about the d-orbital. Write the new basis as

$$\bar{\phi}_{l|z} = \frac{1}{\sqrt{2}}(p_{l|z} - p_{l-|z}) \tag{2.2}$$

where the sign $-$ in the subscript is used to label the p_z orbital at $\vec{R}_{l|O_z} - \vec{e}_c$. These new basis orbital can be made orthogonal using Anderson ansatz[91]. The orthogonal basis orbital can be formed as

$$\begin{aligned} \phi_{l|z} &= \sum_{l'} \lambda^*_{z|l,l'} \bar{\phi}_{l'|z}, \quad \bar{\phi}_{l|z} = \sum_{l'} \lambda(z|l,l')\phi_{l'|z} \\ \lambda_{z|l,l'} &= \frac{1}{N^3} \sum_{\vec{q}\in 1BZ} \frac{i}{\sqrt{\cos q_z}} e^{i\vec{q}\cdot[\vec{R}_l - \vec{R}_{l'}]} \end{aligned} \tag{2.3}$$

where N^3 is the number of total unit cells. The $\lambda_{z|l,l'}$ has been shown to decay rapidly as the distance between the l and the l' unit cell increases (FIG.2.2). Now the d_{3z^2} hybridizes with $\phi_{l|z}$, giving rise to a bonding band with energy

$$[\varepsilon_{de} + \varepsilon_p]/2 - \sqrt{\Delta_e^2 + t_z^2} \tag{2.4}$$

and an anti-bonding band with energy

$$[\varepsilon_{de} + \varepsilon_p]/2 + \sqrt{\Delta_e^2 + t_z^2} \tag{2.5}$$

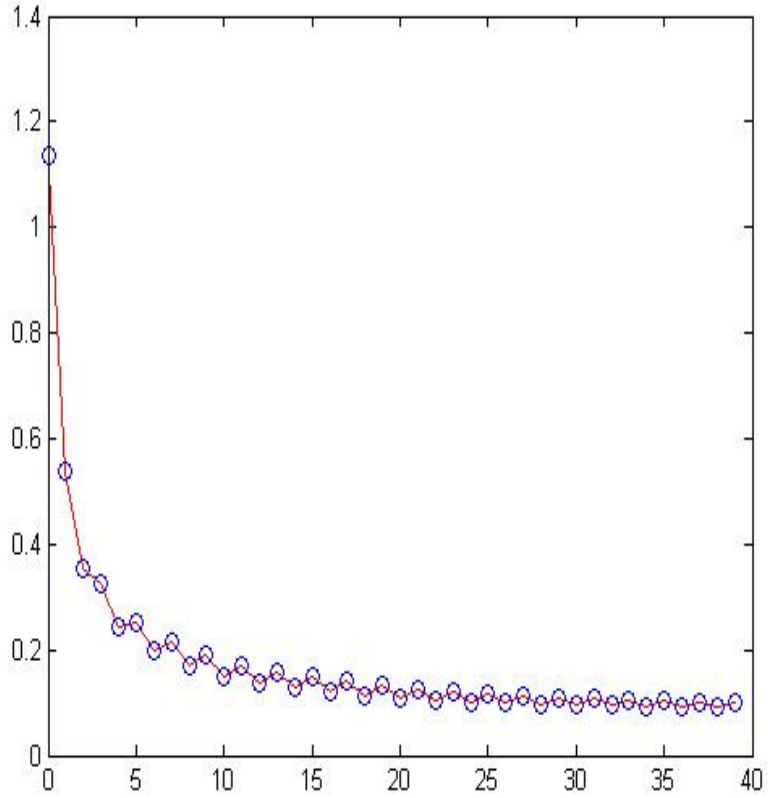

Figure 2.2: The $\lambda_{z|l,l'}$ as calculated from Eq.(2.3). Vertical axis: $\lambda_{z|l,l'}$; horizontal axis: $|\vec{R}_l - \vec{R}_{l'}|$.

Here t_z is the hybridization energy and $\Delta_e = \varepsilon_{de} - \varepsilon_p$ is the energy gap between the e_g-type d orbital and the p orbital. Note that the dispersion has been neglected for simplicity. This approximation is based on the fact that $\lambda_{z|l,l'}$ is a decaying function, as aforementioned. Note that t_z is twice as large as the hybridization energy between neighboring d_{3z^2} and p_z. As for the $d_{x^2-y^2}$ and planar p orbital, similar things can be done. Note that, in this case a $d_{x^2-y^2}$ couples essentially to such a symmetric combination (Zhang-Rice combination) of p orbital[1, 92]:

$$\bar{\phi}_{l|xy} = \frac{1}{2}(p_{lO_x|x} + p_{lO_y|y} - p_{l-O_x|x} - p_{l-O_y|y}) \tag{2.6}$$

Again, these new orbital are not orthogonal and can be orthogonalized to yield the fol-

lowing

$$\begin{aligned} \phi_{l|xy} &= \sum_{l'} \lambda_{xy|l,l'} \bar{\phi}_{l'|xy} \\ \lambda_{xy|l,l'} &= \frac{1}{N^3} \sum_{\vec{q} \in 1BZ} \frac{1}{\sqrt{1-(\cos q_x + \cos q_y)/2}} e^{i\vec{q}\cdot[\vec{R}_l - \vec{R}_{l'}]} \end{aligned} \tag{2.7}$$

which hybridizes with $d_{x^2-y^2}$. Here again, $\lambda_{xy|l,l'}$ decays fast with increasing distance between the l and l'[1]. Also a bonding and an anti-bonding state result, with energies of

$$[\varepsilon_{de} + \varepsilon_p]/2 - \sqrt{\Delta_e^2 + t_{xy}^2} \tag{2.8}$$

and

$$[\varepsilon_{de} + \varepsilon_p]/2 + \sqrt{\Delta_e^2 + t_{xy}^2}, \tag{2.9}$$

respectively. The t_{xy} is the hybrdization energy between the $d_{x^2-y^2}$ and ϕ_{xy}. The dispersion has been ignored for the property of λ_{xy}. Incidentally, we mention that, apart from the combination leading to ϕ_{xy}, there exists an anti-symmetric combination (denoted by ϕ'_{xy}) which leads to a non-bonding band[1].

As we see, in the covalent bonding described above, two p orbital, ϕ_z and ϕ_{xy}, have been concocted with the e_g-type d orbital. The resulting bonding band is mainly of p character while the anti-bonding one of d character. In total one has nine p orbital, whence seven of them should be non-bonding. Besides, all t_{2g}-type d orbital are also non-bonding. All the bonding bands and non-bonding p bands are occupied by electrons, but all the anti-bonding and non-bonding d bands are empty. The bands close to Fermi level are then the non-bonding bands: t_{2g} d bands making up the conduction band while non-bonding p bands the valence band. A gap of around 3ev separates the conduction band from the valence band[19, 93].

Contributions From Born-Mayer Interactions

As shown in the charge density map, Ti ions are besieged by valence electrons taking up the valence band, like a wall confining a ball. When the ion is brought close to the wall, a strong repulsion will be felt due to Pauli exclusion principle[23]: the core electrons of the ion are prevented from penetrating the wall which has already been full of electrons. The considerable band gap makes the wall very exclusive: to admit an external electron would cost 3ev. It is just such short-range force that is ultimately responsible for the stability of solids. As exclusive as it is, this wall can actually be deformed by the motion of the ion. Henceforth, two sources of V_{Ti}^{ie} are expected: one due to Pauli exclusion and the other due to the wall deformability. A few expressions have been proposed for the former. One among them is the Born-Mayer repulsion[94], which adapted to the present need should read

$$V_{BM}^{ie} = V_0 \exp(-|u - u_0|/r_0) \tag{2.10}$$

where u is defined as above while V_0, u_0 and r_0 are parameters characterizing the potential. In the present thesis, however, we prefer to adopt a simple power law,

$$V_{Ti|sri}^{ie} = \gamma_{Ti|sri} u^4 + K_{Ti|sri} u^2 - \alpha_{Ti|sri}(u_x^2 u_y^2 + u_y^2 u_z^2 + u_z^2 u_x^2), \tag{2.11}$$

where $\gamma_{Ti|sri}$, $K_{Ti|sri}$ and $\alpha_{Ti|sri}$ are constants. The $\alpha_{Ti|sri}$ term takes care of the fact that the surrounding electron cloud is not isotropic.

Vibronic Effects In Crystals

The other part of V_{Ti}^{ie} that is associated with the electronic wall deformability, on the other hand, can be taken care of as follows. Such deformability is usually framed using the electron-phonon theory. Electronic energy may be lowered due to level repulsion effects (i.e., when two levels are coupled, the energy of the lower level can be further reduced)

that can be created by phonons. We are not going to pay any heed to the non-bonding p orbital, because they always have very little overlap with the conduction band even in the presence of local lattice deformations. The orbital to be considered are the t_{2g} d-orbital and the $p_{O_{x,y,z}|x,y,z}$ orbital. When $\vec{u}$ is zero, these orbital don't mix, as prescribed by symmetry. Upon displacing the Ti ion (i.e., creating phonons), however, electronic transitions between these two bands can take place. The possible transition channels must be compatible with the underlying symmetry. To illustrate this, we take the band stemming d_{xy} for instance. Look at $d_{l|xy}$ and the surrounding p orbital, $p_{lO_x|x}$, $p_{l-O_x|x}$, $p_{l-O_y|y}$ and $p_{l-O_y|y}$. These two kinds of orbital are endowed with different symmetries under reflection about the $x-z$ and $y-z$ planes. The d_{xy} changes sign under reflection with respect to either plane, while p-orbital changes sign only under one of the two. Therefore, no transitions could take place without phonons. Nevertheless, an electron can transit by simultaneously creating a local deformation that breaks the symmetry. For example, to enable transitions between the $d_{l|xy}$ and $p_{lO_x|x}$, one can displace the Ti ion in the y-direction: the symmetry involved here is the reflection about the $x-z$ plane, under which d_{xy} changes sign but $p_{O_x|x}$ remains the same. Now the displacement along the y-direction has the same symmetry as d_{xy}, thus conserving the associated parity. Formally, one writes for the one-phonon process $\hat{R}_{xz}(d_{xy}\otimes p_{O_x|x}\otimes u_y) = (-d_{xy})\otimes p_{O_x|x}\otimes(-u_y) = d_{xy}\otimes p_{O_x|x}\otimes u_y$. Here $\hat{R}_{xz}$ signifies the reflection operation. In the second quantization formalism, we can write down the corresponding coupling like this: $\xi_{xy}d^{\dagger}_{l|xy}u_y p_{lO_x|x}+h.c.$, where ξ_{xy} is the coupling parameter. In a similar fasion, we can write down for $p_{l-O_x|x}$ an analogous term: $\xi_{xy}d^{\dagger}_{l|xy}u_y p_{lO_x|x}+h.c.$, while for $p_{lO_y|y}$ and $p_{l-O_y|y}$ the same thing can be written down except for changing u_y to u_x. To achieve a compact and symmetric form, we introduce the following symmetric

orbital,

$$\begin{aligned}
\Phi_{l|x,y,z} &= \sum_{l'} \Lambda^{*}_{x,y,z|l,l'} \bar{\Phi}_{l'|x,y}, \quad \bar{\Phi}_{l|x,y} = \sum_{l'} \Lambda_{x,y|l,l'} \Phi_{l'|x,y} \\
\bar{\Phi}_{l'|x,y,z} &= \frac{p_{l'-O_{x,y,z}|x,y,z} + p_{l'O_{x,y,z}|x,y,z}}{\sqrt{2}} \\
\Lambda_{x,y,z|l,l'} &= \frac{1}{N^3} \sum_{\vec{q}\in 1BZ} \frac{1}{\sqrt{\cos q_{x,y,z}}} e^{i\vec{q}\cdot[\vec{R}_l - \vec{R}_{l'}]}
\end{aligned} \tag{2.12}$$

Here $\Lambda(\rho|x,y,z)$ has similar property as $\lambda(\rho|x,y,z)$: a fast decaying function. Now we arrive at

$$H_{Ti|xy} = \sqrt{2}\xi_{xy} \sum_{l} d^{\dagger}_{l|xy} \sum_{l'} \{u_{l|y}\Lambda_{x|l,l'}\Phi_{l'|x} + u_{l|x}\Lambda_{y|l,l'}\Phi_{l'|y}\} + h.c. \tag{2.13}$$

By cyclic permutations of the axis, we can obtain the electron-phonon couplings involving d_{yz} and d_{zx}. They read

$$\begin{aligned}
H_{Ti|yz} &= \sqrt{2}\xi_{yz} \sum_{l} d^{\dagger}_{l|yz} \sum_{l'} \{u_{l|y}\Lambda_{z|l,l'}\Phi_{l'|z} + u_{l|z}\Lambda_{y|l,l'}\Phi_{l'|y}\} + h.c. \\
H_{Ti|zx} &= \sqrt{2}\xi_{zx} \sum_{l} d^{\dagger}_{l|zx} \sum_{l'} \{u_{l|z}\Lambda_{x|l,l'}\Phi_{l'|x} + u_{l|x}\Lambda_{z|l,l'}\Phi_{l'|z}\} + h.c.
\end{aligned} \tag{2.14}$$

Considering that $\Lambda_{x,y,z|l,l'}$ are fast decaying functions, we would like to take $\Lambda_{x,y,z|l,l'} \approx \Lambda\bar{\delta}_{l,l'}$, where $\Lambda \approx 1.1348$. This approximation allows one to focus on just a unit cell. Dropping the label and taking into account the orbital energy, we arrive at

$$\begin{aligned}
H_{Ti} &= \varepsilon_{dg}[d^{\dagger}_{xy}d_{xy} + d^{\dagger}_{yz}d_{yz} + d^{\dagger}_{zx}d_{zx}] + \varepsilon_{p}(\Phi^{\dagger}_{x}\Phi_{x} + \Phi^{\dagger}_{y}\Phi_{y} + \Phi^{\dagger}_{z}\Phi_{z}) \\
&+ \tilde{\xi}_{xy} d^{\dagger}_{xy}\{u_y\Phi_x + u_x\Phi_y\} + \tilde{\xi}_{yz} d^{\dagger}_{yz}\{u_y\Phi_z + u_z\Phi_y\} \\
&+ \tilde{\xi}_{zx} d^{\dagger}_{zx}\{u_z\Phi_x + u_x\Phi_z\} + h.c., \quad \tilde{\xi}_{xy,yz,zx} = \sqrt{2}\Lambda\xi_{xy,yz,zx}
\end{aligned} \tag{2.15}$$

which takes exactly the same form as the Hamiltonian obtained by Bersuker for a single TiO_6 cluster[22]. It can be solved to produce six eigenvalues, $\varepsilon_{1,2,...,6}$, which come in pairs:

$$\begin{aligned}
\varepsilon_1 &- \frac{\varepsilon_{dg}+\varepsilon_p}{2} = \frac{\varepsilon_{dg}+\varepsilon_p}{2} - \varepsilon_2 = \sqrt{\Delta_{gp}^2/4 + \tilde{\xi}_{xy}^2(u_x^2+u_y^2)} \\
\varepsilon_3 &- \frac{\varepsilon_{dg}+\varepsilon_p}{2} = \frac{\varepsilon_{dg}+\varepsilon_p}{2} - \varepsilon_4 = \sqrt{\Delta_{gp}^2/4 + \tilde{\xi}_{yz}^2(u_y^2+u_z^2)} \\
\varepsilon_5 &- \frac{\varepsilon_{dg}+\varepsilon_p}{2} = \frac{\varepsilon_{dg}+\varepsilon_p}{2} - \varepsilon_6 = \sqrt{\Delta_{gp}^2/4 + \tilde{\xi}_{zx}^2(u_z^2+u_x^2)}
\end{aligned} \tag{2.16}$$

After filling the lowest three levels with six electrons, we find (in the adiabatic approximation) an effective potential for the motions of Ti ions:

$$K_{elas}u^2 + 2(\varepsilon_2+\varepsilon_4+\varepsilon_6) \tag{2.17}$$

where we have included the aforementioned elastic term, $K_{elas} = K_{Ti|dip} + K_{Ti|sri}$. One should see that, if K_{Ti} is very small, this potential possesses four types of saddle points that can be classified through a cube. When $\xi_{xy} = \xi_{yz} = \xi_{zx}$, they are as follows[22, 18, 95, 96]:

1. One maximum at the center of the cube $u_x = u_y = u_z = 0$;
2. Eight minima at cube corners satifying $|u_x| = |u_y| = |u_z| \neq 0$;
3. Twelve points at edge centers satisfying, e.g., $|u_x| = |u_y| \neq 0, |u_z| = 0$;
4. Six points at face centers satisfying, e.g., $|u_x| = |u_y| = 0, |u_z| \neq 0$.

For small $\vec{u}$, one may approximate V_{Ti} as (after omitting an irrelevant constant)

$$V_{Ti} \approx \gamma(u_x^4+u_y^4+u_z^4+u_x^2u_y^2+u_y^2u_z^2+u_z^2u_x^2) - K(u_x^2+u_y^2+u_z^2) \tag{2.18}$$

This constitutes the basis of the so-called 8CM[41, 62, 63], which we have mentioned in chapter 1 and will discuss in more details later on in this chapter. It should be pointed out

that, in comparison with a TiO_6 cluster, the Ti off-center shift is expected to be enlarged by a factor of λ^2 in a crystal. Additionally, one should see that, in obtaining V_{Ti}, we did not consider the impacts from the covalent bonding which involves the same p-orbital. It is expected that, in comparison with the covalent bonding, the $H_{Ti|xy,yz,zx}$ are just perturbations. Henceforth, the p-character state taking part in the H_{Ti} should be replaced by the bonding state discussed in earlier paragraphs of this subsection. Fortunately, such replacement amounts to renormalizing the coupling coefficients $\xi_{xy,yz,zx}$. Finally, these coefficients should not be all indentical if the crystal structure is not cubic.

2.1.3 V_O

Contributions From Dipolar and Short-range Interactions

The O ions take up three distinct sites, O_x, O_y and O_z, respectively. Every O ion coordinates with two Ti ions and four A ions. The two Ti ions sandwitch the O ion, making a Ti-O-Ti bond pair. In comparison with the Ti ion, the A ions are much far from the O ion and sit in a plane perpendicular to the bond. Similarly, the O potential should also has three origins: the electrostatic interactions with other ions, the short-range repulsion from the valence electrons due to Pauli exclusion principle and the electron-phonon interactions. Consider a particular O ion, say the O_x in certain unit cell. The former two should result in two terms that can be couched as

$$f_O(\theta,\varphi)u^2 = K_{Ot|dip}u_{\bar{x}}^2 + K_{Ol|dip}u_x^2 \tag{2.19}$$

where $\vec{u}$ denotes the displacement of the O ion under consideration and the symmetry has been utilized to derive the second expression, and

$$\gamma_{Ot|sri}(\sum_{\bar{\rho}} u_{\bar{\rho}}^2)^2 + K_{Ot|sri}u_{\bar{\rho}}^2 + \gamma_{Ol|sri}u_\rho^4 + K_{Ol|sri}u_\rho^2 + \alpha_{O|sri}\sum_{\bar{\rho}} u_\rho^2 u_{\bar{\rho}}^2, \tag{2.20}$$

respectively.

Ti-O Bonding Effects

As for the electron-phonon interactions, there are several situations we have to ponder over. The orbital under immediate influence of the motions of an O ion (core) should be the p orbital centered on this ion. As is said in the last subsection, these p orbital have close relations with both the e_g- and t_{2g}-type d orbital. But not only that, since the O anion is often argued to boast of large polarizability, the admixing of its p orbital with its $3s$ orbital should be in addition included. All other O orbital such as $2s$ and deep-lying orbital are obviously fulfilled and therefore inactive all the time.

First consider how the covalent bonding energy changes when an O ion is displaced. Because of the directionality of covalent bonds, the displacement is expected to cost a significant amount of energy when it is perpendicular to the bond direction. On the other hand, what happens if it's along the bond? Will it be hindered or previliged? If it is hindered, the central positioning is stable; otherwise, the O may find itself instable against motions along bond directions. Considering that the central point is of high symmetry, some instability might well take place, as might happen to Jahn-Teller systems[97] and Peierls transition systems[98].

To explore the physics, we analyze a simple Ti-O-Ti cluster lying along, say, the x-axis. So the oxygen should be labelled as O_x, whose displacement is denoted by $\vec{u}$ as before. The p_x orbital on it is simply written as p for the moment. The left and the right Ti ion are to be tagged $-$ and $+$, whence the $d_{x^2-y^2}$ orbital on these ions are written as d_- and d_+, respectively. A Hamiltonian can be written down to model the cluster,

$$H_{cluster} = \frac{\Delta_{ep}}{2}[d_-^\dagger d_- + d_+^\dagger d_+ - p^\dagger p] + t_-[d_-^\dagger p + h.c.] + t_+[d_+^\dagger p + h.c.] \tag{2.21}$$

Here t_- and t_+ are real and denote the hopping integrals pertaining to the left and the right bond, respectively. When the O is at the center, i.e., $\vec{u} = 0$, one has $-t_- = t_0 = t_+$, with $t_0 > 0$ being a real constant. In general, $t_\pm$ must depend on $\vec{u}$. We write $t_- = \delta_- - t_0$ and $t_+ = \delta_+ + t_0$. We may expand them in powers of $\vec{u}$. For $\vec{u}$ along the bond, i.e, $\vec{u} = (u_x, 0, 0)$, one must have $\delta_- \approx a u_x$ and $\delta_+ \approx a u_x$, where a is a positive coefficient. For $\vec{u}$ perpendicular to the bond, e.g., $\vec{u} = (0, u_y, 0)$, the $\delta_\pm$ must vanish in the first order of u_y by symmetry (the cluster is invariant under rotation about the x-axis). To the second order, however, one has $\delta_- = b u_y^2$ and $\delta_+ = -b u_y^2$, with b another positive coefficient. So, generally, for $\vec{u} = (u_x, u_y, u_z)$, we can write

$$\begin{aligned} t_- &= -t_0 + a u_x + b(u_y^2 + u_z^2) \\ t_+ &= t_0 + a u_x - b(u_y^2 + u_z^2) \end{aligned} \tag{2.22}$$

The model can be easily solved to yield a bonding state, an anti-bonding state and a non-bonding state. To this end, we consider two new d-orbital that are taken to be

$$\begin{aligned} d &= \frac{1}{\sqrt{t_-^2 + t_+^2}}(t_- d_- + t_+ d_+) \\ \bar{d} &= \frac{1}{\sqrt{t_-^2 + t_+^2}}(t_- d_- - t_+ d_+) \end{aligned} \tag{2.23}$$

which are orthogonal. Now we see that the p admixes only with d, not with $\bar{d}$. We arrive at

$$H_{cluster} = \frac{\Delta_{ep}}{2}[d^\dagger d - p^\dagger p] + \sqrt{t_-^2 + t_+^2}(d^\dagger p + p^\dagger d) + \frac{\Delta_{ep}}{2}\bar{d}^\dagger \bar{d} \tag{2.24}$$

The energies of the non-bonding, bonding and anti-bonding states are $\varepsilon_n = \frac{\Delta_{ep}}{2}$, $\varepsilon_b = -\sqrt{\Delta_{ep}^2/4 + t_-^2 + t_+^2}$ and $\varepsilon_a = \sqrt{\Delta_{ep}^2/4 + t_-^2 + t_+^2}$, respectively. Now filling all non-bonding states and the bonding state, we obtain an effective adiabatic potential as $\varepsilon = 2\varepsilon_b$. Keeping

only the leading terms in $\vec{u}$ and dropping an irrelevant constant, we find

$$\varepsilon \approx \frac{8t_0 b}{\Delta_{ep}} u_{\bar{x}}^2 - \frac{4a^2}{\Delta_{ep}} u_x^2, \quad u_{\bar{x}}^2 = u_y^2 + u_z^2 \tag{2.25}$$

This expression clearly confirms our anticipation: the O is prevented from moving to bend the bond while it is instable against motions along the bond. This places the O ion at a particular position: anisotropy can develop, as we will discuss later. Evidently, the as-described covalent bonding effects should not be limited to O ions. They can equally apply to Ti ions. The crucial difference between the Ti ions and O ions lies in the fact that, the former are engaged simultaneously with three cross-linked bond pairs whereas the latter is with just a single pair. The bond network does not favor a Ti ion moving in any direction. Cubic symmetry suggests that, the three bond pairs capturing the Ti ion should exactly have exactly the same effects in their respective orientations. To the lowest non-vanishing order in the displacements, the potentials from these three bonds are additive.

Let's see that, the t_0, a and b introduced above correspond to the zero-th, first and second order effects, respectively. Denote the interactions between an electron and the O ion is $V(|\vec{r} - \vec{u}|) \approx V(|\vec{r}|) - \vec{u} \cdot \nabla V(|\vec{r}|) + \frac{1}{2} u_\nu \frac{\partial^2}{\partial r_\nu \partial r_{\nu'}} u_{\nu'} + ...$, where $\vec{r}$ is the electron position vector relative to the O ion and $\nu, \nu' = x, y, z$. By virture of symmetry, we conclude that $\frac{\partial V(|\vec{r}|)}{\partial r_{y,z}} = 0$. Therefore, these coefficients can be expressed as integrals as follows:

$$\begin{aligned} t_0 &= \int_\Omega \psi_{d_{x^2-y^2}} V(|\vec{r}|) \psi_p \\ a &= \int_\Omega \psi_{d_{x^2-y^2}} \frac{\partial V(|\vec{r}|)}{\partial r_x} \psi_p \\ b &= \frac{1}{2} \int_\Omega \psi_{d_{x^2-y^2}} \frac{\partial^2 V(|\vec{r}|)}{\partial r_y^2} \psi_p \end{aligned} \tag{2.26}$$

The integral is over the space Ω where the atomic wave functions $\psi_{p,d_{x^2-y^2}}$ (at the O and

the right Ti ion sites) have significant overlap. Assuming Coulombic form of $V(|\vec{r}|) \sim \frac{1}{|\vec{r}|}$, we get

$$\begin{aligned} \frac{\partial V(|\vec{r}|)}{\partial r_x} &\sim -\frac{1}{|\vec{r}|^2}\frac{r_x}{|\vec{r}|} \\ \frac{\partial^2 V(|\vec{r}|)}{\partial r_y^2} &\sim \frac{3}{|\vec{r}|^4}\frac{r_y}{|\vec{r}|} - \frac{1}{|\vec{r}|^3} \end{aligned} \tag{2.27}$$

Now that the region Ω is concentrated in a small spot lying on the x-axis, we may approximately take $\vec{r} \sim (r_x, 0, 0)$. Thus, we find

$$\begin{aligned} t_0 &\sim \int_\Omega \psi_{d_{x^2-y^2}} \frac{1}{r_x} \psi_p \approx \frac{1}{r_\Omega} \int_\Omega \psi_{d_{x^2-y^2}} \psi_p \\ a &\sim \int_\Omega \psi_{d_{x^2-y^2}} \frac{1}{r_x^2} \psi_p \approx \frac{1}{r_\Omega^2} \int_\Omega \psi_{d_{x^2-y^2}} \psi_p \\ b &\sim \frac{1}{2}\int_\Omega \psi_{d_{x^2-y^2}} \frac{1}{r_x^3} \psi_p \approx \frac{1}{2}\frac{1}{r_\Omega^3} \int_\Omega \psi_{d_{x^2-y^2}} \psi_p \end{aligned} \tag{2.28}$$

where r_Ω indcates a point inside the region Ω. From the above, we infer that

$$2t_0 b \sim a^2 \tag{2.29}$$

This suggests that, $\varepsilon \approx \frac{4a^2}{\Delta_{ep}^2}(u_{\bar{x}}^2 - u_x^2)$.

Now we provide some justifications for the cluster treatment used to derive ε. Look at a $-[Ti-O]_N-$ chain. The original question is, what is the energy cost of displacing one of the O ions in this chain? Very generically, such displacement should create an impurity state[99], which may lie below the valence band, or above the conduction band or inside the gap. Such state is often found localized in proximity of the impurity (i.e., the displaced O ion). Therefore, its energy is primarily determined by ions close to the impurity. In other words, a proper cluster should suffice for illustrating the physics.

O Ion Polarizability Effects

We proceed to consider the effects from O shell polarizability. It engages the O $2p$ and $3s$ orbital, which are separated in energy by Δ_{sp}. If the O ion takes the central position, then no mixing between these orbital can take place. Upon displacing this ion, the $3s$ becomes hybridized with one of the $2p$ orbital, and the O shell is said to be polarized. No mixing (in the one-phonon process) within $2p$ can occur, due to symmetry. Obviously, the model can be written as

$$H_{polariz} = \frac{\Delta_{sp}}{2}(s^\dagger s - \sum_{\nu=x,y,z} p_\nu^\dagger p_\nu) + \bar{a} \sum_{\nu=x,y,z} (s^\dagger p_\nu + p_\nu^\dagger s) u_\nu \tag{2.30}$$

Here $\bar{a}$ is a coefficient. This model can be solved in the same fasion as we deal with $H_{cluster}$. One just needs to see that the $3s$ couples actually only to the following $2p$ orbital, which is a linear combination of $p_{x,y,z}$,

$$P = \frac{1}{\sqrt{u_x^2 + u_y^2 + u_z^2}}(u_x p_x + u_y p_y + u_z p_z) = \frac{1}{u}\sum_\nu u_\nu p_\nu \tag{2.31}$$

One can construct two other p orbital by linear combinations that are mutually orthogonal and orthogonal to P. Denote them by P_n and P'_n. The model then becomes

$$H_{polariz} = \frac{\Delta_{sp}}{2}(s^\dagger s - P^\dagger P) + \bar{a}u(s^\dagger P + P^\dagger s) + \frac{\Delta_{sp}}{2}(P_n^\dagger P_n + P_n'^\dagger P'_n) \tag{2.32}$$

This gives rise to two non-bonding states with energy $\Delta_{sp}/2$, one bonding state with energy $-\sqrt{\Delta_{sp}^2/4 + \bar{a}^2u^2}$ and one anti-bonding state with energy $\sqrt{\Delta_{sp}^2/4 + \bar{a}^2u^2}$. Filling all the non-bonding states and the bonding state, one obtains an effective potential as

$$-2\sqrt{\Delta_{sp}^2/4 + \bar{a}^2u^2} \approx const - \frac{2\bar{a}^2}{\Delta_{sp}}u^2 \tag{2.33}$$

Note that this potential is isotropic, in the sense that, it is regardless of the direction of $\vec{u}$, standing in sharp contrast with what ensues from $H_{cluster}$. Again, the O shell polarizability effects should also be felt by Ti ions and similar potential should be generated, but there is an essential difference: the potential becomes anisotropic, because the $3s-2p$ hybridization due to displacing a Ti ion discriminates between the case when the displacement is along and that when it is perpendicular to the bond. Besides, the polarizability effects should be smaller on Ti ions than on O ions. Moreover, one should note that, such effects always favor non-central positioning.

O Cage Tilting: A Vibronic Point of View

Now we turn to investigating the electronic origin of the O_6 cage tilting phenomenon, which has been observed in STO and $LaAlO_3$ (LAO)[73, 100]. Here we show that *such tilting can be generated by phonon-aided electronic transitions among the same orbital that have been shown to underlie the Ti off-center shifts*. In this respect, we claim that the O cage tilting and the Ti off-center shifts bear the same cause. The orbital are t_{2g}-type d orbital and the p orbital that take part in covalent bonding. Take $d_{l|xy}$ and $p_{lO_x|x}$ for example. No transitions happen in the absence of phonons. The former is anti-symmetric while the latter is symmetric under reflections about the x-z plane. Therefore, to enable transitions through O phonons, one must displace the O ion along y direction, namely, $u_{lO_x|y}$. The same logic applies to other p orbital sitting around the d orbital. In summary, a Hamiltonian can be jotted down to account for this kind of process:

$$H_{tilting|z} = h\sum_{l} d^{\dagger}_{l|xy}\{p_{l-O_y|x}u_{l-O_y|x} + p_{lO_y|x}u_{lO_y|x} + p_{lO_x|x}u_{lO_x|y} + p_{l-O_x|x}u_{l-O_x|y}\} + h.c. \quad (2.34)$$

where h is the coupling coefficient. Generally, to show any instability associated with the phonon sub-system, one needs to evaluate the correlation function as prescribed in

eq.(15) in chapter 1. However, here we are mainly interested in two cases. Writting $u_{lO_x|y} = u_o \exp(i\vec{q}\vec{R}_l)$ and $u_{lO_y|x} = u_o \exp(i\vec{q}\vec{R}_l)$, the two cases correspond to $\vec{q} = (0,0,0)$ and $\vec{q} = (\pi,\pi,0)$, respectively. In the former, the O ions belonging to the same unit cell are displaced toward each other, resulting in higher electrostatic energy and therefore disfavored. The latter case corresponds to the O cage tilting and the electrostatic repulsion is averted. We therefore consider only the $\vec{q} = (\pi,\pi,0)$ case. Substituting the expression in the above Hamiltonian, we find

$$\begin{aligned} H_{tilting|z} &= hu_o \sum_l d^\dagger_{l|xy}\{p_{lO_y|x} - p_{l-O_y|x} + p_{lO_x|x} - p_{l-O_x|x}\} + h.c. \\ &= 2hu_o \sum_l d^\dagger_{l|xy}\bar{\phi}_{l|xy} + \bar{\phi}^\dagger_{l|xy} d_{l|xy} \\ &= 2hu_o \sum_{l,l'} \lambda_{xy|l,l'}\{d^\dagger_{l|xy}\phi_{l'|xy} + \phi^\dagger_{l'|xy} d_{l|xy}\} \end{aligned} \tag{2.35}$$

where we have used the expressions of $\bar{\phi}_{xy}$ and ϕ_{xy} introduced in the last subsection. Again, using the fact that $\lambda_{xy|l,l'}$ decays rapidly for l' distant from l, we can neglect the dispersion effects. Relating the u_o to the tilting angle φ in terms of the lattice constant a_0 as $u_o = a_0\varphi$ and focusing on a particular unit cell, we find

$$H_{tilting|z} = 2ha_0\varphi\lambda(d^\dagger_{xy}\phi_{xy} + \phi^\dagger_{xy} d_{xy}) \tag{2.36}$$

Now solving it together with the on-site energy, $\varepsilon_{dg} d^{\dagger_{xy}} d_{xy} + \varepsilon_p \phi^\dagger_{xy}\phi_{xy}$, we find a bonding and an anti-bonding state with energies

$$\varepsilon_b = \frac{\varepsilon_{dg} + \varepsilon_p}{2} - \sqrt{\Delta^2_{gp}/4 + 4h^2 a_0^2 \varphi^2} \tag{2.37}$$

and

$$\varepsilon_a = \frac{\varepsilon_{dg} + \varepsilon_p}{2} + \sqrt{\Delta^2_{gp}/4 + 4h^2 a_0^2 \varphi^2}, \tag{2.38}$$

respectively. Now filling two electrons in the bonding state, we find an effective adiabatic potential for the O cage tilting as $2\varepsilon_b$, which can be expanded to yield

$$\varepsilon \approx -\frac{8h^2a_0^2}{\Delta_{gp}}\varphi^2 \tag{2.39}$$

The physically irrelevant constant has been dropped. It is seen that, the electronic energy is lowered for finite φ, indicating the tilting instability. Therefore, we have proved that, the O cage tilting instability can be caused by electron-phonon interactions. The $H_{tilting|z}$ described above accounts for the tilting about the z-axis. In exactly the same manner, one can show that, the $\{d_{yz}, p_{O_y|y}, p_{O_z|z}\}$ leads to tilting around the x-axis and $\{d_{zx}, p_{O_z|z}, p_{O_x|x}\}$ the tilting about the y-axis.

2.2 Two-Body Inter-ion Interactions

2.2.1 Dipolar Interactions

A term is called 'interaction' if it engages simultaneously the variables of more than one body. As usual, we only consider two-body interactions, which are defined as the two-body part of the energy change that occurs when two ions are displaced simultaneously. Such interactions can be mediated in several ways. In the first place, there are the dipolar interactions. For two ions at $l\kappa$ and $l'\kappa'$, respectively, this dipolar energy is given by

$$\begin{aligned} & \frac{z_{l\kappa}z_{l'\kappa'}}{R^3_{l\kappa,l'\kappa'}}\{\vec{u}_{l\kappa}\vec{u}_{l'\kappa'} - 3u_{l\kappa}u_{l'\kappa'}\cos\theta_{l\kappa}\cos\theta_{l'\kappa'}\} \\ = & \frac{z_{l\kappa}z_{l'\kappa'}u_{l\kappa}u_{l'\kappa'}}{R^3_{l\kappa,l'\kappa'}}\{\hat{u}_{l\kappa}\hat{u}_{l'\kappa'} - 3\cos\theta_{l\kappa}\cos\theta_{l'\kappa'}\} \end{aligned} \tag{2.40}$$

where $\cos\theta_{l\kappa} = \hat{u}_{l\kappa}\hat{R}_{l\kappa,l'\kappa'}$. As expected, the dipolar interaction is anisotropic in the sense that, it relies on the direction of $\vec{u}_{l\kappa,l'\kappa'}$. Besides, it is marginally long range: it goes as

$R^{-3}_{l\kappa,l'\kappa'}$. What is particularly complicated is that, it consists of two portions with opposite effects: e.g., if $z_{l\kappa}z_{l'\kappa'} > 0$, the $\hat{u}_{l\kappa}\hat{u}_{l'\kappa'}$-term favors the ions being displaced in opposite directions but the $\cos\theta_{l\kappa}\cos\theta_{l'\kappa'}$-term wants them to displace in the same manner along the line joining them. Note that, an important quantity involved in dipolar interactions is the effective charge, $z_{l\kappa}$, whose definition and values vary from model to model[101, 102]. Despite such controversy, two basic facts have been recognized: (1) the O effective charges should actually be represented as a tensor, instead of a scalar, as can be deduced from the anisotropy seen in the O ions' crystal environment; (2) these charges often deviate from their nominal values signifcantly. Thus, one assigns an O ion the charge z_t and z_l correponding respectively to the motions perpendicular to and along the Ti-O-Ti bond. According to first principles studies, both are negative and with $z_l \approx 2.8z_t \approx -5.71$ in units of elementary charge. The Ti and Ba charges are positive and can be represented as a scalar, $z_{Ti} \approx 7.25$ while $z_{Ba} \approx 2.77$ and $z_{Sr} \approx 2.56$[102].

Despite its claimed importance in driving structural phase transitions, we try to argue that, the dipolar interactions may not be the crucial ingredient. First, we note that, this kind of interactions between a Ti and its adjacent O ions would favor the Ti ion to displace oppositely to apical O ions but in the same direction as the planar O ions. This contradicts experiment: in the tetragonal phase of BTO, all O ions are shifted oppositely to the central Ti ion[10]. Second, there is a reasoning that, lattice instability can not arise from Coulombic interactions[96]. Thus, we make a major assumption: we include them only between a Ti and its nearest O ions. With this assumption, the expression can be simplified. Look at a Ti and the O on its right side (O_x). Their dipolar energy reads

$$\beta^l_{dip} 2u_{Ti|x}u_{O_x|x} + \beta^t_{dip} u_{Ti|y,z}u_{O_x|y,z}, \tag{2.41}$$

where $\beta^l_{dip} = \frac{8|z_l|z_{Ti}}{a_0^3} > 0$ and $\beta^t_{dip} = -\frac{8|z_t|z_{Ti}}{a_0^3} < 0$. We have taken into account the tensor

property of z_O. See that these two coefficients bear opposite signs, which, as already said, would have planar and apical O ions to be displaced differently but for other forces.

2.2.2 Electron-Mediated Interactions

In addition, inter-ion interactions can arise indirectly through coupling to valence electrons. Electronic transitions could happen in the presence of two local phonons at $l\kappa$ and $l'\kappa'$ and as a result, electronic energy changes. This change is not simply a sum of the changes caused individually by phonons at these sites. Rather, there are interferences or say cooperative effects that are manisfested as phonon-phonon interactions. The shell model mentioned in chapter **1** can be used for illustration. Look again at a $Ti-O-Ti$ cluster. All three ions couple to the O shell (i.e., the valence electrons). Motions of the left Ti ion exert influences on that of the shell, which then transmits the effects to the O and the right Ti ion. The net effect appears as if interactions existed between these ions. Two ions can be efficiently coupled only if they both contribute significantly to an electronic transition. Therefore, the physics should be again local and may be studied on a Ti-O-Ti cluster or a TiO_6 cage. Let's begin with the cluster. First note that interactions between the O and a Ti and that between the Ti ions can be induced by polarizing the O ion (i.e., causing electronic transitions between the 2p and 3s orbital). It is easy to estimate the strength of such couplings. To do this, one just needs replace the $\bar{a}u_\nu$ in $H_{polariz}$ by the following terms

$$\bar{a}u_\nu + a_\nu(u_\nu(+) + u_\nu(-)) \tag{2.42}$$

Here a_ν are coefficients satisfying $a_y = a_z$ and $a_x a_y < 0$ as well as $\bar{a}a_x > 0$. The relations about their signs can be easily checked by examing the symmetries of the atomic wave functions and that of the local phonon as well as the sign of the electron-ion potential.

After solving the resulting Hamitonian one finds the following couplings:

$$\begin{aligned}
(1) \quad &: \quad -\frac{8\bar{a}a_\nu}{\Delta_{sp}} u_\nu u_\nu(\pm) = \beta^l_{pol} u_x u_x(\pm) + \beta^t_{pol}(u_y u_y(\pm) + u_z u_z(\pm)) \\
(2) \quad &: \quad \frac{8a^2_\nu}{\Delta_{sp}} u(+)_\nu u(-)_\nu \\
\beta^l_{pol} &= -\frac{8\bar{a}a_x}{\Delta_{sp}} < 0, \quad \beta^t_{pol} = -\frac{8\bar{a}a_y}{\Delta_{sp}} > 0
\end{aligned} \tag{2.43}$$

Clearly, (1) signifies a Ti-O coupling while (2) stands for a Ti-Ti coupling due to O polarizability and is anti-ferroelectric in nature. Similarly, we can obtain an effective potential from $H_{cluster}$ with the following replacements of $\delta_\pm$

$$\delta_\pm \Longrightarrow a[u_x - u_x(\pm)] \pm b[(u_y - u_y(\pm))^2 + (u_z - u_z(\pm))^2] \tag{2.44}$$

This leads to the following Ti-O coupling

$$\begin{aligned}
&: \quad \beta^l_{clu} u_x u_x(\pm) + \beta^t_{clu}[u_y u_y(\pm) + u_z u_z(\pm)] \\
\beta^l_{clu} &= \frac{4a^2}{\sqrt{\Delta^2_{ep} + 8t_0^2}} > 0, \quad \beta^t_{clu} = -\frac{8t_0 b}{\sqrt{\Delta^2_{ep} + 8t_0^2}} < 0
\end{aligned} \tag{2.45}$$

On the other hand, no Ti-Ti coupling has been found to the truncated order.

2.2.3 Summary: The Importance of Polarization Effects

Summarizing what's presented above, one may conclude that, the effective Ti-O coupling may be written as

$$V_{Ti-O} = \sum_l u_{lTi|\rho}\{\beta^l[u_{lO_\rho|\rho} + u_{l-O_\rho|\rho}] + \beta^t \sum_{\bar{\rho}}[u_{lO_{\bar{\rho}}|\rho} + u_{l-O_{\bar{\rho}}|\rho}]\} \tag{2.46}$$

Here $\beta^l = \beta^l_{dip} + \beta^l_{clu} - |\beta^l_{pol}|$ and $\beta^t = \beta^t_{pol} - |\beta^t_{dip}| - |\beta^t_{clu}|$. *One can read the importance of the O polarizability in these expressions*: were not for it, one would have $\beta^t < 0$, which is not consistent with observations. The β^t_{pol} is crucial to have a Ti ion and its neighboring planar O ions shifted oppositely in the tetragonal phase. It should be pointed out that, the observed pattern of ion shifts in tetragonal phase can not be explained by O-O repulsion, because of the symmetry of the O cage. Actually, O-O interactions have been demonstrated very weak in general.

2.2.4 Correlations Between O Cage Tilting and Ti Off-Center Shifts

The last element to be discussed in this subsection is the correlations between the off-center Ti shift and the O cage tilting. We have already shown that, these two modes can arise from a single origin: the phonon-assisted electronic transitions between the bonding p orbital and the non-bonding t_{2g}-type d-orbital. These transitions can be rendered by local phonons on both the Ti and O sites. Previously, we had considered these two categories of phonons separately and individually. When simultaneously input, correlations between them are expected. This comes at the root of the correlations to be discussed between Ti off-center shift (a polar mode) and O cage tilting (a non-polar mode). We shall neglect any possible slight tetragonal distortions and therefore take $\xi_{xy} = \xi_{yz} = \xi_{zx} \equiv \xi$. It is instructive to examine a TiO_6 cluster for the moment, which has the same symmetry as the whole crystal. Again look at the d_{xy} for illustration. As we have discussed before, this orbital can couple to $p_{O_{x,y}|x,y}$. Due to Ti phonon, the coupling reads $\sqrt{2}\xi d^\dagger(u_y\bar{\Phi}_x + u_x\bar{\Phi}_y) + h.c.$. Due to O cage tilting, it reads $\sqrt{2}ha_0\varphi d^\dagger(\bar{\phi}_x + \bar{\phi}_y)$. Evidently, the $\bar{\phi}$ and $\bar{\Phi}$ have different symmetries and have zero overlaps, hence leading to *competition between the off-center*

shift and the tilting mode. To show this, we examine the following Hamiltonian

$$\begin{aligned} : \quad & \frac{\Delta_{gp}}{2}(d_{xy}^{\dagger}d_{xy} - \bar{\phi}_x^{\dagger}\bar{\phi}_x - \bar{\phi}_y^{\dagger}\bar{\phi}_y - \bar{\Phi}_x^{\dagger}\bar{\Phi}_x - \bar{\Phi}_y^{\dagger}\bar{\Phi}_y) \\ + \quad & \sqrt{2}\xi d^{\dagger}(u_y\bar{\Phi}_x + u_x\bar{\Phi}_y) + h.c. + \sqrt{2}ha_0\varphi d^{\dagger}(\bar{\phi}_x + \bar{\phi}_y) \end{aligned} \tag{2.47}$$

which has included both types of couplings and can be solved easily. One ends up with the following adiabatic potential

$$K_{Ti}(u_x^2 + u_y^2) + K_O\varphi^2 - 2\sqrt{\Delta_{gp}^2/4 + 2\xi^2(u_x^2 + u_y^2) + 2h^2a_0^2\varphi^2} \tag{2.48}$$

We have included the elastic terms as headed by K_{Ti} and K_O. The minima of this potential occur either at $u_x = u_y = \varphi = 0$ or where

$$\xi^2(u_x^2 + u_y^2) + h^2a_0^2\varphi^2 = Const \tag{2.49}$$

This $Const$ is almost independent of ξ and h if both K_{Ti} and K_O are sufficiently small. From this equation, it is self-evident that, the O tilting competes with Ti off-center shift. Our discussions are based on a single TiO_6 cluster, however the conclusions should not change even the whole crystal is considered. Using symmetric orbital, the crystal problem boils down to the TiO_6 problem, as we have shown many times before. Another concern is that, we did not consider d_{yz} and d_{zx}, which are expected to affect the results but only quantitatively.

Although the correlations between the polar Ti mode and the non-polar O tilting have been demonstrated interesting, we will not consider them explicitely and they will only be touched where necessary.

2.3 The Model and Its Approximate Forms

2.3.1 Model Hamiltonian

After discussing the various channels of potentials regarding either the on-site or the inter-site part, we are now at a stage to write down the full Hamiltonian for the Ti-O system. Hereafter we denote the displacement of a Ti ion by $\vec{u}$ (with magnitude of u) while that of an O ion by $\vec{U}$ (magnitude of U). Expectedly, we put

$$H_{\mathrm{TiO_3}} = Kin_{Ti} + Kin_O + V_{Ti} + V_O + V_{Ti-O} \tag{2.50}$$

where $Kin_{Ti,O}$ give the kinetic energy

$$Kin_{Ti} = \sum_l \frac{P_l^2}{2M}, \quad Kin_O = \sum_{l,\rho} \frac{p_{l|O_\rho}^2}{2m} \tag{2.51}$$

with P_l is the momentum of the l-th Ti ion of mass M and $p_{l|O_\rho}$ of the momentum of the as-labelled O ion of mass m.

Although the potential terms have already been discussed in the above, we here would like to give a brief synopsis to recapture the logic. As for $V_{Ti} \equiv \sum_l V_{l|Ti}$, the on-site term for Ti ions, we can always assume the following form as accorded by the Ti symmetry,

$$V_{l|Ti} = \gamma u_l^4 + \alpha(u_{l|x}^2 u_{l|y}^2 + u_{l|y}^2 u_{l|z}^2 + u_{l|z}^2 u_{l|x}^2) - K u_l^2 \tag{2.52}$$

According to our discussions in the last section, the coefficients of each term can be written as

$$\gamma = \gamma_{Ti|sri} + \gamma', \quad \alpha = -\gamma' - \alpha_{Ti|sri}, \quad K = K' - K_{elas} \tag{2.53}$$

Here γ' and K' are related to eq.2.17. By expansion, one may put $\gamma' \approx \frac{8\tilde{\xi}^4}{\Delta_{gp}^3}$ and $K' \approx \frac{4\tilde{\xi}^2}{\Delta_{gp}}$. In the strong electron-phonon coupling case, one can have $K > 0$. This will be assumed

from now on, as required by experiments and first-principles computations. Were not for the short-range force, one would get $\gamma + \alpha = 0$. First principles computations indicate that, for a variety of compounds, this relation is approximately fulfilled: e.g., for STO, $\gamma + \alpha \sim 4\%$. Further, these computations show $K > 0$ and $\gamma > 0$. As long as these inequalities are satisfied, one ends up with a set of minima located away from $u = 0$. If $\alpha > 0$, they are found along the axis, e.g., $u_x \neq 0$ and $u_y = u_z = 0$; otherwise, along the diagonals, as detailed before.

Similarly, the O symmetry accords the following form to $V_O = \sum_{l,\rho} V_{lO_\rho}$,

$$V_{lO_\rho} = \gamma_t (\sum_{\bar{\rho}} U^2_{l\rho|\bar{\rho}})^2 + K_t \sum_{\bar{\rho}} U^2_{l\rho|\bar{\rho}} + \gamma_l U^4_{l\rho|\rho} + K_l U^2_{l\rho|\rho} + \alpha_O U^2_{l\rho} \sum_{\bar{\rho}} U^2_{l\rho|\bar{\rho}} \tag{2.54}$$

Obviously, we have assumed rotational symmetry about the Ti-O-Ti bond. In previous analysis it was shown that,

$$K_t = K_{Ot|dip} + K_{Ot|sri} + \frac{8t_0 b}{\Delta_{ep}} - \frac{2\bar{a}^2}{\Delta_{sp}} \tag{2.55}$$

Although this expression does not allow the evaluation of the value of K_t, we may safely assume that $K_t > 0$. As we shall argue in next chapter, this assumption is compatible with experiments. If so, we may neglect the fourth order term in $U_{\rho|\bar{\rho}}$ as well as the cross term. Therefore, we may write

$$V_{lO_\rho} \approx K_t \sum_{\bar{\rho}} U^2_{l\rho|\bar{\rho}} + \gamma_l U^4_{l\rho|\rho} + K_l U^2_{l\rho|\rho} \tag{2.56}$$

We have

$$K_l = K_{Ol|dip} + K_{Ol|sri} - \frac{4a^2}{\Delta_{ep}} - \frac{2\bar{a}^2}{\Delta_{sp}} \tag{2.57}$$

It is interesting to see that in general $K_t \neq K_l$. Reasonably, we may take

$$K_t > K_l \tag{2.58}$$

because (1) the short range potential mainly stems from the O shell, which is likely to generate isotropic repulsion, i.e., $K_{Ot|sri} \sim K_{Ol|sri}$ and (2) in the dipolar potential, by evaluating the leading terms of $f_O(\theta, \varphi)$, it is likely that $K_{Ot|dip} > K_{Ol|dip}$ (see that $|z_{Ti} z_O| > |z_A z_O|$ and $R_{TiO} < R_{AO}$, where R denotes the corresponding distances).

Finally, some words are added on the V_{Ti-O}. The form as writen in eq.2.46 obviously has left out the correlations between the O cage tilting and Ti off-center shifts. The latter, by eq.2.48, comes from higher order Ti-O couplings. A complete handling is very difficult and won't be pursued in this thesis. Rather, we will only discuss some of its consequences in the fourth chapter. Before that, we shall simply assume eq.2.48 for V_{Ti-O}.

A complete treatment of H_{TiO_3} is just considerably difficult and we need various approximate forms in practice. Before laying down these forms we write down the Hamiltonian in the q-space:

$$\begin{aligned}
H_{TiO_3} &= \frac{1}{2M}\sum_{\vec{q}} P(\vec{q})P(-\vec{q}) + \frac{1}{2m}\sum_{\vec{q}} p_{O_\rho}(\vec{q})p_{O_\rho}(-\vec{q}) \\
&+ \frac{1}{N}\sum_{\vec{q}_1,\vec{q}_2,\vec{q}_3,\vec{q}_4;\rho,\rho'} \upsilon_{\rho\rho'} u_\rho(\vec{q}_1)u_\rho(\vec{q}_2)u_{\rho'}(\vec{q}_3)u_{\rho'}(\vec{q}_4)\bar{\delta}(\vec{q}_1+\vec{q}_2+\vec{q}_3+\vec{q}_4) \\
&- K\sum_{\vec{q};\rho} u_\rho(\vec{q})u_\rho(-\vec{q}) + \sum_{\vec{q};\rho}[K_l U_{\rho|\rho}(\vec{q})U_{\rho|\rho}(-\vec{q}) + K_t \sum_{\bar{\rho}} U_{\rho|\bar{\rho}}(\vec{q})U_{\rho|\bar{\rho}}(-\vec{q})] \\
&+ \gamma_l \frac{1}{N}\sum_{\vec{q}_1,\vec{q}_2,\vec{q}_3,\vec{q}_4;\rho} U_{\rho|\rho}(\vec{q}_1)U_{\rho|\rho}(\vec{q}_2)U_{\rho|\rho}(\vec{q}_3)U_{\rho|\rho}(\vec{q}_4)\bar{\delta}(\vec{q}_1+\vec{q}_2+\vec{q}_3+\vec{q}_4) \\
&+ \sum_{\vec{q};\rho} u_\rho(\vec{q})[\beta_l(\vec{q})U_{\rho|\rho}(-\vec{q}) + \sum_{\bar{\rho}} \beta_t(\vec{q})U_{\bar{\rho}|\rho}(-\vec{q})]
\end{aligned} \tag{2.59}$$

where $P(\vec{q})$, $p_{O_\rho}(\vec{q})$, $u_\rho(\vec{q})$ and $U_{\rho|\rho}(\vec{q})$ are the Fourier transforms of P_l, $p_{l|O_\rho}$, $u_{l|\rho}$ and $U_{l\rho|\rho}$,

respectively. In addition,

$$\upsilon_{\rho\rho'} = (\gamma - \alpha/2)\bar{\delta}_{\rho,\rho'} + \alpha/2 \tag{2.60}$$

and

$$\beta_l(\vec{q}) = 2\beta_l \cos\frac{q_\rho}{2}, \quad \beta_t(\vec{q}) = 2\beta_t \cos\frac{q_{\bar{\rho}}}{2} \tag{2.61}$$

In what follows, we discuss several approximate forms of H_{TiO_3}.

2.3.2 Anisotropic Rotor Model: ARM

This model was introduced in [2]. The main approximation comes at simplifying the Ti on-site term $V_{l|Ti} + \frac{P_l^2}{2M}$. It applies when the inter-well energy barrier in $V_{l|Ti}$ is very high, which is the case with compounds like BTO and STO as experimentally suggested. To illustrate the point, we for the moment assume α vanish so that the minima of V_{Ti} comprises a sphere with radius of $\sqrt{\frac{K}{2\gamma}}$. Suppose the energy barrier is high enough. Thus, low energy fluctuations perpendicular to this sphere should be heavily suppressed. Freezing these fluctuations gives rise to a picture in which the Ti ion moves like a rotor. For non-vanishing α, one ends up with a non-uniform sphere, where the rotor description still works provided the non-uniformity is imposed. A formal derivation of the ARM is given below.

To keep the notations clean, we drop the l-label. It is convenient to write $\vec{u} = u(\hat{n}_x, \hat{n}_y, \hat{n}_z) \equiv u\hat{n}$, with which we have $V_{Ti} = \gamma(\hat{n})u^4 - Ku^2$, where $\gamma(\hat{n}) = \gamma + \frac{\alpha}{2}[1 - (n_x^4 + n_y^4 + n_z^4)]$. We also split the kinetic energy as $\frac{P^2}{2M} = -\frac{\hbar^2\nabla^2}{2M} = \frac{\hbar^2}{2Mu^2}\{\hat{\Omega}^2 - \frac{\partial}{\partial u}u^2\frac{\partial}{\partial u}\}$. Here $\hbar\hat{\Omega}$ is the angular momentum. Now one takes the average of $Kin_{Ti} + V_{Ti}$ over the radial part of the wave function, i.e.,

$$H_{ARM;Ti} \equiv \int_0^\infty \Psi^*(u,\hat{n})(Kin_{Ti} + V_{Ti})\Psi(u,\hat{n})u^2 du \tag{2.62}$$

where $\Psi(u,\hat{n})$ denotes the ground state wave function of $[Kin_{Ti}+V_{Ti}]_{\alpha=0}$. Note that $\Psi(u,\hat{n})$ is variable separable and one arrives at

$$\begin{aligned} H_{ARM;Ti} &= \frac{\hbar^2}{2I}\hat{\Omega}^2-\tilde{\alpha}(n_x^4+n_y^4+n_z^4) \\ \frac{1}{u_0^2} &= \langle\frac{1}{u^2}\rangle, \quad I=Mu_0^2, \quad \tilde{\alpha}=\frac{\alpha}{2}\langle u^4\rangle \end{aligned} \tag{2.63}$$

up to an irrelevant constant. Further, we write $\vec{u}\approx u_0\hat{n}$.

One may solve $H_{ARM;Ti}$ numerically. To this end, we choose the spherical harmonics, $|lm\rangle$, as the basis. In this representation, $\hat{\Omega}^2$ is diagonal, $\langle l'm'|\hat{\Omega}^2|lm\rangle=\sqrt{l(l+1)}\bar{\delta}_{l,l'}\bar{\delta}_{m,m'}$. To compute the matrix element of $n_{x,y,z}^4$, one may proceed in two ways. We here adopt the most straightforward one, in which we just need the matrix elements of $n_{x,y,z}$. They are computed like this: we at first express $n_{x,y,z}$ in terms of $Y_l^m=\langle\theta,\varphi|l,m\rangle$ and then make use of the Wigner 3-j symbols for the involved integrals. It is easy to show that

$$n_x=\sqrt{\frac{2\pi}{3}}(Y_1^{-1}-Y_1^1), \quad n_y=i\sqrt{\frac{2\pi}{3}}(Y_1^{-1}+Y_1^1), \quad n_z=\sqrt{\frac{2\pi}{3}}Y_1^0 \tag{2.64}$$

Now the matrix element involves evaluating integrals of the following kind,

$$\begin{aligned} \int(Y_{l_1}^{m_1})^*\cdot Y_{l_2}^{m_2}\cdot Y_{l_3}^{m_3} &= (-1)^{m_1}\int(Y_{l_1}^{-m_1})^*\cdot Y_{l_2}^{m_2}\cdot Y_{l_3}^{m_3} \\ &= (-1)^{m_1}C_{l_1l_2l_3}\times W_{0,0,0}^{l_1,l_2,l_3}\times W_{m_1,m_2,m_3}^{l_1,l_2,l_3} \end{aligned} \tag{2.65}$$

Here $C_{l_1l_2l_3}=\sqrt{\frac{(2l_1+1)(2l_2+1)(2l_3+1)}{4\pi}}$ and W_m^l represents the Wigner 3-j symbols[103]. The integration is taken over the entire solid angle. After obtaining $n_{x,y,z}$, the $n_{x,y,z}^4$ can be found by self-multiplying them four times. Eventually, the H_{ARM} is established and can be solved on a computer.

To be complete, we need to add the following to $H_{ARM|Ti}$ so as to get the ultimate H_{ARM},

$$\begin{aligned} : \quad & \sum_{l,\rho} \frac{p^2_{l|O_\rho}}{2m} + \tilde{K}_l \sum_{l,\rho} U^2_{l\rho|\rho} + \tilde{K}_l \sum_{l,\rho} \sum_{\bar{\rho}} U^2_{l\bar{\rho}|\rho} \\ + \quad & u_0 n_{l|\rho} [\beta_l (U_{l\rho|\rho} + U_{l-\rho|\rho}) + \beta_t (U_{l\bar{\rho}|\rho} + U_{l-\bar{\rho}|\rho})] \end{aligned} \tag{2.66}$$

where we have assumed $\langle u \rangle \sim u_0$.

2.3.3 Eight-Corner Model: 8CM

Assume $\alpha < 0$ so that there are eight minima of the V_{Ti} situated at the corners of a small cube with length of u_0. The 8CM ensues from the ARM in the large $|\tilde{\alpha}|$ limit, where only a few states about the trough are used. These states correpsond to the eight minima on the sphere. One may write them as $|\nu\rangle, \quad \nu = 1, ..., 8$. The $H_{ARM|Ti}$ then becomes

$$H_{8CM|Ti} = \sum_{\nu,\nu'} t_{\nu\nu'} |\nu\rangle\langle\nu'| \tag{2.67}$$

where the sum is over pairs and $t_{\nu\nu'}$ depends on the distance between the ν-th and ν'-th corners. We write t_1 for the nearest pair. Evidently, $t_1 > 0$ decreases as u_0 increases. For BTO, such quantum effects are often ignored. But for STO, it should be important[72]. One should note that, this model has exlcuded any intra-corner motions.

The $H_{8CM|Ti}$ can be solved using permutation symmetry of the said cube. The resulting eight eigenstates can be sorted in two groups, each with a singlet lying above a triplet (since $t_1 > 0$). This is shown in FIG. 2.3

2.3.4 Double-Well Approximation: DWA

This model focuses on motions along one axis, say, z and averages out other components. It may be suitable for describing some basic aspects of phase transitions involving

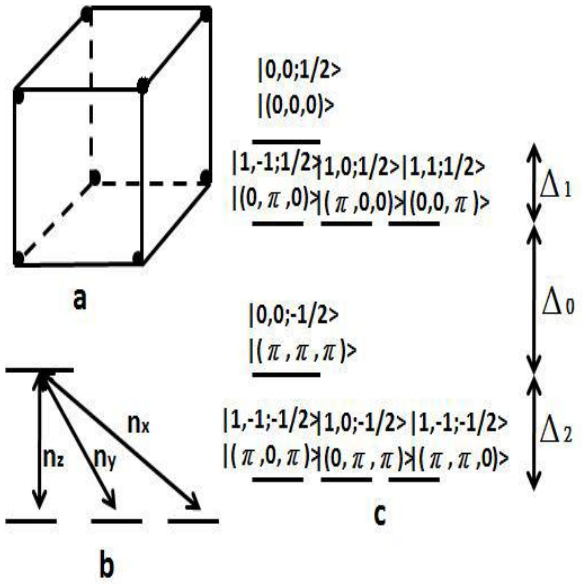

Figure 2.3: A sketch of the 8CM and its specturm.

axial ordering, such as the tetragonal-cubic, orthorhombic-tetragonal and rhombohedral-orthorhombic transitions. Take the tetragonal-cubic transition for example. Suppose the ordering occurs in z-direction. We then average out x- and y-components. This is attained by handling V_{Ti} as follows:

$$\begin{aligned} V_{Ti} \implies & \gamma u_z^4 - K u_z^2 + \langle \gamma(u_y^4 + u_x^4) - K(u_y^2 + u_x^2) \rangle + (2\gamma + \alpha)(u_z^2 \langle [u_x^2 + u_y^2] \rangle + \langle u_x^2 u_y^2 \rangle) \\ \implies & V_{DWA} = \gamma u_z^4 - \tilde{K} u_z^2, \quad \tilde{K} = K - (2\gamma + \alpha)\langle [u_x^2 + u_y^2] \rangle \approx K - \frac{2}{3}(2\gamma + \alpha) u_0^2 \end{aligned} \tag{2.68}$$

Here $\langle ... \rangle$ indicates thermal average, whose temperature dependence depends on which model is used. In BTO, a Ti ion has been experimentally demonstrated to be described by the 8CM, in which $u_{x,y}^2$ can be deemed essentially as constants. Thus, with this model, the averages are nearly temperaure independent. In this thesis, we shall adopt this picture. Note that V_{DWA} features two wells provided $\tilde{K} > 0$.

2.3.5 Pseudo-Spin Model: PSM

The PSM to DWA is as the 8CM to the H_{TiO_3}. Take V_{DWA} for instance. To motivate the (pseudo)spin, let's put $u_z = l_0\sigma$, where $l_0 = \sqrt{\frac{\tilde{K}}{2\gamma}}$. Thus, the potential becomes

$$V_{DWA} = \frac{\tilde{K}^2}{4\gamma}(\sigma^4 - 2\sigma^2) \tag{2.69}$$

which takes minimum at $\sigma^2 = 1$. Although σ is not fixed at $\sigma_z = \pm 1$, fluctuations should be small provided l_0 is large and the temperature is low. In this limit, one may replace σ with σ_z. We then interpret σ_z as the pseudospin. The σ is sometimes refered to as soft spin. At the same time, the kinetic energy is effected as a transverse field that flips a spin coherently, $\frac{P_z^2}{2M} \to E_T\sigma_x$. Here $\sigma_{z,x}$ are Pauli matrice and E_T is the spin flip energy.

2.3.6 Adiabatic Treatment

Considering that the O mass is a third of the Ti mass, i.e., $m/M \sim 0.3$, one may decouple their motions adiabatically. For bilinear interactions like V_{Ti-O}, such decoupling is quite simple. Take $\vec{u}_l$ as a slow variable and $\vec{U}_{l\rho}$ as the fast one. Consider an O_x for illustration. It couples to two Ti ions simultaneously. The impacts of V_{Ti-O} on its motions along x-axis can be dealt like this:

$$\begin{aligned} K_l U_{x|x}^2 &+ \beta_l U_{x|x}(u_{-|x} + u_{+|x}) = K_l \tilde{U}_{x|x}^2 - \frac{\beta_l^2}{4K_l}(u_{-|x} + u_{+|x})^2 \\ \tilde{U}_{x|x} &= U_{x|x} + \frac{\beta_l}{2K_l}(u_{-|x} + u_{+|x}) \end{aligned} \tag{2.70}$$

Now replacing $u_{\pm|x}$ with their averages, the O-subsystem and Ti-subsystem become distangled. Clearly, three effects can arise from V_{Ti-O} from this perspective: (1) the O ion is displaced by an amount of $d_l = \frac{\beta_l}{2K_l}\langle u_{+|x} + u_{-|x}\rangle$ and (2) a coupling between the two Ti ions has been produced, i.e., $-\frac{\beta_l^2}{2K_l}u_{-|x}u_{+|x}$, which always favors ferro-type coupling, and

(3) a self-energy comes about Ti ions, $-\frac{\beta_l^2}{4K_l}u_{\pm|x}^2$.

Applying the above technique to H_{TiO_3}, one ends up with two decoupled subsystems that are governed by the following Hamiltonians, respectively,

$$\begin{aligned} H_{Ti} &= Kin_{Ti} + \tilde{V}_{Ti} - \sum_{<l,l'>,\rho,\rho'} J^{\rho,\rho'} u_{l|\rho} u_{l'|\rho'} \\ H_O &\approx Kin_O + \tilde{K}_l U_{l\rho|\rho}^2 + K_t \sum_{\bar{\rho}} U_{l\rho|\bar{\rho}}^2 \end{aligned} \tag{2.71}$$

Here $J^{\rho,\rho'} = \bar{\delta}_{\rho,\rho'} J^{\rho}$, with $J^{\rho} = \frac{\beta_l^2}{2K_l} \equiv J_l$ if the line joining the l- and l'-th Ti ions lies along the ρ direction and $J^{\rho} = \frac{\beta_t^2}{2K_t} \equiv J_t$ if this line is perpendicular to that direction. The $\tilde{K}_l = K_l + \gamma_l \langle U_{\rho|\rho}^2 \rangle$ denotes the effective elastic constant that is defined via a self-consistent harmonic approximation to be expounded in the next subsection. The $\tilde{V}_{Ti}$ has taken into account the aforementioned self-energy. Conspicuously, H_{Ti} is no more than the conventional ϕ^4 model[104], which often serves to exemplify the basics of quantum field theory and quantum phase transitions[142, 106].

2.3.7 Self-Consistent Harmonic Treatment

Considerable difficulty rests with dealing with the anharmonic terms, such as the quartic terms in V_{Ti} and V_O. Concerned with how the vibration frequencies are affected by such anharmonic terms, one may employ the so-called self-consistent harmonic approximation (SCHA)[107, 10]. Often it is used in handling double-well potential, such as the V_{DWA} shown above. In this method, one goes as follows, taking V_{DWA} for example,

$$\gamma u_z^4 - \tilde{K} u_z^2 \Longrightarrow (\gamma \langle u_z^2 \rangle - \tilde{K}) u_z^2 \equiv \frac{1}{2} M \omega_{SCH}^2 u_z^2 \tag{2.72}$$

which defines the SCHA effective frequecy ω_{SCH} as

$$\omega_{SCH}^2 = \frac{2}{M}(\gamma\langle u_z^2\rangle - \tilde{K}) \tag{2.73}$$

The $\langle u_z^2\rangle$ is then expressed in terms of ω as follows,

$$\langle u_z^2\rangle = \frac{\hbar}{2M\omega_{SCH}} \coth \frac{\hbar\omega_{SCH}}{2k_BT} \tag{2.74}$$

These two equations make a closed set and can be solved numerically. At high temperature, the classical limit is recovered. By equipartition law, one has $\langle u_z^2\rangle \approx \frac{k_BT}{M\omega_{SCH}^2}$, which gives rise to

$$\frac{M\omega_{SCH}^2}{2} \approx \frac{\gamma k_BT}{M\omega_{SCH}^2} - \tilde{K} \tag{2.75}$$

Solve it to have

$$M\omega_{SCH}^2 = \sqrt{\tilde{K}^2 + 2\gamma k_BT} - \tilde{K}, \tag{2.76}$$

from which one infers (1) if $\tilde{K}$ is very small, then $\langle u_z^2\rangle \sim \sqrt{T}$ while (2) if $\tilde{K}$ is very large, then $\langle u_z^2\rangle \sim constant$. From an mean-field (MF) point of view, we can define a critical temperature T_c at which $\chi_0 J_0 = 1$, where $\chi_0 = (M\omega_{SCH}^2)^{-1}$ is the bare susceptibility and J_0 denotes the molecular field strength. Thus, case (1) results in $T_c \approx \frac{J_0^2}{2\gamma k_B}$ and (2) leads to $T_c \approx \frac{J_0\tilde{K}}{\gamma k_B}$. Especially, we notice that, the MF susceptibility $\chi^{-1} = \chi_0^{-1} - J_0 = M\omega_{SCH}^2 - J_0$ goes as $\sqrt{T} - \sqrt{T_c}$ in case (1) but as $T - T_c$ in case (2). Experimentally, it seems the latter case that was observed in both BTO and STO.

This high temperature behavior is expected to break down at low temperatures. In fact, at extremely low temperatures, the coth function approaches unity and the position fluctuation is no more than that of a simple oscillator over its ground state. Thus, the frequency

satifies the following equation,

$$\frac{M}{2}\omega_{SCH}^2 = \frac{\hbar\gamma}{2M\omega_{SCH}} - \tilde{K} \tag{2.77}$$

which always has a single positive solution inside $[0, \frac{\hbar\gamma}{2M\tilde{K}}]$. Its exact form looks cubersome and is not needed. We again look at two extreme cases. In (1) small $\tilde{K}$ case, the solution is located about $(\frac{\hbar\gamma}{M^2})^{1/3}$. On the other hand, in (2) large $\tilde{K}$ case, it is about $\frac{\hbar\gamma}{2\tilde{K}M}$. See that the parameter $\tilde{K}$ actually controls the potential well separation and depth. Now the $\langle u_z^2 \rangle$ goes as $\frac{1}{2}(\frac{\hbar^2}{M\gamma})^{1/3}$ in (1) but as $2l_0^2$ with $l_0 = \sqrt{\frac{\tilde{K}}{2\gamma}}$ in (2).

Here we deduce a poor man's criteria for ferroelectricity by comparing two temperature scales. Let's note that, the classical limit eq.2.76 suggests that, an instability is bound to happen at any non-vanishing J_0. However, as temperature goes down, departure from this limit gradually dominates and eventually the quantum limit eq.2.77 sets in. Suppose this crossover occurs at a temperature T^*. If the classical temperature T_c introduced above lies far below the T^*, the instability can eventually be stabilized by quantum effects. Therefore, the criteria is deciphered as $T_c > T^*$. A rough estimate of T^* can be obtained by considering an oscillator under increasing temperature. Thermal effects become discerbible only for temperatures higher than that corresponding to the gap between the oscillator ground state and the first excited state, which is $\hbar\omega_{SCH}$ with ω_{SCH} satifying eq.2.77. This provides an expression for T^*, i.e., $T^* = \frac{\hbar\omega_{SCH}}{k_B}$. Now, the criteria translates into the following inequalities,

$$\begin{aligned} (1) \quad &: \quad \frac{\hbar^4\gamma^4}{M^2} < \frac{J_0^6}{8}, \quad \text{for small } \tilde{K} \\ (2) \quad &: \quad \frac{\hbar^2}{2MJ_0} < 4l_0^4, \quad \text{for huge } \tilde{K} \end{aligned} \tag{2.78}$$

Let's note that this criteria actually summarizes the effects of quantum fluctuations on

ferroelectricity. For case (2), it might be conventient to work with $l_c^4 \equiv \frac{\hbar^2}{8MJ_0}$. Therefore, the condition becomes $l_0 > l_c$.

As useful as it is, the SCHA basically grabs only the coherent inter-well motions. Under certain circumstances, the intra-well motions can become prevailing and take up most time, while at the same time inter-well motions get incoherent. These features are missed in SCHA. To have some feel for the applicability of SCHA, we derive some simple rules. Let's at first presume well-defined intra-well states. Expand the potential about, let's say, $u_z = l_0$ and one finds to the second order in $\delta = u_z - l_0$ that $2\tilde{K}\delta^2 - \frac{\tilde{K}^2}{4\gamma}$. The motions of δ can then be approximated as that of an oscillator with frequency $\omega_{well} = \sqrt{\frac{4\tilde{K}}{M}}$. Self-consistency implied in the expansion requires $\langle\delta^2\rangle$ to be smaller than l_0^2. For very small M, a well cannot accommodate many states and quantum fluctuations dominate, and thus, $\langle\delta^2\rangle = \frac{\hbar}{2M\omega_{well}} = \frac{\hbar}{4\sqrt{\tilde{K}M}}$, which leads to $M > \frac{\hbar^2}{16\tilde{K}l_0^4}$. For huge M, many states can be admitted in a well, and thermal fluctuations are more relevant, giving rise to $\langle\delta^2\rangle = \frac{k_BT}{M\omega_{well}^2}$ and $T < \frac{4\tilde{K}l_0^2}{k_B}$. In the quantum case, for a well to accommodate at least one state, one should have $\frac{1}{2}\hbar\omega_{well} < \frac{\tilde{K}^2}{4\gamma}$. It follows that $M > \frac{4\hbar^2}{\tilde{K}l_0^4}$. From a quantum point of view, intra-well motions are reasonable only if at least two levels can be admitted within a well, namely, $\frac{3}{2}\hbar\omega_{well} < \frac{\tilde{K}^2}{4\gamma}$, or equivalently, $M > 36\frac{\hbar^2}{\tilde{K}l_0^4}$. Therefore, SCHA is likely to be valid for temperatures above $T_{SCHA} = \frac{4\tilde{K}l_0^2}{k_B}$ and particle mass smaller than $M_{SCHA} = 36\frac{\hbar^2}{\tilde{K}l_0^4}$.

2.4 Other Models

At this stage, it should be appropriate to give a brief overview of the models that have engrossed certain amount of attention in studying ferroelectrics. We shall cover a few of them below. They are chosen because of their intimacy with the model presented above.

2.4.1 Vanderbilt Model

Considering that the most relevant degrees of freedom to ferroelectricity should be the soft mode (transverse optical) and the strain (accoustic), Vanderbilt et al. developed an *ab-initio*-type computational scheme to comprehend the instability physics[18, 48]. Their model Hamiltonian E^{tot} is expressed in terms of a local variable $\vec{u}$, which is actually proportional to the dipole associated with a unit cell, and strain variables η (following their notation). The strain variables are split into their homogeneous part η_H and inhomogeneous one η_I. The E^{tot} encapsulates a self-energy term of the local mode E^{self}, a dipolar interaction term E^{dip} representing the electrostatic energy and a short-range interaction term E^{short} taking care of the short-range interaction between the local variables, in addition to an elastic energy term E^{elas} due to strains and an interaction between the local dipoles and the strains. In this model, E^{self} takes a form that coincides with that of V_{Ti} in H_{TiO_3} developed in the last section.

The Vanderbilt model has gained tremendous momentum in the past few years[108, 109], because of its power in studying ground state properties. Although only one optical mode plus the accoustic modes is included, the model is still too complicated for analytical study. Therefore, its efficiency is largely based on computers. All parameters are obtained based on density functional theory and then input in the model, which is further subjected to molecular dynamics simulations or Monte Carlo study to extract useful information. This model is basically the same as the one employed to explain NMR data regarding the Ti off-center shifts. Note that, the local variable essetially amounts to the Ti displacement: the local variable is a linear combination of the displacements of all the atoms in a unit cell, with the weight predominantly centered on the Ti atom. Most work based on this model focuses on ground state properties and static properties. Although qualitatively correct, the transition temperatures are often underestimated in comparison with observations. Obviously, since it captures only the lower frequency modes, it can not shed light on the

complete optical spectrum.

An essential difference between the Vanderbilt model and the model developed in this thesis is that, the former keeps only one optical mode in addition to all accoustic modes and their couplings, whereas the latter includes all optical modes and their interactions. That is why the latter can be used to study IR or Raman spectrum covering the entire frequency regime but the former fails to do so.

2.4.2 Migoni-Bussmann Model

Motivated by the extraordinary activity of O anions in crystal environment, Migoni et al. came up with a non-linear shell model that includes an intra-ionic coupling energy in the relative displacement between the O core and its shell[28, 94]. In particular, this coupling is tailored to be anisotropic: it is quartic along the O-Ti chain but quadratic in the O-A plane. Such anharmonicity is anticipated to cause phonon softening and nano-cluster (self-induced intrinsic inhomogeneity) relaxation phenonema[68, 112], as already exhibited in early work[67, 110, 111]. Simplified and modified versions have appeared subsequent to the orginal proposal, among which the most often used in recent years assumes that the physics can be captured by a one-dimensional toy system[29]. This toy system is comprised of a chain of $TiO_3 - A$ units. The TiO_3 is treated as a core-shell object while the A is simply a rigid ion. A harmonic nearest neighbor interaction between the A and the TiO_3 shell is assumed, in addition to a double-well-type anharmonic coupling between the core and the shell within the same TiO_3. No other but the nearest neighbor core-core interactions are imposed. Explicitly, the energy reads (in their notations)

$$\begin{aligned} \frac{1}{2}\sum_n [M_1 \dot{u}_{1n}^2 &+ m_2 \dot{u}_{2n}^2 + f'(u_{1n+1} - u_{1n})^2 + f(v_{1n} - u_{2n})^2 \\ &+ f(v_{1n+1} - u_{2n})^2 + g_2 w_{1n}^2 + \frac{1}{2} g_4 w_{1n}^4] \end{aligned} \tag{2.79}$$

where M_1 and m_2 denote the mass of the TiO_3 core and that of the A ion, respectively, while the $w = v_{1n} - u_{1u}$ is the relative displacement between the core and the shell. The shell is taken massless. The values of the introduced parameters are listed in TABLE2.1. Note that, $g_4 > 0$ and $g_2 < 0$, resulting in an effective on-site double-well potential for the core.

Table 2.1: Parameters for the Migoni-Bussmann model. Units: f, f', g_2: $10^4 g s^{-2}$; g_4: $10^{22} erg$; m_1, m_2: $10^{-22} g$.

Compounds	f	f'	g_2	g_4	m_1	m_2
STO16	14.41	1.27	-1.41	1.57	1.55	1.46
STO18	14.41	1.27	-1.41	1.57	2.17	1.46
KTaO3	4.07	0.58	-0.49	0.51	2.88	0.65

This model has been applied to a number of problems and produced many interesting results[113, 114, 115, 116, 117, 118, 119], which may be surprising at first glance since it does not explicitly specify the character of the Ti ions at all. It is widely believed that, such character holds the key to ferroelectricity in perovskites. This puzzle may be resolved by observing that, this model has actually similar mathematical structure to that of the Vanderbilt model, which partly explains its success. Both contain two types of variables coupled to each other, with one of which subjected to certain multi-well potential. They differ in physical interpretations. In the Vanderbilt model, the anharmonicity is due to Ti ions while in the Migoni-Bussmann model it is supposed to stem from O ions. The strains in the former play the part of the A-sublattice variables in the latter. The former model has very clear atomistic basis, while the latter is elusive, especially in its modified versions, where the Ti and O have been lumped together. Despite all these, the Migoni-Bussmann model can hardly explain the isotope exchange effect observed in STO system.

It should be noted that, the latest version of this model as sketched in eq.2.79 is similar to H_{TiO_3} in mathematical structure. In both models, multi-well potentials appear with certain constituents (anharmonicity centers), which are coupled then to other phonon-type

variables. However, they differ greatly in physical interpretations.

2.4.3 Girshbirg-Yacoby Model

This is a typical spin-phonon model, in which a spin component and a phonon component are taken into account. Although it was instigated by Kobayashi[32, 120], its applications to perovskites were only considered in the work of Girshberg et al.[33, 34, 88, 36, 83]. The basic impetus behind their work is to account for the apparent coexistence of the so-called displacive and order-disorder phenomena. By 'displacive', what is usually meant is the observation of a mode whose frequency disperses to zero as the system approaches transitions. By 'order-disorder', one may have in mind either a robust multi-well potential surface or a relaxation displaying critical slowing down (i.e., relaxation time tending to infinity). Therefore, in their model, two types of degrees of freedom have been included, namely, a soft phonon assumed to carry the displacive part and a pseudospin to take the order-disorder part. The Hamiltonian in their notations then reads,

$$\begin{aligned} : \quad & \sum_{\vec{p}} \Upsilon(\vec{p}) \sigma^z_{\vec{p}} \sigma^z_{-\vec{p}} + \sum_i \Omega_0 \sigma^x_i + \sum_{\vec{q}} \omega(\vec{q}) b^\dagger_{\vec{q}} b_{\vec{q}} \\ + \quad & \frac{1}{\sqrt{N}} \sum_{\vec{k}} \frac{f(\vec{k})}{\omega_0(\vec{k})} \sqrt{\frac{\omega_0(\vec{k})}{2}} (b_{\vec{k}} + b^\dagger_{-\vec{k}}) \sigma^z_{-\vec{k}} \end{aligned} \tag{2.80}$$

where σ denotes the Pauli matrice to describe the pseudospin, while $b^\dagger_{\vec{q}}$ ($b_{\vec{q}}$) generates (annihilates) a phonon with energy $\omega(\vec{q})$. The zone center phonon is supposed to be the soft phonon, whose frequency depends on temperature in a Barrett form. According to these authors, $\omega(\vec{q})$ and $\omega_0(\vec{q})$ correspond to the renormalized and bare frequencies, respectively. Further, Ω_0 is assumed to be the spin flip frequency. Obviosuly, they have assumed that, the pseudospin encapsulates the Ti motions.

They have also attempted to construct a miscroscopic theory to interpret the origin of

the psedugospin and the soft phonon[34, 88]. Their scenario is morally based on vibronic (i.e., electron-phonon) interactions. They included both transverse and longitudinal optical phonons, which are then supposed to be strongly coupled to electrons. Coupling to the former was held by them to produce interband (valence-conduction) electronic transitions that would soften the transverse phonons, whereas coupling to the latter was assumed to cause intraband transitions that would lead to small polaron formation and new equilibrium positions for the ions. Such a picture has several loopholes. Firstly, it contradicts the idea that the Ti off-center shift should be due to inter-band transitions. Secondly, the off-center shift predicted by them has a clear temperature dependence, which however has not been observed. Perhaps, a more urgent question is, what is the nature of the soft phonon in their model?

A striking similarity between this model and the H_{8CM} can be noticed. A Ti ion is taken as a spin in both the H_{8CM} and the Girshberg-Yacoby model, but it is coupled to unidentified phonons in the latter whereas O vibrations in the former. In comparison with H_{TiO_3}, both have ignored that, a Ti ion should in reality be a soft spin, instead of a regid one.

2.5 Summary

We have discussed meticulously the eight-well potential model as encapsulated in eq. (2.59). The discussions were largely based on microscopic considerations. It is essential to have experimenal evidences for the necessity of this model. As we will argue in the coming two chapters, there are indeed many circumstances where this model provides the crucial link in comprehending the observations. In such cases, the double-well potential model turns out to be insufficient. Surely, there are cases where the latter model captures the physics. It should be noted that, both the anisotropic rotor model and eight corner model are no more than representatives of the eight-well potential model: they share the

eight-well structure. The former two are easier to handle mathematically.

Chapter 3

APPLICATIONS TO BTO

In this chapter, we discuss the dielectric properties of BTO in light of the model we set up in the last chapter. We shall at first perform very general discussions on the relation between ferroelectricity and the topograph of V_{Ti}. Then we go on to clarify the identity of each observed transverse optic mode and show how such assignment could agree with experiments, followed by considering several specific issues such as axial dispersions and spectral weight transfer phenomena.

3.1 Preliminary Remarks

We begin with the equations of motions, which formally read

$$\begin{aligned} \dot{P}_\rho(\vec{q}) &- F_\rho(\vec{q}) = -\frac{\partial[V_{Ti} + V_{Ti-O} + V_{ext}]}{\partial u_\rho(-\vec{q})}, \quad \dot{u}_\rho(\vec{q}) = \frac{P_\rho(\vec{q})}{M} \\ \dot{p}_{\rho|\rho'}(\vec{q}) &- F_{\rho|\rho'}(\vec{q}) = -\frac{\partial[V_O + V_{Ti-O} + V_{ext}]}{\partial U_{\rho|\rho'}(-\vec{q})}, \quad \dot{U}_{\rho|\rho'}(\vec{q}) = \frac{p_{\rho|\rho'}(\vec{q})}{m} \end{aligned} \tag{3.1}$$

Here the V_{ext} signifies the coupling between the dipole

$$\vec{d_l} = z_{Ti}\vec{u}_l + (z_l U_{lx|x} + z_t[U_{ly|x} + U_{lz|x}], z_l U_{ly|y} + z_t[U_{lx|y} + U_{lz|y}], z_l U_{lz|z} + z_t[U_{lx|z} + U_{ly|z}]) \tag{3.2}$$

and an external electric field formed as $\vec{E}_l = \vec{E}_0 \cos(\vec{q}\vec{R}_l)$, namely, $V_{ext} = -\sum_l \vec{d}_l \cdot \vec{E}_l = -[\vec{d}(\vec{q}) + \vec{d}(-\vec{q})] \cdot \vec{E}_0$. The uniform susceptibility function then obtains for $\vec{q} \sim 0$, $\chi_{\rho,\rho'}(\omega) = \frac{\partial d_\rho(\omega)}{a_0^3 \partial E_{\rho'}(\omega)}$, where $\vec{d}(\omega)$ and $\vec{E}(\omega)$ are the Fourier tansforms of $\vec{d}(t)$ and $\vec{E}(t)$, respectively. We write $\chi_{zz} = \chi_c$ and $\chi_{xx} = \chi_a$ for convenience. In addition, the F-forces are included due to environment, which each can be split into a friction and a noise, as to be specified where appropriate. Although the equations are written in classical forms, they should be understood also as for the quantum mechanical case with proper interpretations of the symbols.

As seen in the expression of H_{TiO_3} eq. (2.59), the quartic terms give rise to scatterring between phonons with different momenta, and therefore, in general $\vec{q}$ is not a good quantum number and cannot be conserved. Throughout the thesis, we are mostly considering how a compound responds to an external electric field that is either static or carried by long wavelength electromagnetic waves. It is desirable to have an effective theory that involves explicitly only the long wavelength phonons. To this end, approximations are in need. As the first approxiamtion, we may assume as in section **2.3.5** that the quartic term in V_O can be either simply dropped or dealt with using SCHA, so that V_O becomes harmonic in effect. This approximation may be justified: (1) experimetally, the modes assigned to O vibrations display little temperature dependence (see chapter 1 and the next section); (2) the O mass is likely to be smaller than M_{SCHA}, rendering the use of SCHA. In the second approximation one may introduce a self energy to handle the quartic terms in V_{Ti}. This consists of a single substituion,

$$\begin{aligned} : \quad & \frac{\partial}{\partial u_\rho(-\vec{q})} \sum \upsilon_{\rho\rho'} u_\rho(1) u_\rho(2) u_{\rho'}(3) u_{\rho'}(4) \bar{\delta}(1+2+3+4) \\ \Longrightarrow \quad & \sum_{\rho\rho'} \int_{-\infty}^{t} \Sigma_{\rho\rho'}(\vec{q}; t-t') u_{\rho'}(\vec{q}, t') \, dt' \end{aligned} \tag{3.3}$$

where $\Sigma_{\rho\rho'}(\vec{q}; t-t')$ stands for the self energy term, which can be calculated only approxi-

mately through e.g. diagramatic methods. It is often to neglect the frequency dependence of such term, i.e., $\Sigma_{\rho\rho'}(\vec{q};t-t') \approx \Sigma_{\rho\rho'}(\vec{q})\bar{\delta}(t-t')$. Also, it is thought that $\Sigma_{\rho\rho'} = \Sigma_{\rho'\rho}$. With the above substitution, decoupling between different $\vec{q}$ modes have been achieved. However, the above self-energy treatment can not be valid if the quartic terms are extremely anharmonic, which is the case with BTO. Despite this, this treatment shall prove useful in dealing with certain aspect of such potential, as to be described below. Considering BTO is a prototypical ferroelectric, we shall postulate, in accord with observations as carefully discussed in section **1.6**, that $K > 0$ and $\tilde{K}_l > 0$ as well as $K_t > 0$, all with negligible temperature dependence in most cases. In addition, $\gamma > 0$ while $\alpha < 0$, with $\alpha + 3\gamma > 0$ necessary for lattice stability. These inequalities allow us to have 8CM as a starting point for discussions. Nevertheless, the 8CM has a defect: only inter-corner motions are counted on.

There are circumstances where the intra-corner motions hold the key. To take into account both types of motions, one may from the outset represent them separately by writing the Ti displacement vector as $\vec{u} = l\vec{S} + \vec{D}$. Here $\vec{S} = (\pm 1, \pm 1, \pm 1)$ give the positions of the eight corners and can be deemed as spin-type variables, and $\vec{D}$ stands for the deviation from a corner by definition. Obviously, the values of $\vec{D}$ must be consrained so that the physical space remains the same as in the original representation. This constraint can be automatically satisfied if the deviations are assumed small in comparison with l, as is often the case with the low energy sector of a system's phase space. Noting the symmetry between the values of $\vec{S}$, it might be convenient to write $\vec{D} = (S_x Y_x, S_y Y_y, S_z Y_z)$. In terms of this $\vec{Y}$, one may expand up to quadratic terms the V_{Ti} as

$$a\vec{Y}^2 + b[Y_x Y_y + Y_y Y_z + Y_z Y_x], \quad a = M\omega_{cor}^2 = \frac{2\gamma - \alpha}{3\gamma + \alpha}K, \quad b = \frac{4\gamma + 2\alpha}{3\gamma + \alpha}K \tag{3.4}$$

Consider a Ti ion moving in this potential. The eigen-frequencies can be obtained by

solving the following secular equation

$$\begin{vmatrix} M(\omega^2-\omega_{cor}^2) & -b & -b \\ -b & M(\omega^2-\omega_{cor}^2) & -b \\ -b & -b & M(\omega^2-\omega_{cor}^2) \end{vmatrix} = 0 \tag{3.5}$$

which gives

$$M^3(\omega^2-\omega_{cor}^2)^3 = 2b^3 + 3b^2M(\omega^2-\omega_{cor}^2) \tag{3.6}$$

Three solutions are expected to exist, since the matrix is hermitian. These solutions are close to one another as long as b is not large in comparison with a, as is the case with BTO (see next subsection). Basically this is because γ and α have opposite signs but nearly equal in magnitude. Therefore, the intra-corner motions as described by $\vec{Y}$ can be regarded as simple harmonic. As for the inter-corner motions, the 8CM can be employed. Unsurprisingly, couplings between these two types of motions are bound to be induced by those anharmonic terms not included in the above expansion in $\vec{Y}$.

According to the arguments presented above, the degrees of freedom of the system can be taken to be $\vec{S}$ and $\vec{Y}$ in addition to those $\vec{U}$ of the O ions. As we discussed, both $\vec{Y}$ and $\vec{U}$ describe harmonic oscillators, which involve three different frequencies ω_{cor}, $\omega_l \equiv \sqrt{\frac{2\tilde{K}_l}{m}}$ and $\omega_t \equiv \sqrt{\frac{2K_t}{m}}$. On the other hand, the properties of $\vec{S}$ are not that clear. Actually, the $\vec{S}$ and the $\vec{Y}$ are intimately correlated, as anticipated from the fact that they were created from the same origin. An important consequence is that, their spectral intensities put together have to be nearly conserved and hence, when the $\vec{S}$ roars in the spectrum, the $\vec{Y}$ has to decline, and vice versa. Such phenomena are obviously in parallel with the discussions on double-well potential, where the inter- and intra-well motions compete in intensity. Analogous reasoning (section **2.3.6**) applies here: as the fluctuations in $\vec{Y}$ increase, more spectral intensity will be inhabited by $\vec{S}$. We shall present quantitative

discussions later on.

This preliminary analysis prescribed above is intended to guide us in identifying the character of the observed dielectric modes in BTO.

3.2 Length Scales: A Poor Man's Criteria For Ferroelectricity

The 8CM refers to a cube in describing the effective Ti states. This cube has an edge length of $2l = 2\sqrt{\frac{K}{2(\alpha+3\gamma)}}$. In chapter 2, we have already seen how a SCHA treatment of a double-well model could lead to a criteria for ferroelectric instability. There two important length scales were introduced, l_0 and l_c. What is peculiar about these scales is that, l_0 gives pure information about the landscape of the potential surface and has nothing to do with the ion that moves in this potential while the l_c characterizes sheerly this ion and has nothing to do with the potenial. The derived criteria consists of a simple inequality, $l_0 > l_c$, which looks very beautiful. We may establish an approximate relationship between l_0 and l like this: see that $l_0 = \sqrt{\frac{\tilde{K}}{2\gamma}}$ and $\tilde{K} \leq K - 2(2\gamma + \alpha)l^2$ according to eq.(2.68), where we have used that $u_0^2 \geq 3l^2$ by 8CM. Hence, one gets $l_0 \geq l$, which shows that l sets a lower bound for l_0. The quantity of $l_0 - l$ is small if $\tilde{K}$ is large but big otherwise.

According to eq.(2.78), l_c is related to the molecular field strength J_0 as $l_c = \frac{\hbar^2}{2MJ_0}$. In the large $\tilde{K}$ limit, as supposed here, one can follow the route designed in section **2.3.4** to reduce the double-well model to a PSM of Ising type. Applying MF theory to the PSM, one can relate the J_0 to the transition temperature T_c as $J_0 l_0^2 = k_B T_c$. The condition that $l_0 > l_c$ then becomes

$$\frac{\hbar^2}{8MJ_0} = \frac{\hbar^2}{8Mk_BT_c l_0^{-2}} < l_0^4, \quad \text{or equivalently,} \quad l_0^2 > \tilde{l}_c^2 \equiv \frac{\hbar^2}{8Mk_BT_c} \tag{3.7}$$

Using experimental values of T_c, $\tilde{l}_c$ can thus be evaluated. They are listed in TABLE.3.1 for various ferroelectrics. Unfortunately, I have not come up with a reliable way of estimating l_0 and l. Note that, the l_c for STO18 seems fairly large, indicating that l_0 has to be as great as $\sim 7pm$. This may not contradict the observation that l might be less than $5pm$, for the reason that $l_0 \geq l$ and that the $\tilde{K}$ may not be so large as required for the use of the inequality $l_0 > l_c$.

Table 3.1: Estimated $\tilde{l}_c$ for various compounds.

Compounds	BTO	STO18	KNbO3	NaNbO3
T_c	405K	24K	708K	73K
$\tilde{l}_c$	1.57pm	6.32pm	0.85pm	2.66pm

3.3 Character of The Dielectric Modes

3.3.1 Qualitative Discussions

We at first talk about the modes situated about $170cm^{-1}$ and $510cm^{-1}$. These modes were given different names in the cubic phase and the tetragonal phase. In particular, they are called TO_2 and TO_4 in cubic phase with dielectric function ϵ, but f_2 and f_4 in tetragonal phase with ϵ_a while LM and AM also in tetragonal phase yet with ϵ_c. The characteristics such as temperature dependences of line width and positions have been carefully discussed in chapter 1. We give a brief summary here: they are

- observed in all phases (ϵ, ϵ_a and ϵ_c) with their characteristics essentially unchanged;
- likely of resonance type in the sense that they are sharp and underdamped, with very small damping rate;
- essentially temperature independent;

- not only found in BTO, but also in STO and with basically the same characteristics;
- about 4% downward shifted on average if O^{16} is exchanged for O^{18}.

All these features point to insignificant anharmonicity associated with these modes. In our model as explained at the beginning of this chapter, the only modes that are comparable to these modes are those connected with O vibrations, which have frequencies of ω_l and ω_t, respectively. As shown in chapter 2, $\omega_l < \omega_t$ due to covalent bonding effects. Therefore, we assert that the $170cm^{-1}$ mode should be primarily attached to the O vibrations along the Ti-O-Ti direction while the $510cm^{-1}$ one to perpendicular O vibrations.

We proceed to other modes, which have contrasting properties in comparison with the O modes assigned above. Consider in the first place ϵ_c in the tetragonal phase. As discussed in chapter 1, ϵ_c displays two strongly correlated modes, apart from those O modes. They have been denoted by DM and SM, respectively. Their most pertaining features are summarized below:

- Both were seen very sensitive to temperatures;
- DM was firmly established as a relaxation mode;
- SM was found likely to be a resonance mode;
- Complete spectral intensity transfer has been found between them: as the tetragonal-cubic transition is approached, all the intensity of SM has been found quickly transfered to the DM; when the transition point is receding, however, the SM has been found absorbing most intensity while the DM is nearly not discernible.

The last point crucially shows that, according to the model presented in the last chapter, both DM and SM should originate from the Ti motions. They are expected to correspond basically to the inter- and intra-corner motions, respectively. The anharmonicity with Ti motions is compatible with the first point. Actually, computer simulations[60]

also vindicate this assignment: the relaxation rate of DM was shown to be of the same magnitude of the rate associated with local dipole reorientation between previlaged and disfavored (due to molecular field built in the ordered phase) directions.

Let's see how the proposed scenario interprets the modes perceived in ϵ and ϵ_a. Consider ϵ_a at first, which quantifies the response to an external electric field applied along a-axis (In the tetragonal phase, the spontaneous polarization $\vec{P}_s$ is supposed to be along the c-direction, i.e., z-direction). It probes the $U_{x,y,z|x}$ and $u_x = lS_x + D_x$. Note that, in tetragonal phase, $\langle u_x \rangle = 0$. Within 8CM, this indicates that the previlaged corners (those with $S_z = 1$) are equally populated regardless of S_x: no ordering in S_x. Henceforth, differing from the case with ϵ_c, in which S_z contributes little (except near T_c) while Y_z overwhelms, the case with ϵ_a has S_x at work while Y_x suppressed, for reasons similar to those stated in discussing DWA and SCHA. We thus expect three peaks, among which two should stem from O vibrations and are hence located around $170cm^{-1}$ (f_2) and $510cm^{-1}$ (f_4) while the third (f_1) comes from thermal Ti motions among the four previlaged corners ($\vec{S} = (\pm, \pm, 1)$). In this picture, f_1 roughly meaures how fast a Ti ion hops among the corners. The hopping rate obviously depends on temperature (e.g., Arrhenius' law). As temperature goes up, f_1 is expected to increase, in consistency with observations[58]. In fact, Burns et al. observed that f_1 increases from about $35cm^{-1}$ at room temperature to about $60cm^{-1}$ near $T_c = 405K$.

Now we divert to ϵ in the cubic phase. Obviously, the O vibrations should still manifest themselves as two peaks about$170cm^{-1}$ (TO_2) and $510cm^{-1}$ (TO_4), respectively. As regards the Ti motions in this phase, one has to see that there is no previlaged corner in the 8CM. In other words, intra-corner motions are again suppressed (vanishing spectral weight) and only inter-corner motions can be detected. Imagine applying an electric field in the z-direction. As in ϵ_a, the inter-corner hopping rate along z-axis, or say, the rate of fliping S_z between 1 and -1 should depend on temperature in a similar way. Especially,

as the phase transition gets closer, this rate is expected to decrease, a phenomenon known as critical slowing down. Just at the transition, the flip period diverges and the rate becomes zero. Such slowing down will show up in hyper-Raman scattering as a central peak. Up till now, we have spoken of three peaks in ϵ. Surprisingly, there is an additional peak, which could exist if robust nano-polar clusters were formed in the phase. Suppose one-dimensional clusters, i.e., chains, can form in the cubic phase. Within each chain, the Ti ions are each assumed to occupy preferentially four of the respective eight corners just as in tetragonal phase, and the previleged fours for each ion are the same with respect to the corresponding cube. In other words, each chain is ordered within itself, but no ordering between chains. Such ordering must be stable, i.e., the chain size should not be sensitive to temperatures. Since these chains are randomly oriented, there must be chains lying perpendicular to c-axis. For such chains, the applied electric field probes actually the f_1 mode that is usually associated with ϵ_a. If such chains really exist, f_1 should exist around $60cm^{-1}$ at the critical point, where the S_z hopping rate vanishes. Indeed, the as-prescribed scenario is compatible with experiments, as discussed in chapter 1.

In summary, we have explicated all the observed modes in terms of the model presented in chapter 2. The explanation has employed two assumptions: (1) there is complete spectral weight transfer between inter- and intra-corner motions and (2) chain formation. Point (1) finds support from various existing simulations, while point (2) seems lacking sufficient discussions in the literature. We'll turn to them later. It is appropriate to stress that, *no other models have been capable of giving a picture as complete as the one presented above.*

3.3.2 ϵ_c: The Dielectric Constant Along Polar Axis

We here discuss quantitatively ϵ_c, which characterizes the response of the polarization in z-direction to an external electric field in the same direction. Since the tetragonal phase is involved, we may focus on the dynamics along c-direction and forget about other

directions. Therefore, we employ the DWA to do the work. Now the Hamiltonian relevant to this case can be cast as

$$\begin{aligned} H_c &= \frac{P_j^2}{2M} + \gamma Z_j^4 - \tilde{K} Z_j^2 + \frac{p_{j|\rho}^2}{2m} + \frac{1}{2} m\omega_l^2 Z_{jz}^2 + \frac{1}{2} m\omega_t^2 (Z_{jx}^2 + Z_{jy}^2) \\ &+ Z_j\{\beta_l(Z_{jz} + Z_{j-z}) + \beta_t(Z_{jx} + Z_{j-x} + Z_{jy} + Z_{j-y})\} \end{aligned} \tag{3.8}$$

where we have written $Z_j = u_{j|z}$ and $Z_{j\rho} = U_{j\rho|z}$ and the P as well as p refer to the z-components. Summation over j is implicit.

The double-well potential on Ti ions can be dealt with following the afore-prescribed recipe: if intra-well motions take up a negligible amount of intensity, then SCHA can be invoked; other wise, one has to consider this type of motions in addition to the inter-well motions. It is the latter case that is present with ϵ_c, as affirmed before. Thus, we put $Z_j = l_0\sigma_j + D_j$, with σ_j incurring the inter-well dynamics and D_j the intra-well part. Differing from the rigid spin variable $\vec{S}$ used in preceding discussions, the σ introduced here is free from the restriction that $\sigma^2 = 1$. Rather, it is allowed to fluctuate, which equals to displacing the intra-well oscillator a bit. The required slightedness can be ensured in the large l_0 limit, which is realistic for BTO.

In terms of these variables, the double-well potential becomes

$$\begin{aligned} &: \frac{\tilde{K}^2}{4\gamma}(\sigma_j^4 - 2\sigma_j^2) + D_j^2\tilde{K}(3\sigma_j^2 - 1) + 2D_j\sigma_j\tilde{K}l_0(\sigma_j^2 - 1) \\ &+ \text{higher order terms in } D_j \text{ to be ignored} \end{aligned} \tag{3.9}$$

Evidently, the first term just works to prevent σ_j from large fluctuations. Such fluctuations disappear in the limit $\tilde{K}^2/\gamma \to \infty$. The following two terms represent couplings between σ_j and D_j. Now that the fluctuations are small in σ^2, we may safely replace in these two terms the σ^2 by its thermodynamic average $\langle\sigma_j^2\rangle = \bar{\sigma}^2$, as done in Hartree

approximation in electronic theory. In the large l_0 limit, no coherent hopping between $\sigma_j = 1$ and $\sigma_j = -1$ exists. Therefore, the inter-well dynamics are utterly incoherent. On the other hand, the intra-well motions are that of a simple harmonic oscillator with frequency $\omega_{well} = \sqrt{\frac{2\tilde{K}(3\bar{\sigma}^2-1)}{M}}$.

At the same time, the original Ti-O interaction terms give rise to couplings between σ_j and $Z_{j\rho}$, which reads

$$l_0\sigma_j\{\beta_l(Z_{jz} + Z_{j-z}) + \beta_t(Z_{jx} + Z_{j-x} + Z_{jy} + Z_{j-y})\} \tag{3.10}$$

and between D_j and $Z_{j\rho}$, which reads

$$D_j\{\beta_l(Z_{jz} + Z_{j-z}) + \beta_t(Z_{jx} + Z_{j-x} + Z_{jy} + Z_{j-y})\} \tag{3.11}$$

In obtaining the equations of motions, one has to treat σ_j separately from variables D_j and $Z_{j\rho}$, because the former has no inherent dynamics and performs only incoherent motions due to environment while the latter perform largely coherent motions that are governed by their own properties through dynamical laws. According to these laws, we have

$$\begin{aligned}
M\ddot{D}_j &= -M\omega_{well}^2 D_j - \{\beta_l(Z_{jz} + Z_{j-z}) + \beta_t(Z_{jx} + Z_{j-x} + Z_{jy} + Z_{j-y})\} \\
&- 2\tilde{K}l_0(\bar{\sigma}^2 - 1)\sigma_j + z_{Ti}E_j - M\Gamma_{well}\dot{D}_j \qquad (3.12)\\
m\ddot{Z}_{jx} &= -m\omega_t^2 Z_{jx} - \beta_t\{l_0(\sigma_j + \sigma_{j+_x}) + D_j + D_{j+_x}\} + z_t E_j - m\Gamma_t\dot{Z}_{jx} \\
m\ddot{Z}_{jy} &= -m\omega_t^2 Z_{jy} - \beta_t\{l_0(\sigma_j + \sigma_{j+_y}) + D_j + D_{j+_y}\} + z_t E_j - m\Gamma_t\dot{Z}_{jy} \\
m\ddot{Z}_{jz} &= -m\omega_l^2 Z_{jz} - \beta_l\{l_0(\sigma_j + \sigma_{j+_z}) + D_j + D_{j+_z}\} + z_l E_j - m\Gamma_l\dot{Z}_{jz}
\end{aligned}$$

where we have included the external electric field E_j and friction terms $\Gamma_{well,l,t}$ to account for line broadening and damping.

To establish the time dependence of σ_j, there have appeared a few ways. In one way,

the dynamics of σ_j are described as stochastic process and master equations were used. This can be exemplified in Glauber method, which is more suitable for discrete-valued variables, but σ_j is contiuous. In another way, σ_j is construed as the cooridnate of certain virtual particle with vanishing mass interacting with a subsystem of harmonic oscillators that simulate the heat bath, so that the normal dynamical laws can be directly used; the physical results are then obtained by letting the mass vanish. This method is microscopic but cumbersome. We here employ a method based on Langevin descriptions that was developed for massive Brownian particles and glassy dynamics[121, 122, 123]. In this method, the heat bath is dealt with in a phenomenological way and assumed mainly to bear two effects: producing noisy forces and causing dissipation. Thus, equations of motion for σ_j are given as

$$M_\sigma l_0 \ddot{\sigma}_j = -\frac{\partial H_c}{\partial l_0 \sigma_j} - M_\sigma \Gamma_\sigma l_0 \dot{\sigma}_j + \eta_j(t) + z_\sigma l_0 E_j \tag{3.13}$$

where M_σ denotes the virtual mass to vanish later, $z_\sigma l_0$ the effective charge associated with inter-well motions (see that z_σ does not have the dimension of charge but $z_\sigma l_0$ does) and $\eta_j(t)$ a random Gaussion force satisfying the following statistical properties by virtue of Einstein relation,

$$\langle \eta_j(t) \rangle = 0, \quad \langle \eta_j(t) \eta_i(t') \rangle = 2 k_B T M_\sigma \Gamma_\sigma \bar{\delta}_{ij} \bar{\delta}(t - t') \tag{3.14}$$

Now dividing both sides of eq.3.13 by $(l_0 \beta)^{-1} = k_B T / l_0$, we find

$$M_\sigma l_0^2 \beta \ddot{\sigma}_j = -\frac{\partial H_{eff}}{\partial \sigma_j} - M_\sigma \Gamma_\sigma \beta l_0^2 \dot{\sigma}_j + \tilde{\eta}_j(t) + z_\sigma \beta l_0^2 E_j \tag{3.15}$$

where $H_{eff} = \beta H_c$, and the $\tilde{\eta}$ satisfies

$$\langle \tilde{\eta}_j(t) \rangle = 0, \quad \langle \tilde{\eta}_j(t) \tilde{\eta}_i(t') \rangle = 2\beta l_0^2 M_\sigma \Gamma_\sigma \bar{\delta}_{ij} \bar{\delta}(t - t') \tag{3.16}$$

Keep $\tau = \beta l_0^2 M_\sigma \Gamma_\sigma$ finite but let M_σ vanish to yield

$$\tau \dot{\sigma}_j = -\frac{\partial H_{eff}}{\partial \sigma_j} + \tilde{\eta}_j(t) + \tilde{z} E_j, \quad \tilde{z} = z_\sigma \beta l_0^2 \tag{3.17}$$

which provides the basis for discussing the σ dynamics. Explicitly, we have

$$\begin{aligned} \tau \dot{\sigma}_j &= r(\sigma_j - \sigma_j^3) - \beta \mu l_0 D_j + \tilde{\eta}_j(t) + \tilde{z} E_j \\ &- \beta l_0 \{ \beta_l (Z_{jz} + Z_{j-z}) + \beta_t (Z_{jx} + Z_{j-x} + Z_{jy} + Z_{j-y}) \} \end{aligned} \tag{3.18}$$

Here $r = \beta \bar{r} = \frac{\tilde{K}^2}{\gamma k_B T}$ and $\mu = 2\tilde{K}(\bar{\sigma}^2 - 1)$.

Now we conduct Fourier tranforms to turn the equations of motion established above into their frequency-momentum representation. Multiplying both sides of each equation by $\exp(i\{\vec{q}\vec{R}_j - \omega t\})$ and then integrating over the entire time domain as well as summing over all unit cells, we arrive at

$$\begin{pmatrix} G_D^{-1} & \mu l_0 & \beta_l C_z & \beta_t C_x & \beta_t C_y \\ \mu l_0 & G_\sigma^{-1} & l_0 \beta_l C_z & l_0 \beta_t C_x & l_0 \beta_t C_y \\ \beta_l C_z & \beta_l l_0 C_z & G_l^{-1} & 0 & 0 \\ \beta_t C_x & \beta_t l_0 C_x & 0 & G_x^{-1} & 0 \\ \beta_t C_y & \beta_t l_0 C_y & 0 & 0 & G_y^{-1} \end{pmatrix} \begin{pmatrix} D(\vec{q}, \omega) \\ \sigma(\vec{q}, \omega) \\ Z_z(\vec{q}, \omega) \\ Z_x(\vec{q}, \omega) \\ Z_y(\vec{q}, \omega) \end{pmatrix} = \begin{pmatrix} z_{Ti} E(\vec{q}, \omega) \\ z_\sigma l_0^2 E(\vec{q}, \omega) + \beta^{-1} \tilde{\eta}(\vec{q}, \omega) \\ z_l E(\vec{q}, \omega) \\ z_t E(\vec{q}, \omega) \\ z_t E(\vec{q}, \omega) \end{pmatrix} \tag{3.19}$$

Note that, there is no entanglement between variables with different $\vec{q}$. In the above, we

have written $C_\rho = 2\cos\frac{q_\rho}{2}$ and

$$\begin{aligned} G_D^{-1} &= M(\omega_{well}^2 - \omega^2 - i\Gamma_D\omega), \quad G_l^{-1} = m(\omega_l^2 - \omega^2 - i\Gamma_l\omega), \quad G_{x,y}^{-1} = m(\omega_t^2 - \omega^2 - i\Gamma_t\omega) \\ G_\sigma^{-1} &= \beta^{-1}\{r[\Sigma(\vec{q},\omega) - 1] - i\omega\tau\}, \quad X(\vec{q},\omega) = \sqrt{\frac{1}{2\ N^3}}\sum_j \int_{-\infty}^{\infty} dt \exp(i\{\vec{q}\vec{R}_j - \omega t\})X_j(t), \\ &\text{with } X = \sigma, D, Z_{x,y,z}, E, \tilde{\eta} \end{aligned} \tag{3.20}$$

Note that in G_σ^{-1} we have introduced a self-energy term (see the first subsection for details), $\Sigma(\vec{q},\omega)$, which is supposed to solve the following equation:

$$\sum_j \int_{-\infty}^{\infty} \sigma_j^3(t) e^{i(\vec{q}\vec{R}_j - \omega t)} dt = \Sigma(\vec{q},\omega)\sigma(\vec{q},\omega) \tag{3.21}$$

Its frequecy dependence is often neglected, as to be done in what follows. Under such approximation, the form of G_σ belongs to a relaxation mode with effective relaxation rate $r(\Sigma_{\vec{q}} - 1)\tau^{-1}$. More clearly, we rewrite it as

$$G_\sigma = \frac{\beta}{r(\Sigma_{\vec{q}} - 1)} \cdot \frac{1}{1 - i\omega\frac{\tau}{r(\Sigma_{\vec{q}} - 1)}} \tag{3.22}$$

Since we are mainly interested in the small $\vec{q}$ repsonses, we then look at when $\vec{q} = 0$, in which case $C_\rho = 2$ regardless of ρ. Therefore, this case possesses a bigger symmetry. Because of this symmetry, we construct two combinations from $Z_x(\vec{q} = 0,\omega)$ and $Z_y(\vec{q} = 0,\omega)$, namely,

$$Z_t(\omega) = Z_x(\vec{q} = 0,\omega) + Z_{jy}(\vec{q} = 0,\omega), \quad \bar{Z}(\omega) = Z_x(\vec{q} = 0,\omega) - Z_y(\vec{q} = 0,\omega) \tag{3.23}$$

It can be easily shown that, the mode $\bar{Z}$ has no couplings to the external electric field $E(\omega) = E(\vec{q} = 0,\omega)$ and to all the rest variables such as $Z_l(\omega) = Z_z(\vec{q} = 0,\omega)$, $\sigma(\omega) = \sigma(\vec{q} = 0,\omega)$ and $D(\omega) = D(\vec{q} = 0,\omega)$ as well as $Z_t(\omega)$. Therefore, this mode can be simply

disregarded from now on, since it can be neither directly nor indirectly detected by E at all. The dynamic equation (3.19) can then be reduced to exclude this mode. One finds,

$$\begin{pmatrix} G_D^{-1} & \mu & 2\beta_l & 2\beta_t \\ \mu & G_\sigma^{-1} & 2\beta_l & 2\beta_t \\ 2\beta_l & 2\beta_l & G_l^{-1} & 0 \\ 2\beta_t & 2\beta_t & 0 & G_t^{-1} \end{pmatrix} \begin{pmatrix} D(\omega) \\ l_0\sigma(\omega) \\ Z_l(\omega) \\ Z_t(\omega) \end{pmatrix} = \begin{pmatrix} z_{well}E(\omega) \\ z_\sigma l_0 E(\omega) + (l_0\beta)^{-1}\tilde{\eta}(\omega) \\ z_l E(\omega) \\ z_t E(\omega) \end{pmatrix} \tag{3.24}$$

Here $G_t^{-1} = \frac{1}{2}G_x^{-1}$, G_σ^{-1} is obtained through multiplying the G_σ^{-1} in eq.3.19 by l_0^{-2}. We have chosen $z_{well} \neq z_\sigma l_0$. Hereafter, the 4×4 dynamical matrix, which captures all the information regarding dielectric responses, is to be called $\Xi(\omega) = \Xi'(\omega) + i\Xi''(\omega)$ containing a real part and an imaginary part. Now the dipole (z-component) is given as $d(\omega) = z_{well}\langle D(\omega)\rangle + z_\sigma l_0^2\langle\sigma(\omega)\rangle + z_l\langle Z_l(\omega)\rangle + z_t\langle Z_t(\omega)\rangle$, with $\langle ...\rangle$ indicating the average over the entire noise configuration space. After inverting eq.3.34 and averaging out the noise, the displacement column can be related to the charge colomn as

$$Z(\omega) = \Xi^{-1}(\omega)zE(\omega), \quad Z(\omega) = \langle \begin{pmatrix} D(\omega) \\ l_0\sigma(\omega) \\ Z_l(\omega) \\ Z_t(\omega) \end{pmatrix} \rangle, \quad z = \begin{pmatrix} z_{well} \\ z_\sigma l_0 \\ z_l \\ z_t \end{pmatrix} \tag{3.25}$$

Whence one has $d(\omega) = z'Z = z'\Xi^{-1}(\omega)zE(\omega)$, with the prime indicating the transpose. Eventually, the susceptibility is reached as

$$\chi_c(\omega) = \frac{1}{a_0^3}\frac{d(\omega)}{E(\omega)} = \frac{1}{a_0^3}z'\Xi^{-1}(\omega)z \tag{3.26}$$

From which the relative dielectric function is given as $\epsilon_c = \epsilon_\infty + \frac{\chi_c}{\epsilon_0}$, where ϵ_0 denotes the vacuum permittivity.

The explicit expression of Ξ^{-1} is very complex and won't be used here. We let the computer to do the inversion. Before that, however, it is useful to grip some qualitative message. The structure of χ_c clearly shows that there are four modes that can be probed: σ, D, l and t. There are couplings between these modes. The corresponding Green's function $G_{...}$ is of a prototypical Debye form for σ and of resonance form for others. It is therefore expected that four peaks can be seen in the imaginary part of χ_c vs. ω, in consistency with observations. The coupling between the σ and D is temperature dependent, $\mu = 2\tilde{K}(\bar{\sigma}^2 - 1)$. Besides, the ω_{well} belonging to D also has a T dependence, $\omega_{well}^2 = 2\tilde{K}M^{-1}(3\bar{\sigma}^2 - 1)$. The mode that is responsible for the structural instability should be the σ-mode, instead of the D-mode, because the latter's frequency ω_{well}^2, despite its temperature dependence, is not likely to vanish at T_c, as long as $\bar{\sigma}^2$ is in the vicinity of unity. It might be interesting to have some feel about the temperature dependence of $\bar{\sigma}^2$. Note that it can be split into two portions: $< \sigma >^2 + < \sigma - < \sigma >>^2$. The first portion may be written as $\sim \lambda_1(1 - \frac{T}{T_0})$ while the second one is roughly equal to $k_B T G_\sigma(\omega = 0) \sim \lambda_2(1 - \frac{T}{T_0})^{-1}$ by the fluctuation-dissipation theorem. At low temperatures, the first term dominates and dictates softening behaviors of ω_{well}^2. Although these expressions provide an idea, they are never accurate. As regards the form of Σ_0, we assume $r(\Sigma_0 - 1) \sim 1$ above T_c, so as to produce the mean-field Curie-Weiss law, while below T_c we lend to it such a form: $L_1 \frac{T^*}{T} - L_2$, with $L_{1,2}$ and T^* being parameters. This form is inferable from eqs.(14) and (29) in Ref.[121]. In this thesis, we choose $L_1 \sim L_2 = L$, whose values will be discussed together with that of T^* later.

We have performed numerical computations to obtain ϵ_c. The parameters are listed in TABLE3.2. We have used different charges for the σ- and D-variables, as noted before. The results are displayed in FIG.3.1-FIG.3.3. Let's derive some simple constraints regarding the choice of paramters. To obtain analytical results, we consider one further simplication: the couplings between D and other modes are ignored. At first sight there

is no justifications for this. We however see that, (1) the D-σ coupling as represented by μ is small as long as $\bar{\sigma}^2$ is close to unity; (2) the coupling energy between D and l (also t) should be much smaller than that between σ and l (also t), because $\langle D \rangle$ is likely to be much smaller than l_0. Under such approximation, the static dielectric constant is derived to be

$$\epsilon(0) - \epsilon_\infty = \frac{C}{T \cdot r(\Sigma_0 - 1) - T_c} \tag{3.27}$$

with T_c given as

$$k_B T_c = 4 l_0^2 (\frac{2\beta_t^2}{m\omega_t^2} + \frac{\beta_l^2}{m\omega_l^2}) \tag{3.28}$$

and the Curie constant C by

$$\begin{aligned} C &= \frac{l_0^2}{k_B a_0^3 \epsilon_0} \qquad (3.29) \\ &\times \quad [(z_\sigma l_0)^2 + \frac{\frac{z_l^2 k_B T_c \cdot r(\Sigma_0 - 1)}{l_0^2} - 4 z_l z_\sigma l_0 \beta_l}{m\omega_l^2} + 2\frac{\frac{z_t^2 k_B T_c \cdot r(\Sigma_0 - 1)}{l_0^2} - 4 z_t z_\sigma l_0 \beta_t}{m\omega_t^2} - 8\frac{(z_l\beta_t + z_t\beta_l)^2}{m^2\omega_l^2\omega_t^2}] \end{aligned}$$

Making use of the expression for $r(\Sigma_0 - 1)$, we find on the high temperature side near T_c

$$\epsilon(0) - \epsilon_\infty = \frac{C_h}{T - T_c} \tag{3.30}$$

with

$$C_h = \frac{l_0^2}{k_B a_0^3 \epsilon_0}[(z_\sigma l_0)^2 + \frac{\frac{z_l^2 k_B T_c}{l_0^2} - 4 z_l z_\sigma l_0 \beta_l}{m\omega_l^2} + 2\frac{\frac{z_t^2 k_B T_c}{l_0^2} - 4 z_t z_\sigma l_0 \beta_t}{m\omega_t^2} - 8\frac{(z_l\beta_t + z_t\beta_l)^2}{m^2\omega_l^2\omega_t^2}] \tag{3.31}$$

while on the low temperature side near T_c

$$\epsilon(0) - \epsilon_\infty = \frac{C_l}{T_c' - T}, \quad T_c' = T^* - T_c/L \tag{3.32}$$

where

$$C_l = \frac{l_0^2}{Lk_B a_0^3 \epsilon_0} \times [(z_\sigma l_0)^2 + \frac{\frac{z_l^2 k_B L(T^*-T_c)}{l_0^2} - 4 z_l z_\sigma l_0 \beta_l}{m\omega_l^2} + 2\frac{\frac{z_t^2 k_B L(T^*-T_c)}{l_0^2} - 4 z_t z_\sigma l_0 \beta_t}{m\omega_t^2} - 8\frac{(z_l\beta_t + z_t\beta_l)^2}{m^2\omega_l^2\omega_t^2}] \quad (3.33)$$

It was known experimentally that $C_h \sim 1.5 \cdot 10^5 K$[10], $C_l \sim 4000K$[60, 69], $T_c \approx 410K$ and $T_c' \approx 420K$[60]. From these, we conclude that, $L \sim \frac{C_h}{C_l} \sim 38$ and $T^* \approx 435K$.

As for the charges, we take data from first principles computations[102], which give $z_\sigma l_0 \approx 7.5e$, $z_l \approx -6e$ and $z_t \approx -3e$. We expect z_{well} to be close to $z_\sigma l_0$. In practice, we choose it to be $6e$. The value of l_0 is chosen to be $14pm$, as suggested by NMR probes. With these inputs, we end up with two equations that lend us an estimate of β_l and β_t. As for the temperature dependence of ω_{well} and Γ_{well} as well as the effective relaxation rate $\tau^{-1}r(\Sigma_0 - 1)$, we also use experimental results[59, 60]. In short, although many parameters are engaged, they are mostly set by experiments.

Table 3.2: BTO parameters used in numerical results. $\mu = \mu_0\sqrt{1 - 0.4\frac{T-300K}{410K}}$, with $\mu_0 = 10Kgs^{-2}$

l_0	a_0	β_l	β_t
$10pm$	$400pm$	$20Kgs^{-2}$	$12Kgs^{-2}$
$z_\sigma l_0$	z_l	z_t	Γ_{well}
$7.5e$	$-6.0e$	$-3.0e$	$20cm^{-1} \cdot [1 + 1.6\frac{(T-300K)^2}{12100K^2}]$
ω_{well}	z_{well}	$\tau^{-1}r(\Sigma_0 - 1)$	T^*
$280cm^{-1}\sqrt{1 - 1.2\frac{T-300K}{410K}}$	$6.0e$	$20cm^{-1} + 0.6cm^{-1}K^{-1}(Tc - T)$	$430K$
ω_l	ω_t	Γ_l/ω_l	Γ_t/ω_t
$180cm^{-1}$	$510cm^{-1}$	0.001	0.05

3.3.3 Why is ϵ_a much bigger than ϵ_c?

In the tetragonal phase, in spite of the ordering in z-direction, the system is as disordered as in the cubic phase in the perpendicular directions. Within the same DWA formalism

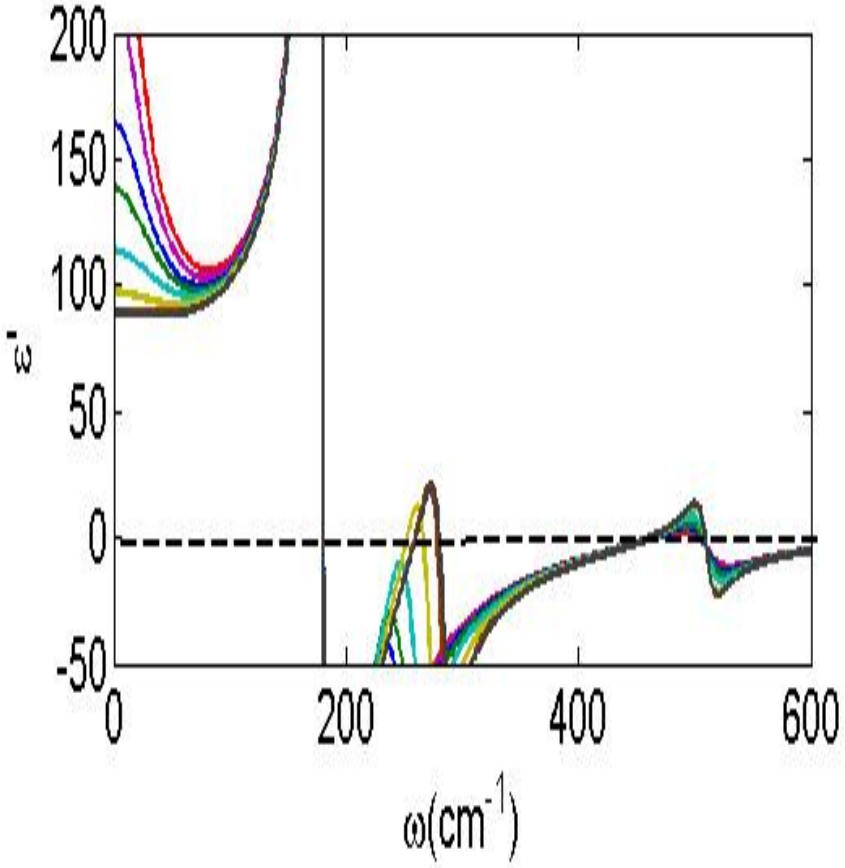

Figure 3.1: $\epsilon^{'}$ of BTO

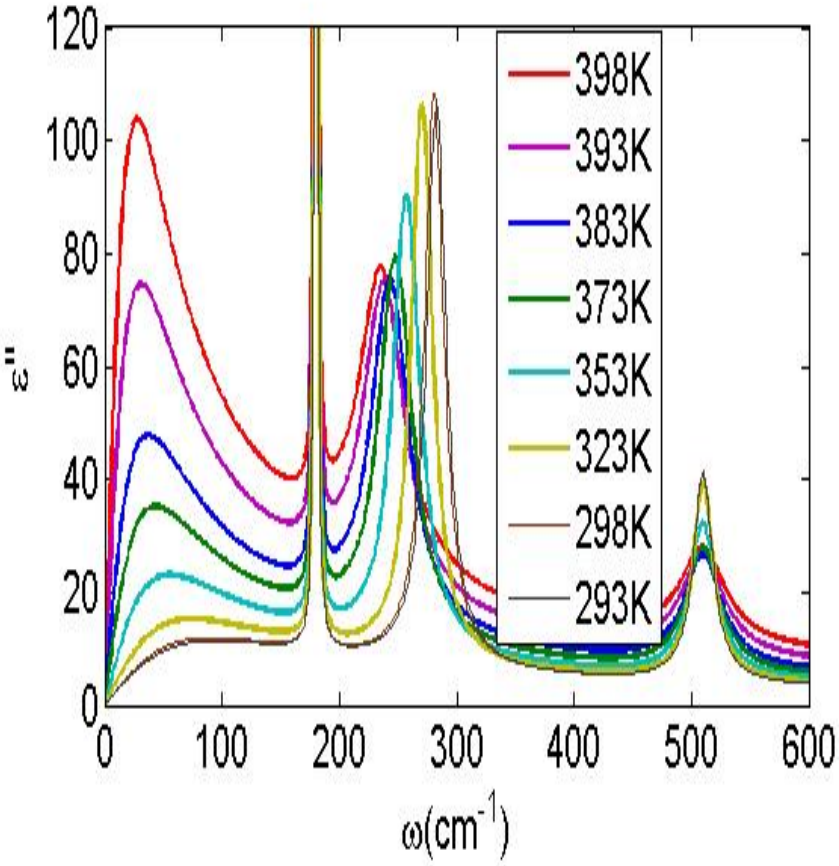

Figure 3.2: ϵ'' of BTO

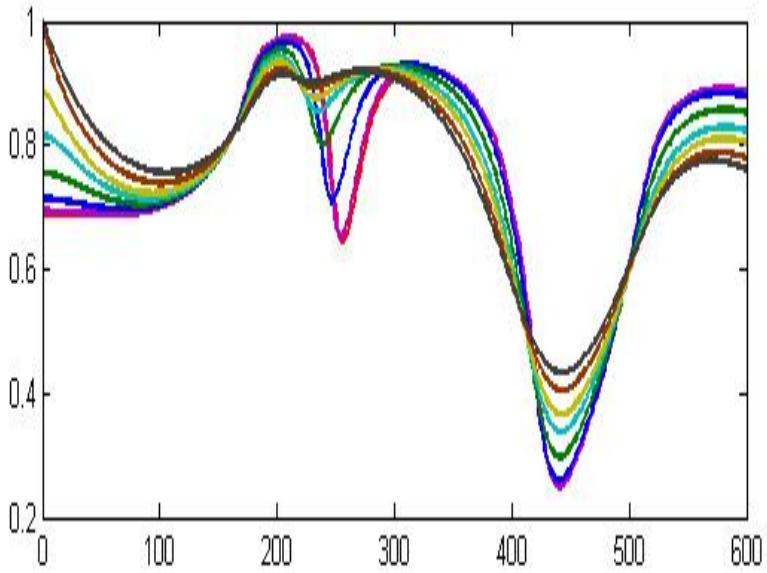

Figure 3.3: Reflectivity of BTO

developed in the last subsection, this fact means negligible spectral intensity for intra-well motions, which can therefore be left out here. The dynamical equation is then written as

$$\begin{pmatrix} G_\sigma^{-1} & 2\beta_l & 2\beta_t \\ 2\beta_l & G_l^{-1} & 0 \\ 2\beta_t & 0 & G_t^{-1} \end{pmatrix} \begin{pmatrix} l_0\sigma(\omega) \\ X_l(\omega) \\ X_t(\omega) \end{pmatrix} = \begin{pmatrix} z_\sigma l_0 E(\omega) + (l_0\beta)^{-1}\tilde{\eta}(\omega) \\ z_l E(\omega) \\ z_t E(\omega) \end{pmatrix} \tag{3.34}$$

which can be used to calculate the ϵ_a following the procedures prescribed before with new parameters. The quantities are defined in a similar fasion as those with ϵ_c. Here our main interest is to explain the significant discrepancy between the magnitudes of ϵ_a and ϵ_c at zero frequency. As mentioned in chapter 1, the ratio ϵ_a/ϵ_c was measured to be as big as 30. This has been a puzzle till now. In light of the argument presented with ϵ_c, we should already have an idea why it is so. Basically, this can be understood via the fluctuation-dissipation theorem, which states that larger fluctuations should lead to larger susceptibility. In the present case, this theorem tranlates as $\chi_{\rho\rho} \sim \beta(\langle d_\rho^2 \rangle - \langle d_\rho \rangle^2)$.

Now that the low-ω contribution stems primarily from σ variables, we may simply put $d_\rho \approx z_{sigma} l_0 \sigma_\rho$; hence, $\chi_{\rho\rho} \sim \beta z_\sigma^2 l_0^2 (\langle \sigma_\rho^2 \rangle - \langle \sigma_\rho \rangle^2)$. At room temperature, in the z-direction the spectral weight essentially rests with D; however, in the x-direction the weight goes with σ, which explains why ϵ_c is much smaller than ϵ_a at room temperature. According to this logic, the gap between ε_a and ε_c should turn even wider as temperature gets closer the tetragonal-orthohombic transition, which has been seen in experiments[69].

We'd like to forward another perspective. Treating the dynamical equation in the same manner as we did with ϵ_c, ϵ_a may be written down as

$$\epsilon_a = \frac{\tilde{C}_h}{T - \tilde{T}_c}, \tag{3.35}$$

with $\tilde{T}_c$ being the tetragonal-orthohombic transition temperature $\sim 280K$. See that here $\tilde{C}_h$ should look the same as C_h but with its own l_0 and T_c replaced with $\tilde{T}_c$. Despite this, it is reasonable to have $\tilde{C}_h \sim C_h$. Now by comparison with eq.3.32, we get

$$\frac{\epsilon_a}{\epsilon_c} = \frac{C_h}{C_l} \cdot \frac{T_c' - T}{T - \tilde{T}_c} \tag{3.36}$$

which gives an easy huge ratio, as required in the experiments. It should be pointed out that, such gap phenomena can be understood only with an order-disorder model (like the 8CM). For purely displacive compound such as $PbTiO_3$, no gap has been found[69].

3.4 Spectral Weight Transfer

Although we have discussed a lot about spectral weight transfer and shown its definiteness, the discussions were very qualitative. An unfortunate shortcoming of separating the inter-well motions from the intra-well motions is the failure to account for the transfer. Without the separation, the model would not be analytically tractable. As a way out there is

computer simulations based on e.g. molecular dynamics, which have been performed by several authors[68, 60]. The coexistence of both types of motions have been well confirmed in their work. It might be appropriate to quote from (excerpt of the 14th paragraph in Ref.[60]) the following

> The need for both modes is obvious in the OD [order-disorder] case: a small-amplitude intrawell vibrational mode has to coexist with large-amplitude interwell hops.

Nevertheless, a detailed investigation of such spectral weight transfer is still wanting.

3.5 Anisotropy Responsible for Chain Formation

Over four decades ago, Comes et al. did diffuse X-ray scattering with BTO, which in their opinion revealed a chain structure originating from correlations along $< 100 >$ directions. This structure was soon applied to explain the remarkably small entropy change upon structural phase transitions in BTO and KNO. It turns out that, for 8CM model to produce the correct entropy change, the correlation length should cover about $6 \sim 20$ unit cells. Let us try to understand this by considering the cubic-tetragonal transition. The entropy change per unit cell can be expressed as $\Delta S = k_B \log(\frac{N_c}{N_t})$, where N_c and N_t are the total numbers of accessible microscopic configurations in the cubic and tetragonal phases, respectively. Suppose every phase can be regarded as consisting of nearly independent D-dimensional clusters. The size of each cluster is then ξ^D, comprised of $[\frac{\xi}{a_0}]^D \equiv n^D$ unit cells. Simple considerations show that, $N_{c,t} \sim L^{\frac{N}{n_{c,t}^D}}$, which yields $\Delta S = k_B N(n_c^{-D} - n_t^{-D}) \log L$. Here N denotes the total number of unit cells, while L is the number of internal states. Since in tetragonal phase n_t is infinity, one then simply has $\Delta S \propto \frac{1}{n_c^D}$. For chain correlations, $D = 1$ and for planar correlations $D = 2$. Assuming zero correlations in the cubic phase would produce ΔS ten times larger than the observed value, which

means $n_c \sim 10$ for $D = 1$. This value agrees well with observations.

Now for finite-range correlations to occur in disordered phase, there must exist anisotropy in inter-cell coupling strengths. Let us consider $D = 1$. Let $\bar{J}$ be the average coupling strength, which relates to transition temperature $T_c = \frac{\bar{J}}{k_B}$. Let $\gamma = \frac{J}{J'}$ represent the anisotropy. Here J and J' stand for intra-chain and inter-chain coupling strengths, respectively. If $\gamma = 1$, $\bar{J} = J = J'$ and above T_c no finite correlations shall happen. But if $\gamma > 1$, chain correlations shall take place even above T_c, since $J > k_B T_c$. One way to estimate this is to treat the inter-chain interaction by mean-field method, which shall yield $\chi_{3D} = \frac{\chi_{chain}}{1-8J'\chi_{chain}}$, where χ_{3D} is the response function of the whole sample while χ_{chain} is the exact response function of an isolated chain. The divergence of χ_{3D} gives T_c, at which, it can be shown that, correlations within a chain has already been well developed.

After the original proposal, more experiments employing probes such as neutrons have led to similar conclusions. Recently, using picosecond soft x-ray laser speckle technique, Tai. et al were able to image the chain structures in BTO directly[70]. They observed that, the cluster's mean distance, which is determined by $\bar{J}$, increases linearly with temperature whereas the mean size, which is determined by J, of clusters does not change significantly. This observation strongly advocates the chain picture. Nevertheless, an explicit atomistic interpretation is still wanting.

According to the present model, we have $\frac{J}{J'} = [\frac{\omega_t}{\omega_l}]^2 \cdot [\frac{\beta_l}{\beta_t}]^2$, which generally deviates from unity and thus entails anisotropy. Now that ω_l is the only quantity that diminishes as temperature goes down, we concluded that the anisotropy shall become more pronounced at low temperatures.

3.6 Displacive vs. Order-Disorder

There is some kind of confusion in the literature regarding the use of these concepts. They may refer to different things depending on the context. Within the spin-phonon scheme such as the one developed by Yacoby et al[83], the 'displacive' is associated with the softening phonon while the 'order-disorder' concerns the spin variable. See that in this scheme, although the spin variable has a definite character (the Ti displacement), the nature of the softening phonon is elusive. On the other hand, within the Migoni-Bussmann jargon[115], the 'order-disorder' refers to the nano-size cluster dynamics and the 'displacive' again links to a soft mode. In the spectroscopic community, one associates them with a soft mode and a central mode, respectively[60]. Despite apparent discords, it is widely agreed that, the 'displacive' indicates a softening resonant mode and the 'order-disorder' connects to a relaxation mode respecting Deybe's law. However, as discussed in **section 1.6.4**, the border is not always sharp, especially in the case of a critical mode.

Chapter 4

APPLICATIONS TO STO

Differing from BTO, which is a ferroelectric, STO is often quoted as an incipient ferroelectric or quantum paraelectric. It is believed that, this compound has already been on the way toward ferroelectricity but somewhat thwarted by quantum fluctuations. Qualitative discussions may be again performed within the SCHA that has been exemplified before in chapter 2 and 3. According to **section 2.3.6**, quantum fluctuations are characterized by l_0 in the large $\tilde{K}$ limit or γ in the small $\tilde{K}$ limit. In the former, if l_0 does not exceed a critical value l_c, then ferroelectricity will be suppressed. A rough estimation of l_c for STO gives $\sim 6.32pm$, as shown in **section 3.2**, indicating $l_0 > 6.32pm$. However, experiments saw that l, the inter-corner separation, should not exceed $5pm$. Thus, l_0 seems not that close to l, implying not big $\tilde{K}$ and therefore significant quantum fluctuations. In such case, intra-well motions become ill-defined and SCHA should be sufficient in describing the Ti motions.

4.1 Dielectric Modes

4.1.1 Dynamical Matrix

In comparison with BTO, the dielectric modes of STO have a few distinct traits. Firstly, in stead of four, only three modes have been observed across all temperatures in every axial direction. This may be basically due to the disappearance of Ti intra-well modes. Secondly, all modes seem of resonant nature and none relaxation behaviors have been perceived. Actually, the damping rate of the lowest mode is no more than a half of the mode frequency, while those of other two modes are nearly the same as that in BTO: less than five percent of the corresponding mode frequencies. This feature is again consistent with the disappearance of intra-well motions. Needless to say, the modes around $170cm^{-1}$ and $510cm^{-1}$ are obviously of O character, in line with the logic presented in preceding chapters. On the other hand, the lowest mode is expected to be attached to Ti motions. Since this mode is of resonant nature, we can assign to it a frequency $\omega_{s|\rho}$ and damping rate $\Gamma_{s|\rho}$, whose Green's function should then be given as $G_{s|\rho}(\omega) = \frac{1}{M(\omega_{s|\rho}^2 - \omega^2 - i\omega\Gamma_{s|\rho})}$. Henceforth, the dynamical equation for STO should look analogous to that belonging to ϵ_a of BTO. It can then be written as

$$\begin{pmatrix} G_{s|\rho}^{-1} & 2\beta_l & 2\beta_t \\ 2\beta_l & G_l^{-1} & 0 \\ 2\beta_t & 0 & G_t^{-1} \end{pmatrix} \begin{pmatrix} u_\rho(\omega) \\ U_{l|\rho}(\omega) \\ U_{t|\rho}(\omega) \end{pmatrix} = \begin{pmatrix} z_{Ti}E(\omega) \\ z_l E(\omega) \\ z_t E(\omega) \end{pmatrix} \tag{4.1}$$

Here ρ indicates the axial directions. Above the oxygen cage tilting transition, the compound is in cubic phase and thus the dynamical matrix should be regardless of the directions. Below it, the tilting causes a tetragonal distortion and one has to distinguish between the c-direction and ab-direction. This difference mainly enters through $G_{s|\rho}$ and occurs at $\omega_{s|\rho}$. Within DWA, the ω_s can be calculated using SCHA or based on numerical

methods. As we will discuss in subsequent sections, all these calculations can be captured by the following form (drop the label ρ)

$$\omega_s^2 = \Omega^2 \coth \frac{T_1}{2T} \tag{4.2}$$

where Ω is the value of ω_s at vanishing temperature and T_1 is a parameter to be determined.

4.1.2 Dielectric Constant

The dielectric constant can be obtained similarly as we did with BTO. At $\omega = 0$, it takes the Barrett form as prescribed in eq.(1.24). Namely,

$$\epsilon(0) = \frac{C}{\frac{T_1}{2}\coth\frac{T_1}{2T} - T_0} \tag{4.3}$$

where the extrapolated Curie constant is given by

$$\begin{aligned} C &= \frac{l_1^2}{k_B a_0^3 \epsilon_0} \\ &\times \left[z_{Ti}^2 + \frac{\frac{z_l^2 k_B T_1 \coth\frac{T_1}{2T}}{2l_1^2} - 4 z_l z_{Ti}\beta_l}{m\omega_l^2} + 2\frac{\frac{z_t^2 k_B T_1 \coth\frac{T_1}{2T}}{2l_1^2} - 4 z_t z_{Ti}\beta_t}{m\omega_t^2} - 8\frac{(z_l\beta_t + z_t\beta_l)^2}{m^2\omega_l^2\omega_t^2}\right] \end{aligned} \tag{4.4}$$

and T_0 has the same expression as for T_c in BTO,

$$k_B T_0 = 4 l_1^2 \left(\frac{2\beta_t^2}{m\omega_t^2} + \frac{\beta_l^2}{m\omega_l^2}\right) \tag{4.5}$$

In the above,

$$l_1 = \sqrt{\frac{k_B T_1}{2M\Omega^2}} \tag{4.6}$$

is a length scale playing a similar role here as l_0 in BTO.

4.1.3 Parameters and The Origin of Isotope-Exchange Induced Ferroelectricity

To pin down the parameters, one may utilize several facts. Look at T_0 first. For pure STO, T_0 has been found to be around $38K$. For STO18, however, it was shown to be $44K$. Let's emphasize that, such increase in T_0 after isotope exchange can hardly be explained by contrived decrease of $m\omega_{l,t}^2$, which actually represent the force constants associated with O vibrations. Except that $K_{t,l}$ are extremely small or negative, we should have $m\omega_{l,t}^2 = K_{l,t}$, which, as is clear from eq.(2.55) and (2.57), are not expected to change in the course of isotope substitution. Therefore, we may conclude that, the increase of T_0 should be attributed to the increase of l_1. This leads us to the second fact: it was observed that T_1 could be enlarged by about $3K$ after isotope exchange: $84K$ and $87K$ for STO16 and STO18, respectively. According to eq.(4.6), one should have

$$\frac{T_0}{2T_1}|_{\mathrm{STO16}} = \frac{A}{M\Omega^2_{\mathrm{STO16}}} \approx 0.2262, \quad \frac{T_0}{2T_1}|_{\mathrm{STO18}} = \frac{A}{M\Omega^2_{\mathrm{STO18}}} \approx 0.2529 \tag{4.7}$$

where $A = \frac{2\beta_t^2}{m\omega_t^2} + \frac{\beta_l^2}{m\omega_l^2}$. We infer that Ω^2 for STO18 is a little smaller than that for STO16. According to eq.(4.3), the quantity $\frac{2T_0}{T_1}$ may be used as an indicator of ferroelectricity, which happens only when that quantity exceeds unity. The values obtained above for STO16 and STO18 are in accord with this statement. One should see that, the main difference between STO16 and STO18 comes from Ω^2, rather than T_1. In fact, even if the T_1 for STO16 were used, one would get $T_0 = 42.5K$ for STO18 provided Ω^2_{STO18} had been in use. Such analysis hints that, the main consequence of O isotope substitution seems to diminish qunatum fluctuations via decreasing the value of Ω^2. This conclusion stands in contrast with those by many other authors, who frequently ascribed the artificial ferroelectricity induced in STO18 to a decrease in the O force constants.

To find out other parameters, we need to know Ω. To this end, we notice that, at room

temperature ω_s was found about $87.7cm^{-1}$ in pure STO[56]. Thus, we have $87.7cm^{-1} \approx \Omega_{\mathrm{STO}16}\sqrt{\coth\frac{84K}{2*300K}}$, from which it follows that $\Omega_{\mathrm{STO}16} \approx 32.7cm^{-1}$. Now from eq.(4.7), one finds $\Omega_{\mathrm{STO}18} \approx 30.9cm^{-1}$. It is very interesting to see that a small change in Ω could result in dramatic changes in dielectric properties. The l_1 is then estimated to be about $13.8pm$ for STO16. The third fact to be used is the value of $C(T=0)$, which is about 10^5K. With the knowledge of l_1, T_0, $\omega_l = 178cm^{-1}$ and $\omega_t = 546cm^{-1}$, equation (4.5) translates into the following equation

$$0.6878 \approx 0.0071\beta_t^2 + 0.0332\beta_l^2 \tag{4.8}$$

where $\beta_{l,t}$ are taken in unit of Kgs^{-2}. Similarly, knowing that $z_l = -5.73e$, $z_{Ti} = 7.26e$ and $z_t = -2.15e$, eq.(4.5) becomes

$$\frac{C}{0.0062 * 10^5K} \approx 52.7 + 3.3227 + 5.5317\beta_l + 0.4412 * \beta_t \tag{4.9}$$

Here again $\beta_{l,t}$ denote the numeric values in unit of Kgs^{-2}. These equations can be roughly satisfied if we choose $\beta_l = 4.4Kgs^{-2}$ and $\beta_t = 2.5Kgs^{-2}$, which give $C \sim 0.6 * 10^5K$. This value is comparable to experimental data.

We have presented some dielectric properties as calculated with the parameters entabulated in TABLE4.1. They are displayed in FIG.4.1 and FIG.4.2.

Table 4.1: STO parameters used in numerical results.

l_1	a_0	β_l	β_t
$13.8pm$	$400pm$	$4.4Kgs^{-2}$	$2.5Kgs^{-2}$
z_{Ti}	z_l	z_t	Γ_s
$7.25e$	$-5.7e$	$-2.15e$	$0.5 * \omega_s$
Ω	T_1	Γ_l/ω_l	Γ_t/ω_t
$32.7cm^{-1}$	$84K$	0.03	0.05

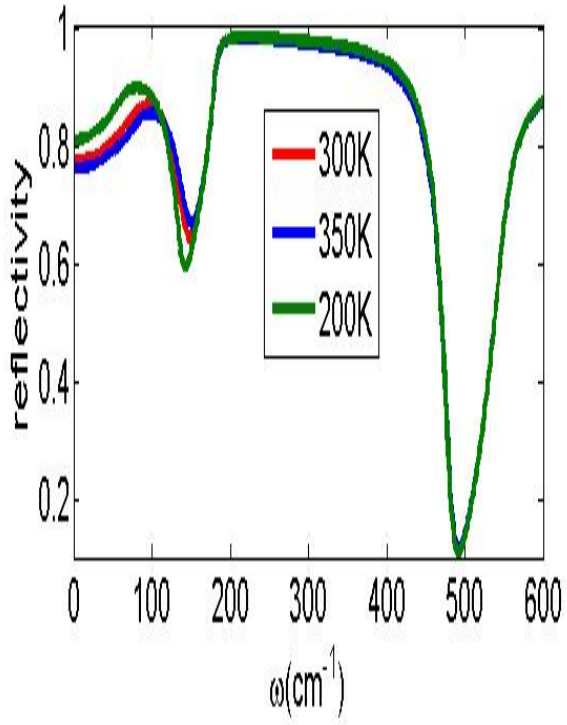

Figure 4.1: Reflectivity of STO

4.2 Quantum Paraelectricity

4.2.1 Introduction

In the last section, we have shown that the dielectric constant of STO should follow basically the Barrett's law, as embodied in eq.(4.3). Note that, the quantity C in this equation has a temperature dependence that gets in through the factor $\coth \frac{T_1}{2T}$. This makes that equation deviate from the standard Barrett's formula, where the C is supposed to be a constant. Nevertheless, the deviation is negligibly tiny: numerically, the fraction taken by the temperature dependent terms in C is given by $\frac{3.3227 \coth \frac{42K}{T}}{78.1425+3.3227 \coth \frac{42K}{T}}$, which is less than 17% as long as $T < 200K$. Henceforth, one may safely fix C at its zero temperature value.

In this section, we try to address an issue that has been carefully portrayed in **section**

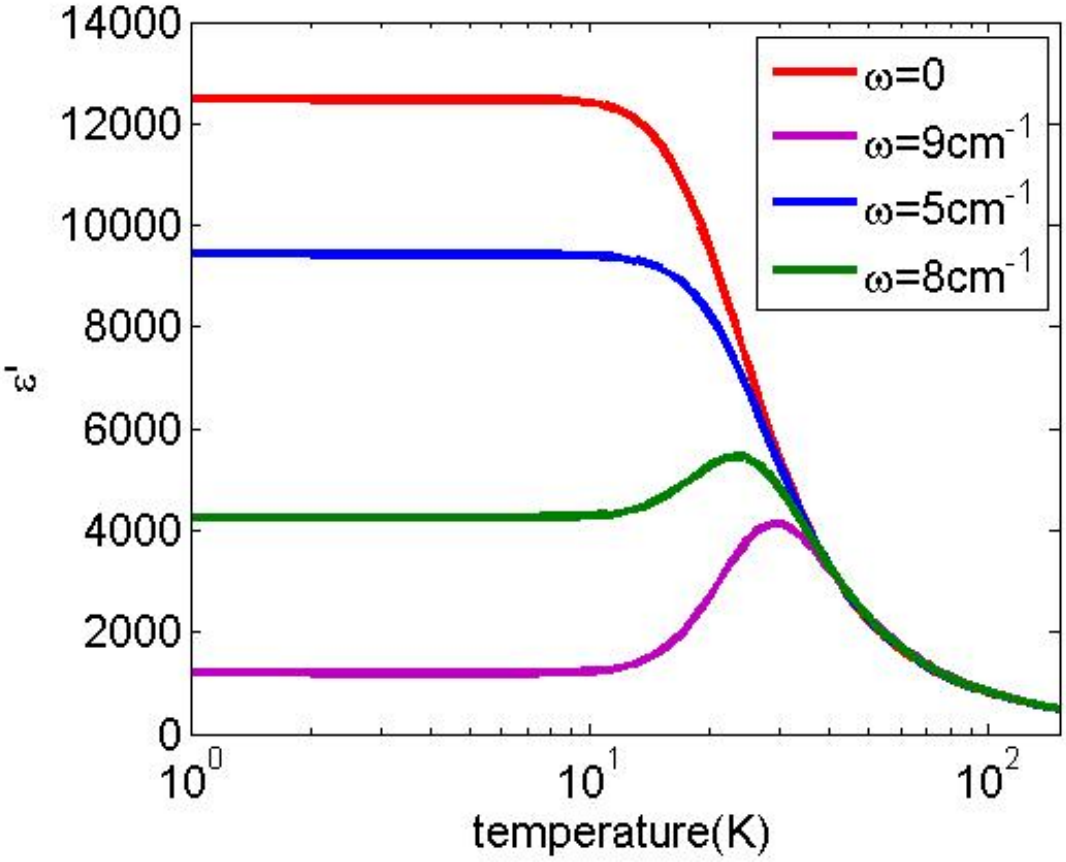

Figure 4.2: ϵ' of STO at various frequencies

1.7.1: to fit the experimental data with Barrett's formula, a contrived increase in T_1 from a low temperature (below $3K$) value to a high temperature one (in the range from $10K$ to $30K$) seems in need. Similar crossover has been observed in a couple of other experiments[126, 81, 127, 128] and modelled with a hyperbolic tangent engaging four parameters [78]. However, the reason for this temperature dependence is unveiled. Recently, Marqués et al. came up with an explanation[79] that deciphers T_1 as the quantum temperature associated with some unidentified phonons[129, 130]. Assuming a special phonon mode distribution, which itself requires justifications, they could find a good agreement with experimental data. Fittings using generalized Barret formula[131] or in terms of the so-called hard anti-phase boundaries[132, 82] have also appeared. In all these schemes, certain extrinsic factors outside the Ti atoms have been invoked. In what follows, however, we show that the proposed T_1 behaviors can be inherent to the double-well potential (DWP) and a corollary of the tunneling between the excited intra-well states belonging to different wells (see FIG.4.3).

4.2.2 Formalism

We employ the Hamiltonian H_c in eq.(3.8) to study ϵ_c within DWA. The O octehedral rotation transition occuring at $\sim 105K$ is ignored here, whose impacts will be investigated in the next section. This allows us to focus on the intrinsic behaviors of Ti ions within DWA. After eliminating the O variables using the adiabatic methods prescribed in **section 2.3.5**, one arrives at a model that has also been studied in Ref.[133, 134, 135]

$$H = \sum_i \{-\frac{\hbar^2}{2M}\frac{\partial^2}{\partial Z_i^2} + \frac{b}{4}Z_i^4 - \frac{a}{2}Z_i^2\} - \sum_{<i,j>} J_{ij} Z_i Z_j \tag{4.10}$$

Here we have set $b = 4\gamma$ and $a = 2\tilde{K}$ and $J_{ij} = \frac{\beta_l^2}{m\omega_l^2}$ for the pair $< i, j >$ lying in the z-direction while $J_{ij} = \frac{\beta_t^2}{m\omega_t^2}$ for that in the xy-plane. It proves convenient to work with

a dimensionless Hamiltonian. To reach this, we introduce $u_i = \frac{Z_i}{\sqrt{2}l_0}$, where $l_0 = \sqrt{a/b}$ as before. At the same time, we write $\lambda^2 = \frac{\hbar^2}{2Ml_0^2}\frac{4b}{a^2} = \frac{2\hbar^2}{Mal_0^4}$ and $V_{ij} = 2J_{ij}l_0^2$. The dimensionless version of H is then given by

$$\frac{4b}{a^2}H = -\sum_i\{-\frac{\lambda^2}{2}\frac{\partial^2}{\partial u_i^2} + 4(u_i^4 - u_i^2)\} - \sum_{<i,j>} V_{ij}u_iu_j \tag{4.11}$$

Now we treat the inter-site term via mean field theory. Thus we find a single-site model, which reads

$$H_m = -\frac{\lambda^2}{2}\frac{\partial^2}{\partial u^2} + 4(u^4 - u^2) - V_0\langle u\rangle u \tag{4.12}$$

where $V_0 = \sum_j V_{ij}$. Note that, the physics is controlled by two parameters, $\lambda \propto l_0^{-2}$ and V_0. The former controls the quantum fluctuations while the latter represents the strength of the molecular field. The potential barrier (which is unity for H_m) separating the wells serves as an intrinsic energy scale. The stability of the double-well potential requires that $V_0 \ll 1$. From now on we fix $V_0 = 0.1$ and study the effects of quantum fluctuations.

Let χ_0 be the susceptibility for $V_0 \equiv 0$. For finite V_0, the susceptibility can be obtained as

$$\chi = \frac{\chi_0}{1 - V_0\chi_0} \tag{4.13}$$

Actually, by definition one has for disordered phase $\langle u\rangle_0 = \int_0^E \chi_0(E')dE'$, where E is the external electric field, from which one has $\langle u\rangle = \int_0^{V_0\langle u\rangle + E} \chi_0(E')dE' \approx \chi_0(V_0\langle u\rangle + E)$, and thus $\chi = \frac{\partial\langle u\rangle}{\partial E}$ obtains the form of the above equation. This shows that, all we need is χ_0, which shall be calculated numerically. To this effect, we introduce the ladder operators that are defined by

$$\begin{aligned} u &= \sqrt{\frac{\lambda^2}{2\omega_0}}(a + a^\dagger) \\ -i\frac{\partial}{\partial u} &= i\sqrt{\frac{\omega_0}{2\lambda^2}}(a^\dagger - a) \end{aligned} \tag{4.14}$$

Here $\omega_0 = 2\sqrt{2}\lambda$ is chosen so that the Hamiltonian is symmetric with respect to a and $a^\dagger$. With this choice, the Hamiltonian becomes

$$H_m = \frac{\lambda^2}{8}(a + a^\dagger)^4 - \sqrt{2}\lambda(a^2 + a^{\dagger 2}) - g(a + a^\dagger) \tag{4.15}$$

where $g = \sqrt{\frac{\lambda}{4\sqrt{2}}}V_0\langle u\rangle$ signifies the molecular field. The computations are most conveniently conducted in the representation in which $a^\dagger a$ is diagonal, namely, $a^\dagger a|n\rangle = n|n\rangle$, $n = 0, 1, ..., N_c$ being non-negative integers. In actual computations, we need truncate the Hilbert space by N_c. We choose $N_c = 100$. Now the matrix elements of a and $a^\dagger$ are $a_{m,n} = \sqrt{n}\delta_{m,n-1}$ and $a^\dagger_{m,n} = \sqrt{n+1}\delta_{m,n+1}$, respectively. The bare susceptibility is computed as $\chi_0 = \frac{\partial\langle u\rangle}{\partial g}|_{g=0}$, where $\langle u\rangle = Tr[\exp(-H_m/T)u][Tr\exp(-H_m/T)]^{-1}$. In consistency with Ref.[135], at essentially zero temperature, there exists a critical value, λ_c, separating the ordered ground state from the disordered one. For $V_0 = 0.1$, λ_c was numerically found of about 0.2. Since ST is para-electric, one must have $\lambda > \lambda_c$. On the other hand, ST can be made ferroelectric with the replacement of $O16$ by $O18$[16], which means an appropriate choice of λ for ST should not be far from λ_c. Therefore, we use $\lambda = 0.3$ for this compound.

4.2.3 Analysis

Exact Results

We have performed the computations for a series of λ from below λ_c to above. To try the Barret fit with eq.(4.3), one has to input three parameters. Considering eq.(4.13), it is natural to fix $T_0 = V_0$. In the meanwhile, $C = \lim_{T\to\infty}[\chi(T)(T - T_0)]$ and $T_1 = 2\lim_{T\to 0}[C/\chi(T) + T_0]$. For all λ, we found $C \approx 1$, as expected from eq.(4.13). However, the as-obtained T_1 shows strong temperature dependence. As exhibited in the inset of FIG.4.3, T_1 begins to rise rapidly at a temperature T^* after a short flat section, a universal feature

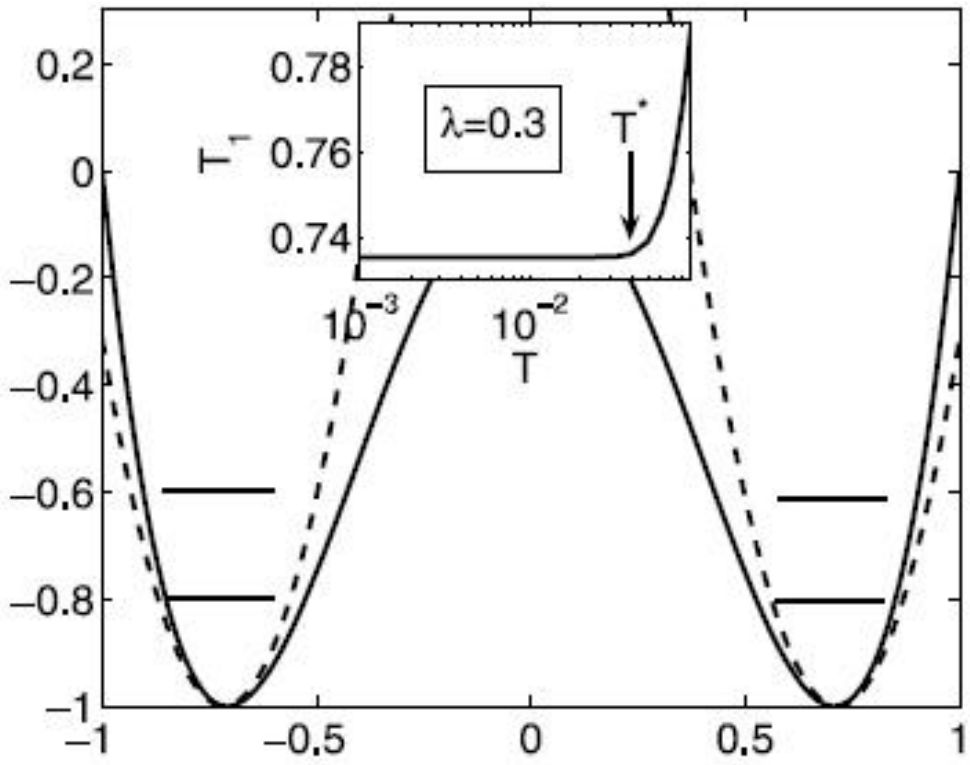

Figure 4.3: Schematic of the DWP and the temperature dependence of T_1.

for all λ. Moreover, the λ-dependence of T^* follows a simple linear behavior, $T^* \propto (\Delta - \Delta_c)$. Here $\Delta = 4\lambda$ is the intra-wall oscillatory energy spacing, which is obtained by expanding the potential around either well (see FIG.4.3). The intimate connections between T^* and Δ implies that: beyond T^*, higher energy intra-well states can be activated and should contribute to the increase of T_1.

Low Temperature Limit

It is noted that, small amplitude oscillations about either well are approximately harmonic with an energy spacing Δ. As long as the ground state energy of this intra-well oscillator, $\frac{\Delta}{2}$, is much less than the barrier, intra-well states and energy levels of either well can

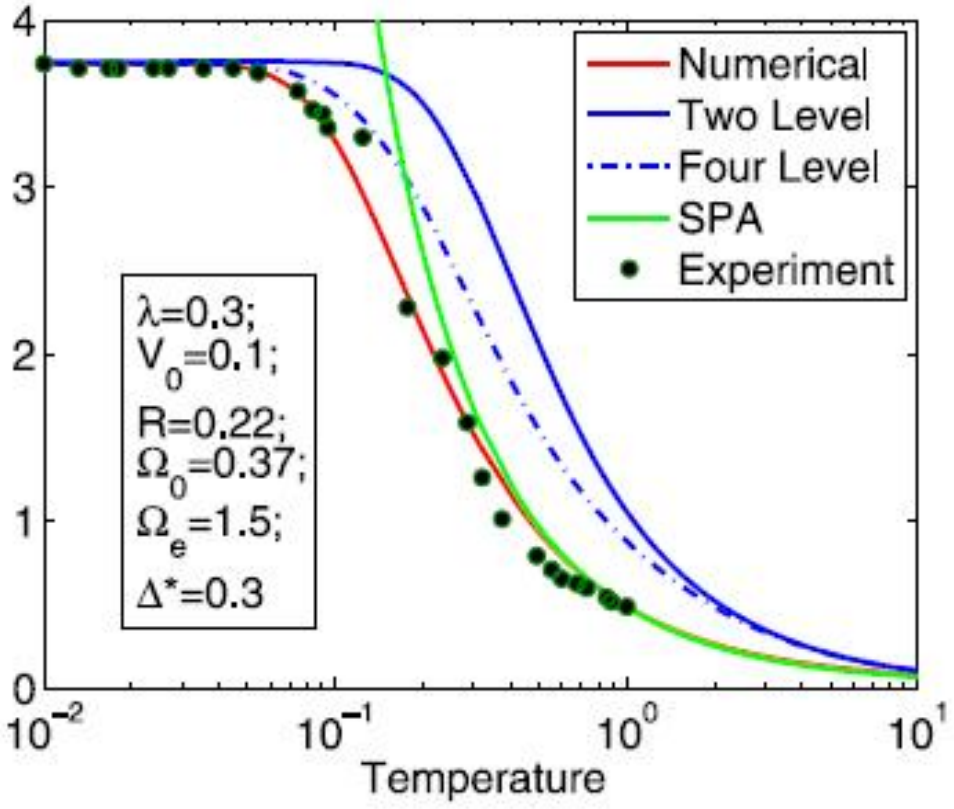

Figure 4.4: Comparison between experimental and theoretical χ. Numerical: χ_0 obtained by numerically solving the MF Hamiltonian; Two Level: $\chi_0 = \chi_2$; Four Level: $\chi_0 = \chi_4$; SPA: $\chi_0 = \chi_{SPA}$. Experimental data has been rescaled as discussed in text.

be defined univocally. Below a characterizing temperature T^*, high energy states are frozen and only the ground states are active[134]. Hence a two-level description should be realistic. The Hamiltonian at $g = 0$ in this reduced sub-space takes on a simple form[83]: $H_2 = \Omega_0\sigma_x$, where Ω_0 is the tunneling energy, which is a constant, and σ_x is the Pauli matrix. The susceptibility by H_2 is well known: $\chi_2 = \frac{1}{\Omega_0}\tanh(\Omega_0/T)$. Plug this as χ_0 in eq.(3) and one gets in the low temperature regime a susceptibility of exactly the same form as χ_B, with $\Omega_0 = T_1/2$.

High Temperature Limit

On the other hand, at temperatures much higher than T^*, the tunneling scenario is expected to fail. In this case, the barrier becomes almost invisible in the presence of thermal fluctuations, and the double-well architecture can be effected by a single-well one. The effective oscillation frequency, ω_s, can then be evaluated with the SCHA. As usual, two equations can be obtained,

$$\begin{aligned} \omega^2 &= 8\lambda^2(\langle u^2\rangle - 1) \\ \langle u^2\rangle &= \frac{\lambda^2}{2\omega}\coth(\omega/T) \end{aligned} \tag{4.16}$$

The susceptibility of an oscillator can be related to its mass and frequency by $\chi_{osi} = \frac{\lambda^2}{\omega^2}$. Combining this with the above equations, we arrive at

$$1 = 4\lambda\chi_{osi}^{3/2}\coth(\frac{\lambda\chi_{osi}^{-1/2}}{T}) - 8\chi_{osi} \tag{4.17}$$

which can be solved numerically. The as-found χ_{osi} is expected to be further affected by anharmonic effects that are not included in SCHA[136]. We thus introduce a temperature independent constant R to account for this, so that the final susceptibility reads $\chi_{SPA} = R \cdot \chi_{osi}$. Upon fitting χ_{SPA} with the exact χ, the R for small λ was numerically found

around 0.2, but larger values needed for bigger λ. Inserting χ_{SPA} as χ_0 in eq.(4.13) gives χ in the high temperature regime.

Four Level Approximation

Here we consider an intermediate case between the two extremes discussed above. We resort to a 4-level description, in which four levels, two (the ground (g) plus the first excited (e) intra-well state) for each well, are considered. These four levels can be written as $|Lg\rangle$, $|Rg\rangle$, $|Le\rangle$ and $|Re\rangle$, with L (R) referring to the left (right) well. Ignoring the mixing between the e- and g-states from different wells, the Hamiltonian can be written as $H_4 = \Omega_g\sigma_x + \Omega_e\tau_x + \Delta\tau_0$, where Ω_e ($\Omega_g = \Omega_0 < \Omega_e$) denotes the tunneling energy between the e (g) states and σ and τ act upon the ground and excited states respectively. We ignore the mixing because the said levels are not matched in energy and hence their mixing is inefficient.

With the results obtained for the 2-level model, one can easily obtain the bare susceptibility as $\chi_4 = p_g\chi_g + p_e\chi_e$, where $\chi_{e,g} = \Omega_{e,g}^{-1}\tanh(\frac{\Omega_{e,g}}{T})$, $p_g = \frac{Z_g}{Z_g+e^{-\Delta/T}Z_e}$, with $Z_{e,g} = 2\cosh(\frac{\Omega_{e,g}}{T})$, and $p_e = 1 - p_g$. For simplicity, we shall write $p_g \approx \frac{1}{1+\exp(-\frac{\Delta^*}{T})}$, which defines Δ^*. The generalization to a many-level description is straightforward. Define an effective frequency by Ω via $\chi_4 = \Omega^{-1}\tanh(\frac{\Omega}{T})$, and clearly this Ω plays the role of the averaged frequency used in Ref.[79]. As T goes to zero, p_g approaches unity and Ω tends to Ω_g. As T increases, Ω (and also T_1) increases. At relatively low temperatures, where the tanh function can be taken as unity, one finds $\frac{1}{\Omega} \approx \sum_{\nu=e,g}\frac{p_\nu}{\Omega_\nu}$, which can be rewritten as $\Omega = \frac{2\Omega_g\Omega_e}{\Omega_+ + \Omega_-\tanh(\frac{\Delta^*}{2T})}$. Here $\Omega_\pm = \frac{1}{2}(\Omega_g \pm \Omega_e)$. As T goes to zero, it approaches Ω_g; as T goes to large, it approaches $\frac{4\Omega_g\Omega_e}{\Omega_g+\Omega_e}$. This behavior resembles that of the formula used in Ref.[78]. In addition, if we include even more levels, the Ω should not saturate at all, but should increase all the way instead.

4.2.4 Conclusions

In light of the above analysis, we should anticipate a crossover from the 2-level mechanism, which prevails at very low temperatures, to the SPA mechanism that dominates at high temperatures. This is wonderfully confirmed in FIG.4.4, where we plot χ with various χ_0, together with the experimental data. It is seen that, with $\chi_0 = \chi_2$, the flat low-temperature segment can be remarkably fitted, whereas the higher temperature part shows a mismatch. On the other hand, with $\chi_0 = \chi_{SPA}$, the high temperature section can be fitted marvelously, whereas the flat part can not be tamed. Note that the numerical results are in good agreement with experimental data over the entire region. This is somewhat unexpected, in the sense that, only two paramters, λ and V_0, are used as inputs and their choices are tightly contrained by physical considerations, as discussed in previous paragraghs.

The experimental data (between $1K$ and $100K$) are taken from Ref.[71] and can be compared with the present computation. The connections between the present calculations and the data can be established by choosing $\frac{a^2}{4b} = 100K$ as the temperature conversion factor and observing that the measured dielectric constant ϵ is related to the computed χ via $\epsilon \approx 8\pi(\frac{l_0}{a_0})^3 \frac{Q^2}{l_0} \cdot \chi$, where a_0 is the lattice constant and Q is the effective charge. Let the pre-factor be about $6.7 \times 10^5 K$ and we find the results as displayed in FIG.4.4.

4.3 Repercussions of O Cage Tilting

4.3.1 Introduction

In the last subsection, we have shown that due to thermal activation of excited intra-well levels the quantum temperature T_1 cannot be a constant. Rather, within DWA, it has to increase with temperature and thus offers an explanation of a long-standing

inexplicable phenomenon as described therein. However, as we will argue below, this picture is oversimplified: one more twist should be added to the story. Another purpose here is to demonstrate the inadequacy of the DWA. The new anomaly to be revealed below requires the presence of the 8CM or the ARM that were depicted in chapter 2.

This anomaly has to do with the O cage rotation transition. For a long time, people have thought that there should be neligible correlations between this transition and the quantum paraelectricity in STO. As we discussed in chapter 2, this picture is not true: the incipient ferroelectricity and the O cage rotation can arise from the same vibronic origin and there exists competitions between them as sketched in eq.(2.49). This equation states that, the rotation will reduce the off-center shifts of Ti ions and therefore diminish the dielectric activity. Aside from this miscroscopic perspective, a phenomenological investigation[137] based on Barrett's formula (non-standard) has also disclosed clear traces left on the dielectric constant by the rotation. In Vogt's context and symbols, the susceptibility (the inverse of the squared frequency which is an average over the E_u and A_{2u} modes) is expressed as

$$\chi(0) = \frac{3^{-1}\hbar\tilde{\lambda}^{-1}\omega_1^{-1}}{\frac{\hbar\omega_1}{2}\coth\frac{\hbar\omega_1}{2k_BT} - \frac{\tilde{v}_0-1}{12\tilde{\lambda}}\hbar\omega_1} \tag{4.18}$$

As regards the physical meanings of the involved parameters, the readers are refered to Ref.[137]. What is needed right now is the ω_1, which defines the quantum temperature $T_1 = \frac{\hbar\omega_1}{k_B}$. Interestingly, to obtain a good fit to observations, the ω_1 was found to follow the rotation angle in this pattern (see also **section 1.7.3**):

$$\omega_1^2(T) = \omega_1^2(T_a)[1 + \alpha\varphi_s^2(T)] \tag{4.19}$$

which is the eq.(30) in Ref.[137]. Here $\varphi_s(T)$ denotes the rotation angle at temperature T (see FIG.4.5) and $T_a = 105K$. So, according to this work, T_1 is expected to decrease as T approaches T_a from below. This decrease cannot be explained within DWA, unless a

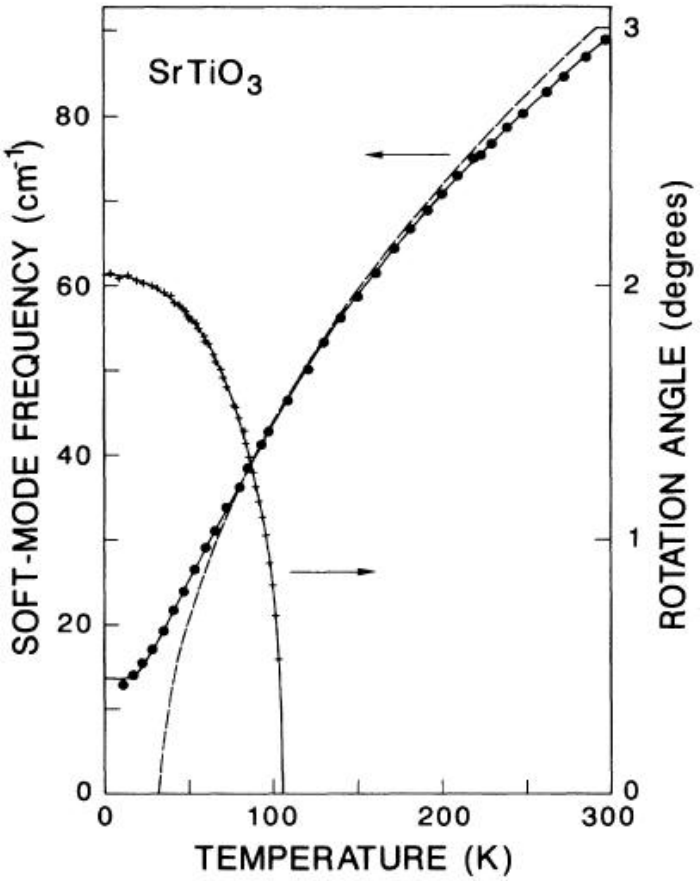

Figure 4.5: The O cage tilting angle as a function of temperature and the soft mode frequency obtained with the tilting counted in. Reproduced with permission from [137].

contrived temperature dependence of ω_1 as the above equation is used.

In light of the discussions on isotope exchange effects in preceding sections, we are also led to the conclusion that subtle correlations exist. Actually, our previous analysis shows that, the FE induced via $O18$ substitution is actually through decreasing the quantum fluctuations on the Ti sites. Although the mass change is very small, the effects are dramatic. There are a flurry of work[138, 139, 140, 141] focusing the quantum aspects of the isotope effects, but few pay attention to such correlations.

Finally, we mention the experimental work by Yamanaka et al[75]. These authors performed high-resolution hyper-Raman scattering (HRS) measurements on STO and the

temperature dependences of the soft polar mode frequency, ω_0, were determined. Although above T_a the ω_0^2 follows perfectly the Curie-Weiss's law, it starts to split into two branches (at ω_a and ω_c, respectively) and deviate from this law significantly after crossing T_a. Then they put $\omega_{a,c}^2$ as a sum of two terms, the first supposed to be the squared frequencies that would result if the AFD did not take place and the second being proportional to the square of the AFD order parameter. After determining the second term independently via other methods, they were able to settle the first one, which actually softens to zero at around $30K$, indicating FE instability. However, this instability was eventually prevented by the O rotation. They concluded that, QF alone could not suppress the FE and the presence of O rotation is essential. In view of the analysis given below, we would say, the actual role of O rotation is to enhance quantum fluctuations and therefore, it should not be deemed as an independent cause.

4.3.2 The Importance of T_1

We notice several reasons to focus on T_1 instead of ϵ. Firstly, the behaviors of T_1 are much more revealing than that of ϵ. Apparent agreements with ϵ can be easily achieved, almost regardless of how the T_1 behaviors are postulated[71, 78, 79]. This can be appreciated by noting that, the factor $(T_1/2)\coth(T_1/2T)$ becomes unity regardless of T_1 for $T \gg T_1/2$. Secondly, T_1 may be regarded as an independent quantity with clear physical meanings, rather than a simple fitting parameter. From a mean-field point of view, ϵ hinges on temperature primarily through the bare electric susceptibility $\tilde{\chi}_0$, which is associated with motions of the local mode $\vec{u}$ belonging to a single unit cell and proportional to the electric dipole as defined in Ref.[18]. Different modeling of $\vec{u}$ leads to different $\chi_0(T)$. Often, one may approximate the behaviors of $\vec{u}$ via a bistable system that is characterized by a frequency $\frac{k_B T_1}{\hbar}$, at which the system rustles. In pseudo-spin modeling, T_1 is simply a constant and measures how fast the spin flips, whereas within DWA, T_1 decreases with

decreasing temperature and eventually saturates at low temperatures[3]. In such cases, one easily derives Barrett formula in relating T_1 to $\tilde{\chi}_0$. However, a broader meaning may be assigned by noting that T_1 actually indicates the low temperature stiffness of the system, because, assuming the validity of Barrett formula, $\tilde{\chi}_0^{-1} \propto T_1$ for $T/T_1 \ll 1$. Thirdly, as already mentioned, the behaviors of T_1 are model dependent, implying they can serve as fingerprints in identifying the nature of the local mode.

4.3.3 Experimental T_1

The empirical T-dependence of T_1 can be found by sloving the following equation,

$$\frac{T_1}{2}\coth(\frac{T_1}{2T}) = T_0 + \frac{A}{\epsilon - \epsilon_\infty} \tag{4.20}$$

with T_0 and A^{-1} as well as ϵ (also ϵ_∞) as inputs known experimentally. However, there is certain subtleness: the high T section of the experimental $\frac{1}{\epsilon}$ seems broken into two or three straight segments, as seen in FIG.4.6. Therefore slight variations may have occured to A and T_0, which can be caused by changes in e.g. the couplings between the local modes belonging to different unit cells. Hence, the temperature dependence of $\frac{1}{\epsilon}$ may be due to (A, T_0) or T_1 or both. One must isolate the latter (as due to T_1) to pursue genuine behaviors of T_1. This is done by using segment-wise (A, T_0), which are obtained by the usual least-square fit method, to deduce T_1. The final T_1 is obtained by grafting the segments together.

We have applied the procedures to not only STO but also two other incipient ferroelectrics: $KTaO_3$ and $CaTiO_3$, so that a comparison can be made. The results are exhibited in FIG.4.6. As we see, for STO, two segments can be seen, which are indicated by the red and blue curves in panel (a) and (b), where the black curve stands for the result after grafting. Similar annotations are given to other panels. In comparison with $CaTiO_3$ and

$KTaO_3$, what is peculiar about ST is the huge dip of T_1 around $T_a \sim 105K$. It is natural to ascribe the dip to the O rotation, which occurs at the same temperature. A meticulous inspection on FIG.4 in Ref.[75] reveals more: the low T parts of ω_0^2 and $\omega_{a,c}^2$ take analogous shapes that are characteristic of zero point fluctuations, the only distinction being that the latter implies stronger such fluctuations. Hence, fluctuations become enhanced after O rotation, consistent with previous analysis. We give a brief summary of the salient features:

- In $CaTiO_3$, T_1 starts with a nearly flat section at low T, followed by a linear section, where T_1 increases monotonically without any discernible saturation at high T. This is qualitatively compatible with the DWA. But quantitatively, we **can't** fit the behavior by this model. No DWA parameter could be found to fit both the flat and the increaing part simultaneously;

- In STO, T_1 does not simply increase with temperature. Rather, it at first diminishes in a very smooth way down to zero around the AFD critical temperature T_a, and then starts to rise up. Up to our knowledge, this dip behavior has never been reported before. And it *can't* be consistent with the DWA at all. Likely, it originates from the O rotation;

- In $KTaO_3$, a similar dip behavior is noticed. But here the dip is very weak and narrow and almost not perceptible. Its nature is unidentified and its presence is unexpected, since no structural instabilites in this compound around $35K$ has been spotted;

- The T_1 behaviors in all the materials under consideration can be understood using an $O(3)$ rotor model in the presence of some cubic intra-cell anisotropy (υ), namely the ARM. It turns out that, two different υs are required for each of ST and KT, corresponding to the low-T and high-T sections, respectively.

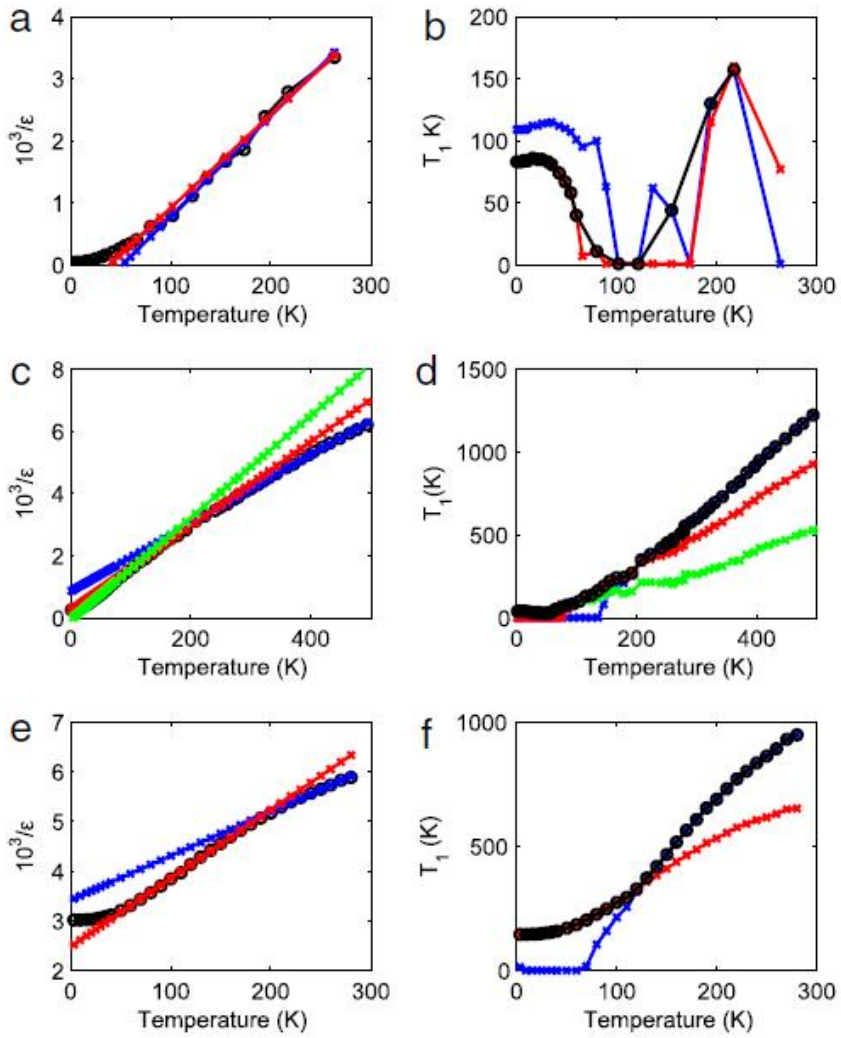

Figure 4.6: The experimental inverse dielectric constants, $1/\epsilon$ and the extracted T_1s by the method described in the text, for STO (a,b), KTO (c,d) and CTO (e,f), respectively. The black curves in the T_1 panals are obtained by grafting relevant segments from the colorful curves, as described in the text.

4.3.4 Interpreting T_1 via ARM

Ingredients of The ARM

We here recapitulate the basics of the anisotropic rotor model that was derived in chapter 2. Since the calculations will be performed in MFA, we just need to write it for a single unit cell. The model reads

$$\begin{aligned} \tilde{H}_{ARM} &= \frac{\hbar^2\hat{\Omega}^2}{2I} + \tilde{\upsilon}(n_x^4 + n_y^4 + n_z^4); \\ \frac{1}{u_0^2} &= \langle\frac{1}{u^2}\rangle, \quad I = Mu_0^2, \quad \tilde{\upsilon} = \frac{\gamma}{2}\langle u^4\rangle \end{aligned} \tag{4.21}$$

There is an intrinsic energy scale $\varepsilon_0 = \frac{\hbar^2}{2I}$, by which we can define a dimensionless constant $\upsilon = \tilde{\upsilon}/\varepsilon_0$. Reasonably, we expect that $\langle u\rangle \approx u_0 \approx l_0$.

Numerical Recipes

We have to calculate the susceptibility $\tilde{\chi}_0$ of an individual unit cell. Let Q be the Born effective charge associated with the local mode $\vec{u}$. The dipole moment is then given by $\vec{P} = Q\vec{u}$, which is coupled to an external electric field $\vec{E} = (0, 0, \tilde{E})$ via $-P_z\tilde{E}$. Then we have $\tilde{\chi}_0 = \frac{\partial\langle P_z\rangle}{\partial\tilde{E}}$. For convenience, we also introduce a dimensionless susceptibility χ_0 so that $\tilde{\chi}_0 = \frac{Q^2\langle u\rangle^2}{a^3\varepsilon_0}\chi_0$, where a denotes the lattice constant and $\chi_0 = \frac{\langle n_z\rangle}{\partial E}$. Here $E = Q\langle u\rangle\tilde{E}/\varepsilon_0$. Now expressing energies in unit of ε_0, we obtain a dimensionless Hamiltonian

$$H_{ARM} = \frac{\hat{\Omega}^2}{2} + \upsilon(n_x^4 + n_y^4 + n_z^4) - En_z, \quad H_{ARM} = \frac{\tilde{H}_{ARM}}{\varepsilon_0}$$

Here the external perturbation has been added explicitly. Note that $\langle n_z\rangle = -\langle\frac{\partial H_{ARM}}{\partial E}\rangle$. Let $\epsilon_N(E)$ be the N-th eigenvalue of H_{ARM}, then $\langle n_z\rangle = -\sum_N \rho_N \frac{\partial\varepsilon_N(E)}{\partial E}$, where $\rho_N = \frac{\exp(-\frac{\varepsilon_N}{t})}{\sum_{N'}\exp(-\frac{\varepsilon_{N'}}{t})}$ is the Boltzman factor. Similarly, $\chi_0 = -\sum_N \rho_N \frac{\partial^2\varepsilon_N(E)}{\partial E^2}$. Here all the derivatives are taken at $E = 0$ and $t = \frac{k_BT}{\varepsilon_0}$ is the reduced temperature.

Now we need to find out all the ε_N by solving the corresponding secular equation. This can be done only numerically. The representation will be chosen to be the spherical harmonics $|l,m\rangle$, namely, $\langle\theta,\varphi|l,m\rangle = Y_l^m(\theta,\varphi)$. In practice, the Hilbert space must be truncated. Presently, we truncate it at $L_c = 12$. Thus, in total L_c^2 eigenvalues will be obtained. $\hat{\Omega}^2$ is diagonal in this repsentation, $\langle l',m'|\hat{\Omega}^2|l,m\rangle = \delta_{l,l'}\delta_{m,m'}l(l+1)$. To compute the matrix elements of $n_{x,y,z}^4$ and $n_{x,y,z}$, we express all these quantities in terms of Y_l^m. It is easy to check that

$$\begin{aligned} n_x &= \sqrt{\frac{2\pi}{3}}(Y_1^{-1} - Y_1^1), \quad n_y = i\sqrt{\frac{2\pi}{3}}(Y_1^{-1} + Y_1^1) \\ n_z &= \sqrt{\frac{4\pi}{3}}Y_1^0 \\ n_x^4 &+ n_y^4 + n_z^4 = \frac{\sqrt{\pi}}{1260}(Y_4^4 + Y_4^{-4}) + \frac{4\sqrt{\pi}Y_4^0}{15} + \frac{6\sqrt{\pi}Y_0^0}{5} \end{aligned} \tag{4.22}$$

Now the required matrix elements can all be built with the following quantity

$$\begin{aligned} \int (Y_{l_1}^{m_1})^* \quad \cdot \quad Y_{l_2}^{m_2} \cdot Y_{l_3}^{m_3} &= (-1)^{m_1}\int Y_{l_1}^{-m_1} \cdot Y_{l_2}^{m_2} \cdot Y_{l_3}^{m_3} \\ &= (-1)^{m_1} C_{l_1 l_2 l_3} \times W_{0,0,0}^{l_1,l_2,l_3} \times W_{m_1,m_2,m_3}^{l_1,l_2,l_3} \\ C_{l_1 l_2 l_3} &= \sqrt{\frac{(2l_1+1)(2l_2+1)(2l_3+1)}{4\pi}} \end{aligned} \tag{4.23}$$

Here the integral is taken over the solid angle, the first line ensues from the property of spherical harmonics and in obtaining the second line we have used Wigner 3-j symbols W_m^l[103]. Now plug the matrix forms of all quantities in H_{ARM} and the eigenvalues can be found in a standard way. Then the χ_0 can be computed with the prescription offered above. All these have been mentioned in chapter 2.

ARM Vs. Experimental

To make comparison with the experimental T_1, we need establish the relation between T_1 and χ_0. From a mean-field point of view, one should have $\tilde{\chi}_0 = \frac{Q^2\langle u\rangle^2}{a^3\varepsilon_0} \cdot \frac{1}{\chi_0^{-1}-\upsilon}$, where υ is a dimensionless constant representing the molecular field strength that is pertains to T_0. Then the dielectric constant can be written as $\epsilon = \epsilon_\infty + \frac{\chi_0}{\epsilon_0} \equiv \epsilon_\infty + \frac{\tilde{A}}{\chi_0^{-1}-\upsilon}$, where ϵ_0 denotes the vacuum permitivity and $\tilde{A} = \frac{Q^2\langle u\rangle^2}{a^3\varepsilon_0\epsilon_0}$. Now we expect that, to have the Curie-Weiss law, χ_0^{-1} should follow a simple linear relation with t, namely, $\chi_0^{-1} \overset{\text{for large } t}{\rightarrow} R(t)\cdot t$, with R approaching a constant at high t. Numerically, we have computed R versus t at various υ and found that, R approaches a seemingly universal constant $R^* \approx 3$ regardless of υ, as illustrated in FIG.4.7. Making use of this knowledge, we may define T_1 with χ_0 by the following equation

$$\frac{1}{R^*\chi_0} = \frac{t_1}{2}\coth(\frac{t_1}{2t}), \quad T_1 = t_1 \times \frac{\varepsilon_0}{k_B} \tag{4.24}$$

which can be solved numerically for every t and then the as-found T_1 can be compared with that is extracted experimentally. This definition is compatible with the way of extracting T_0 and A prescribed in previous sections. In the present jargon, one recognizes that $A = \tilde{A}/R^*$ and $T_0 = (\upsilon/R^*) \times \frac{\varepsilon_0}{k_B}$. Note that the r.h.s of this equation is an even function of and increases with t_1 given t. It has a single minimum of t at $t_1 = 0$. Therefore, if the l.h.s is less than t, no real solution will exist. On such occasions, we always choose $t_1 = 0$. This trick also applies in solving eq.(4.20).

The comparison is summarized in FIG.4.8. The $\varepsilon_0/k_B \approx 175K$, $267K$and $100K$ have been chosen for ST, CT and KT, respectively. These ε_0 correspond to u_0 of the order of $10pm$. A single $\upsilon = 100$ gives a rough fit for $CaTiO_3$ over the entire temperature range under consideration. For $KTaO_3$, however, two different υs are required, namely, $\upsilon \approx 260$ above the dip temperature and $\upsilon \approx 40$ below it. Analogously, two υs are also required for STO, in which the same $\upsilon \approx 40$ can fit the data below the dip. We did not

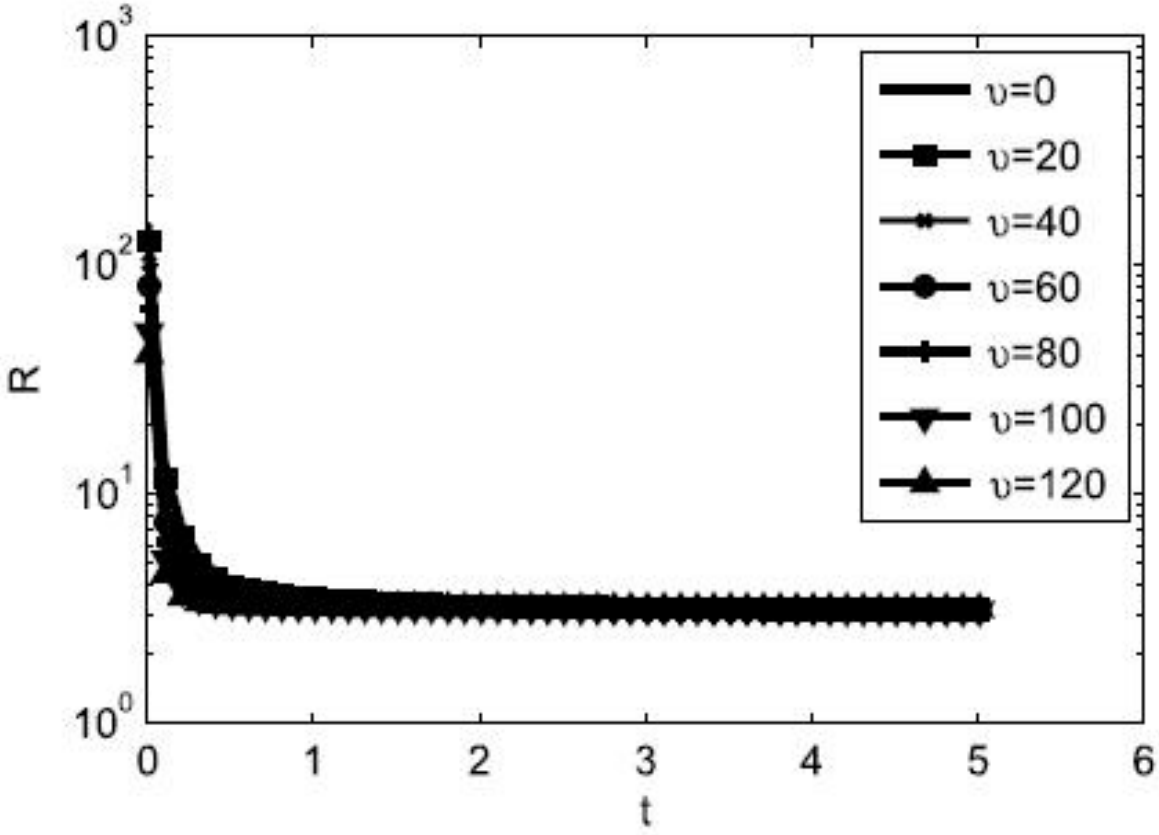

Figure 4.7: The behaviors of R vs. t at various v. All curves fall on top of each other at large t, indicating the universality of the high t limit of R.

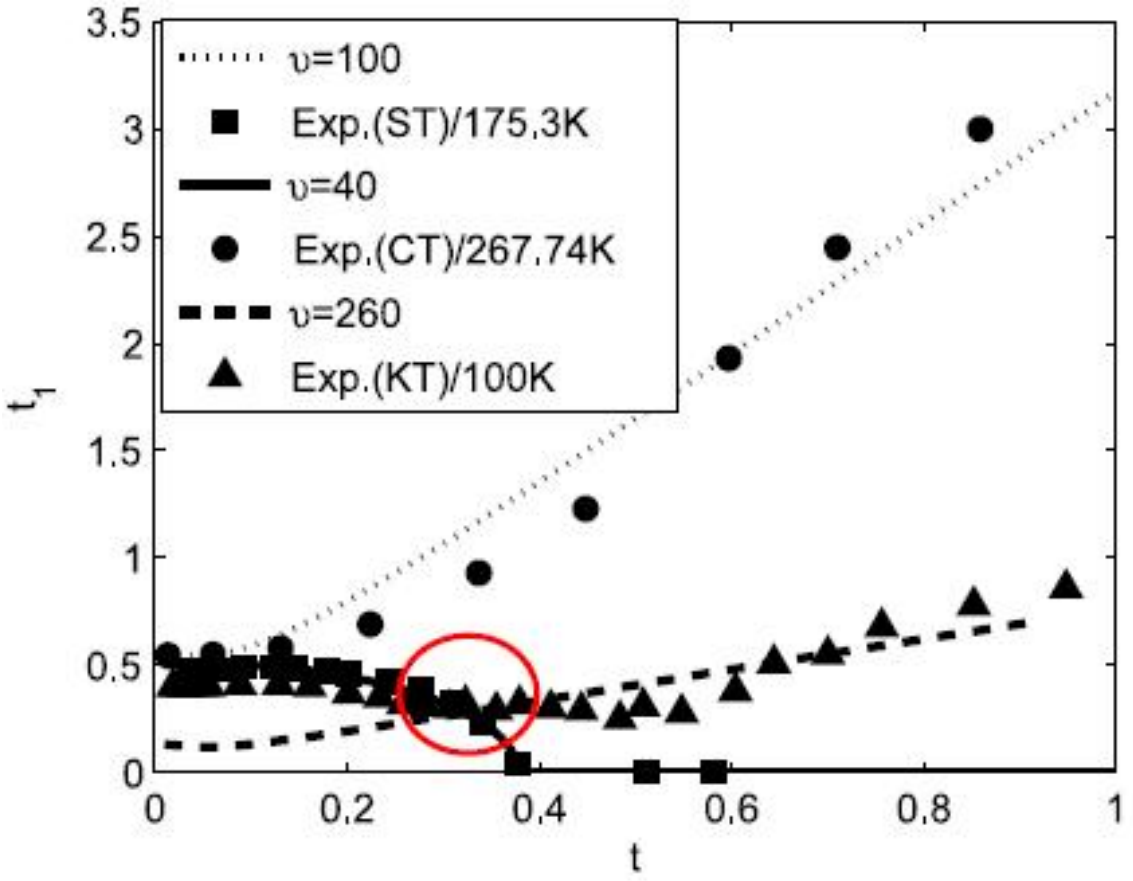

Figure 4.8: Comparison between the theoretical and experimental t_1 against t, with $R^* = R(t = 3000)$.

try to fit the high temperature data of STO, because the data in this range are scarce and inaccurate. Nevertheless, we believe that a different and bigger υ should be at work, considering the case with $KTaO_3$. Obviously, smaller υ means larger QF and vice versa. Therefore, quantum fluctuations in STO and $KTaO_3$ are stronger at low t than at high t. This is consistent with the conclusion drawn in Ref.[75] and Ref.[137].

4.4 Correspondence Between ARM and 8CM

In the last section, we have discussed an anomaly seen in the T-dependence of T_1 and shown that it is explicable in terms of the ARM. On the other hand, it is noted that the 8CM can be taken as the large-anisotropy limit of the ARM. Therefore, it is expected that, the anomaly should also submit to the 8CM. This is indeed the case, as displayed in FIG.4.9. In this figure, we exhibit that the experimental data of STO can be fitted equally well by the 8CM (with only the tunneling t_0 between nearest corners), as indicated by the red curve. Despite the apparent simpleness, there is a subtleness: although both the broken ($t_0 < 0$) and solid (t_0) red curves give nice fit, the broken one seems overally better and closer to the ARM curve (the green one). However, the broken line corresponds to an ill-defined 8CM, because the large-anisotropy limit of the ARM should always correspond to an 8CM with positive t_0. This can be confirmed by solving the ARM and examining the lowest four eigen-levels. There are two features that can be seen in the results: (1) the lowest four states always group into a singlet and a triplet; (2)as long as $\upsilon > 300$ (see the last section for υ), the singlet lies above the triplet, otherwise the structure is inverted, as demonstrated in FIG.4.10. This means that, for large υ, the corresponding t_0 is always positive. Nevertheless, considering the peculiar singlet-triplet architechture, one may relax the values of t_0. Namely, one may allow t_0 to acquire negative values. This generalization allows a full correspondence between the low energy sector of the ARM and

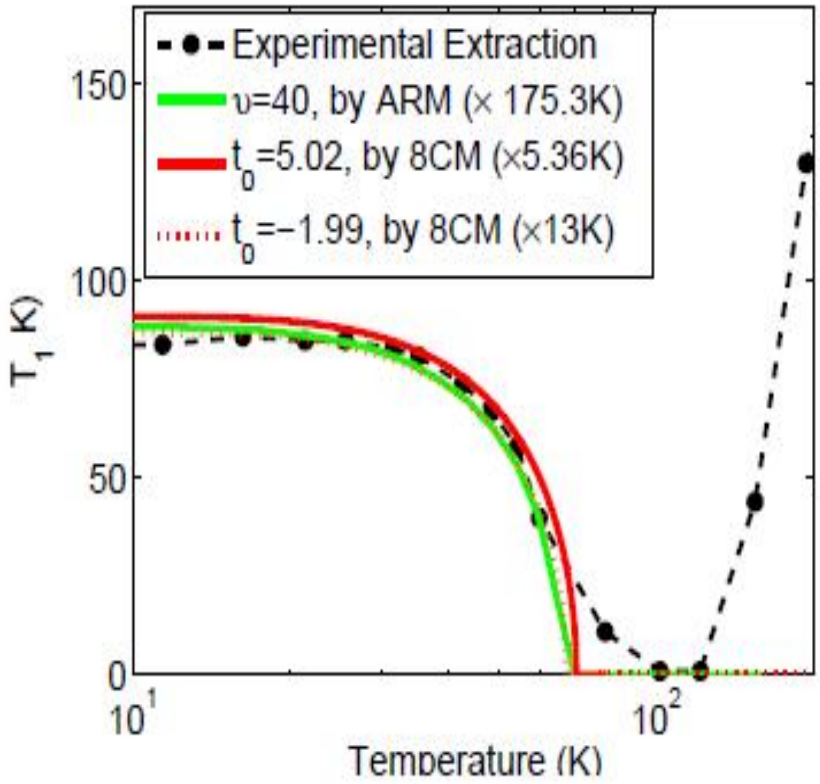

Figure 4.9: Experiment vs. theory (STO). Black dots: experimental extraction as in FIG.4.6. Red solid curve: calculations at $t_0 = 5.02$ with the 8SM. Red dotted curve: calculations at $t_0 = -1.99$ with the 8SM. Green solid curve: calculations at $\upsilon = 40$ with the ARM. Note that, the latter two curves almost coincide. Respective ε_0 are placed in the parentheses.

the 8CM: the 8CM with $t_0 < 0$ maps onto an ARM with small υ whereas the 8CM with $t_0 > 0$ maps onto an ARM with big υ. One should note that, the Hilbert spaces of them are also comparable, which is a prerequisite for the correspondence.

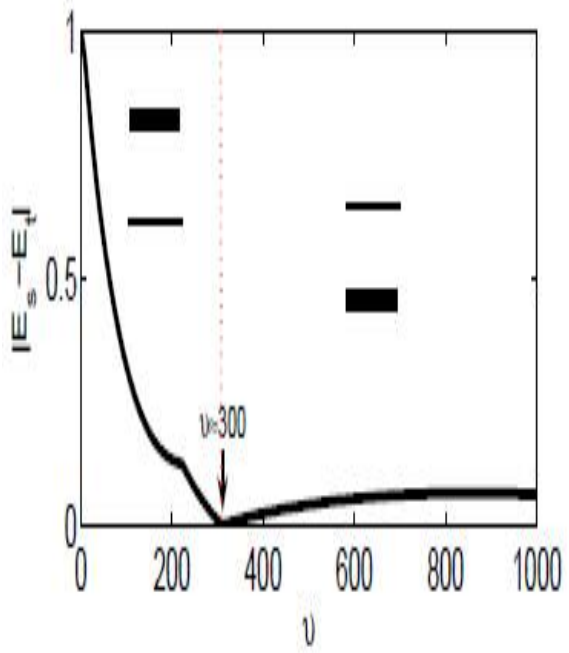

Figure 4.10: The singlet-triplet structure (of the ARM) turns upside down when tuning υ. E_s: singlet energy; E_t: triplet energy. The reversion happens around 300. Inset thick (thin) line stands for the triplet (singlet). The kink in between 200 and 300 marks a discontinuity in $\frac{\partial|E_s-E_t|}{\partial\upsilon}$, implying a transition.

4.5 Under Strong Electric Field

4.5.1 Introduction

Here we investigate what might happen to STO under a sufficiently strong external electric field along, say, the z-direction. We hope the field is strong enough to suppress any fluctuations along this direction, i.e., the variables in that direction are totally frozen. Under such circumstances, out of the eight minima of V_{Ti}, only the four in the field direction have to be included. To focus on the low energy physics, it might be appropriate to consider a model that is morally similar to the ARM or 8CM but with reduced number of variables. Actually we write the model as

$$H_{4SM} = \sum_{i,\nu,\nu'} t_{\nu,\nu'} |\nu; i\rangle\langle i; \nu'| - \sum_{<i,j>} J_{ij} \vec{n}_i \cdot \vec{n}_j \tag{4.25}$$

We shall assume J_{ij} vanishes except for the pair of adjacent sites, in which case it is a positive constant J. Besides, $t_{\nu,\nu'} = t$ for nearest neighboring corners and $t_{\nu,\nu'} = t'$ for next nearest neighboring corners. The readers are referred to FIG.4.11 for the definitions of the quantities involved in this Hamiltonian.

Conspicuously, the physics contained in H_{4SM} are determined by two parameters: $\lambda = t'/t$ and $g = t/J$, in addition to the temperature T. As in H_{IM}, the strength of the C_4 anisotropy is reflected in t, which increases as the anisotropy becomes weaker. In what follows, we will demonstrate that, an $SO(2)$ symmetry can be approximately revived by increasing both t and t'. This recovery is most complete for $\lambda = 1$, at which the gap Δ_2 (see FIG.4.11) disappears. Now that the $SO(2)$ represents a continuous symmetry, by Nambu-Goldstone's theorem[143], massless bosons (NGB) must show up in the phase (actually a pseudo-phase, hereafrer referred to as the S-phase) where this symmetry is spontaneously broken. Such bosons are indeed found and their energy dispersions are

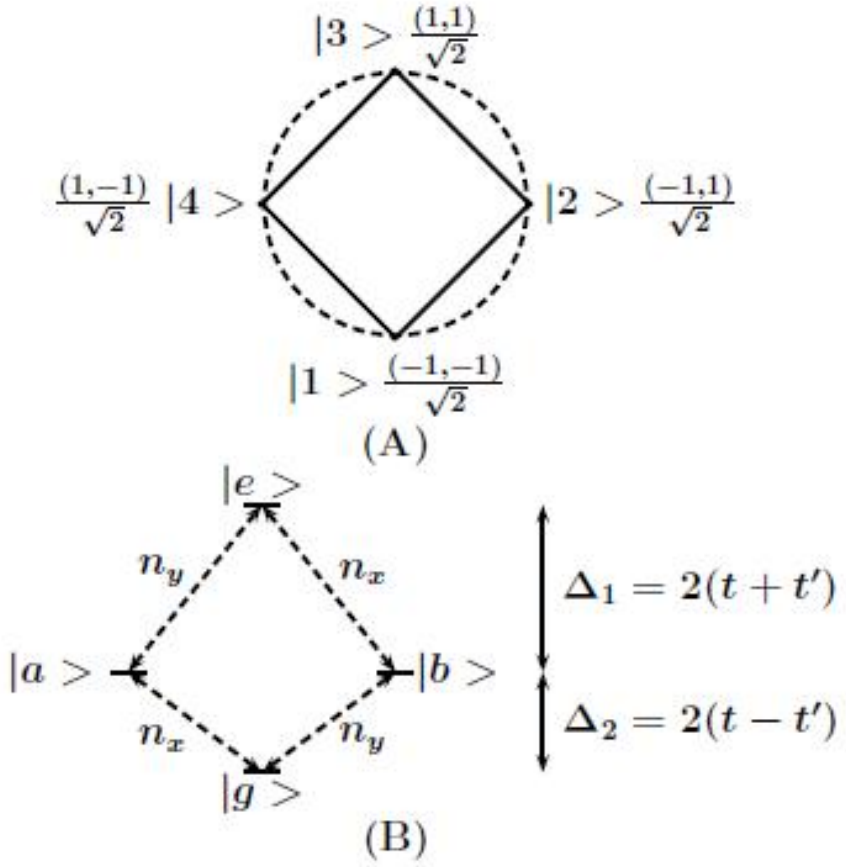

Figure 4.11: The schematic of the 4SM and the energy level structure of the H_0. (A): the O(2) rotor as indicated by the dashed circle and the cube mentioned in the text, whose corners give the eigenstates of $\vec{n}$; (B): the level structure of H_0, characterized by two gaps, Δ_1 and Δ_2, separating the singlets from the doublet. In (A), beside each corner state, $|\nu\rangle$, with $\nu = 1, 2, 3, 4$, the corresponding position vector $\vec{R}_\nu = (X_\nu, Y_\nu)$ is displayed. In (B), the non-vanishing matrix elements of n_x and n_y are visualized. In terms of $\vec{k}$, one has $|e\rangle = |(0,0)\rangle$, $|g\rangle = |(\pi,\pi)\rangle$, $|a\rangle = |(0,\pi)\rangle$ and $|b\rangle = |(\pi,0)\rangle$.

shown to be the same as in the XY-model[144]. It is also shown that, by tuning λ, first-order quantum phase transitions, which are quite rare in other systems[145], could happen. The discontinuous nature of these transitions is argued to be a corrolary of the S-phase. The phase diagram, which displays a pseudo-tri-critical point (PTC), is sketched based on self-consistent mean field calculations.

4.5.2 Phase Diagram

We start with discussing the behaviors of the on-site term (hereafter referred to as H_0) of H_{4SM}. It can be exactly solved due to the translatonal symmetry regarding a single cube. Every eigenstate of H_0 can be assigned a unique wave vector $\vec{k} = (k_x, k_y)$, where k_x (and k_y) can be either π or 0. These $\vec{k}$ states are related to the ν states by Fourier transforms: $|\vec{k}\rangle = \frac{1}{2}\sum_\nu \exp(i\vec{k}\cdot\vec{R}_\nu)|\nu\rangle$. The resulting energy architecture is exhibited in FIG.4.11, where one can see a doublet and two singlets. They are spaced by two gaps $\Delta_1 = 2t(1+\lambda)$ and $\Delta_2 = 2t(1-\lambda)$. Now suppose Δ_1 is very big in comparison with both Δ_2 and J, in which case the low energy physics should be essentially independent of Δ_1. We may then ignore the top state $|e\rangle$ (see FIG.4.11), which has the highest energy among the $\vec{k}$ states. Under this approximation, we argue that, the original $SO(2)$ symmetry is fully restored. To show this, we at first examine the mean-field (MFA) behaviors, which are governed by this Hamiltonian, $H_{SCMF} = \Delta_2(|a\rangle\langle a| + |b\rangle\langle b|) - \{\frac{|g\rangle}{\sqrt{2}}(h_x\langle a| + h_y\langle b|) + h.c.\}$. Here $\vec{h} = J(0)\langle\vec{n}\rangle$, with $J(0) = zJ$ (z is the coordination number, which is 6 for cubic lattice) being the molecular field strength. This H_{SCMF} can be easily solved by a unitary transformation that combines $|a\rangle$ and $|b\rangle$ like this: $|A\rangle = \frac{h_x|a\rangle + h_y|b\rangle}{\sqrt{\vec{h}^2}}$ and $|B\rangle = \frac{-h_y|a\rangle + h_x|b\rangle}{\sqrt{\vec{h}^2}}$. With the new basis, the Hamiltonian becomes $H_{SCMF} = \Delta_2(|A\rangle\langle A| + |B\rangle\langle B|) - \frac{h}{\sqrt{2}}(|A\rangle\langle g| + h.c.)$, where $h = \sqrt{h_x^2 + h_y^2}$. The three eigenvalues (in units with $J(0) = 1$) correspond to the non-bonding $\omega_0 = \Delta_2$, the anti-bonding $\omega_+ = \frac{\Delta_2 + \sqrt{\Delta_2^2 + 2h^2}}{2}$ and the bonding $\omega_- = \frac{\Delta_2 - \sqrt{\Delta_2^2 + 2h^2}}{2}$. At $T = 0$, the self-consistent condition, $\langle\vec{n}\rangle = -\nabla_{\vec{h}}\omega_-$, allows us to get the magnitude of

the order parameter (OP, i.e., $n_s = |\langle \vec{n} \rangle|$) as

$$n_s \equiv |\langle \vec{n} \rangle| = \sqrt{\frac{1 - \Delta_2^2}{2}} \tag{4.26}$$

regardless of its direction. The fact that all ω here depend only on the length of the OP implies the free energy density, F, also depends only on n_s. Therefore, the $SO(2)$ symmetry is indeed fully restored. Clearly, this restoration hinges critically on the possibility of decoupling $|B\rangle$ from $|g\rangle$, which would be impossible if the effects from $|e\rangle$ were not negligible. To facilitate later discussions, the phase that results from a spontaneous breaking of this approximate $SO(2)$ symmetry shall be called the S-phase, whose OP is just determined by eq.(4.26).

To gain more insight, we return to the exact H_{4SM}. For simplicity, we focus on $T = 0$. Apparently, for very small t, the effects from $|e\rangle$ are significant and the F should depend on both the magnitude and direction of the OP in a fasion that observes C_4 symmetry. The phase that results from spontaneously breaking the C_4 symmetry shall be called the C-phase. As t increases, the direction dependences of F should be less and less visible. Now the question is, does there exist a transition from the C- to the S-phase? We have numerically solved the H_{4SM} within the MF frame and found no sharp transition, but a strong crossover is clearly discernible for λ close to 1. The results are shown in FIG.4.13 and FIG.4.12. By virture of C_4 symmetry, exact MF solutions can exist in only three types: the C-type with $\langle \vec{n} \rangle = \frac{n_c}{\sqrt{2}}(1, 1)$ pointing to the cube corners, the M-type with $\langle \vec{n} \rangle = n_m(1, 0)$ pointing to the edge centers and the third (O) a trivial one corresponding to the disordered phase. The solutions with their Fs as a function of t or λ are shown in FIG.4.12 at $T = 0$. From FIG.4.12(A,B), the quantum phase transition at $t = t_c$ is clear, separating the ordered phase from the disordered one. Expectedly, t_c increases as λ increases. The remarkable thing is that, t_c can be precisely predicted with eq.(4.26), even

though this equation is obtained ignoring $|e\rangle$. According to eq.(4.26), $t_c = \frac{0.5}{1-\lambda}$, which gives $t_c = 0.5$ at $\lambda = 0$ and $t_c = 5$ at $\lambda = 0.9$, in complete agreement with numerical computations. All these hint that, $|e\rangle$ is indeed negligible, at least around t_c. Close inspection on the differences between what happens with $\lambda = 0$ and $\lambda = 0.9$ reveals a crossover in the latter, as manifested in the turning point seen around $t = 0.3$ in n_c. Crossing this point, there is a great drop in the $|F_c - F_m|$. We decipher this drop as the signature of the aforementioned crossover from the C- to the S-phase. To support this claim, we in FIG.4.13 plot the susceptibility of n_c with respect to t. One can see two downward peaks in $\frac{\partial n}{\partial t}$, one of which is broad while the other is very sharp. Obviously, comparing with FIG.4.12(A,B), the sharp peak indicates a real transition while the broad one alludes to a strong crossover. To demonstrate the invariance of F under $SO(2)$ in the S-phase, we have solved the MF equations for all OP directions and only very tiny variations can be observed in F. Based on $\frac{\partial n}{\partial t}$, we have sketched a phase diagram in the t-T plane in the inset of FIG.4.13. The foremost aspect is the existence of a point where three phases meet, resembling the tri-critical point in the case of water, thence the name PTC. That the S-phase occupies a large volume reminds its robustness.

In FIG.4.12(C,D) the results versus λ are shown. Surprisingly, *first-order* quantum phase transitions, which are characterized by a discontinuity in the first derivative of F, are found to occur at $0 < \lambda_{c1} < 1$ and $\lambda_{c2} > 1$. In the region $(\lambda_{c1}, \lambda_{c2})$, one finds the ordered phase while outside it the disordered phase exists. Obviously, such transitions are also predicted by eq.(4.26). In line with our analysis, the ordered phase here should primarily bear the characters of the S-phase. Generally, a first-order phase transition involves a change in the number of total active freedom of degrees, which is believed also at work in the present case. Across the transition from the S-phase to the disordered phase, the $|e\rangle$ state gets released. In other words, the disordered phase has four active states per site but the S-phase has essentially only three, whence a change in the number of states.

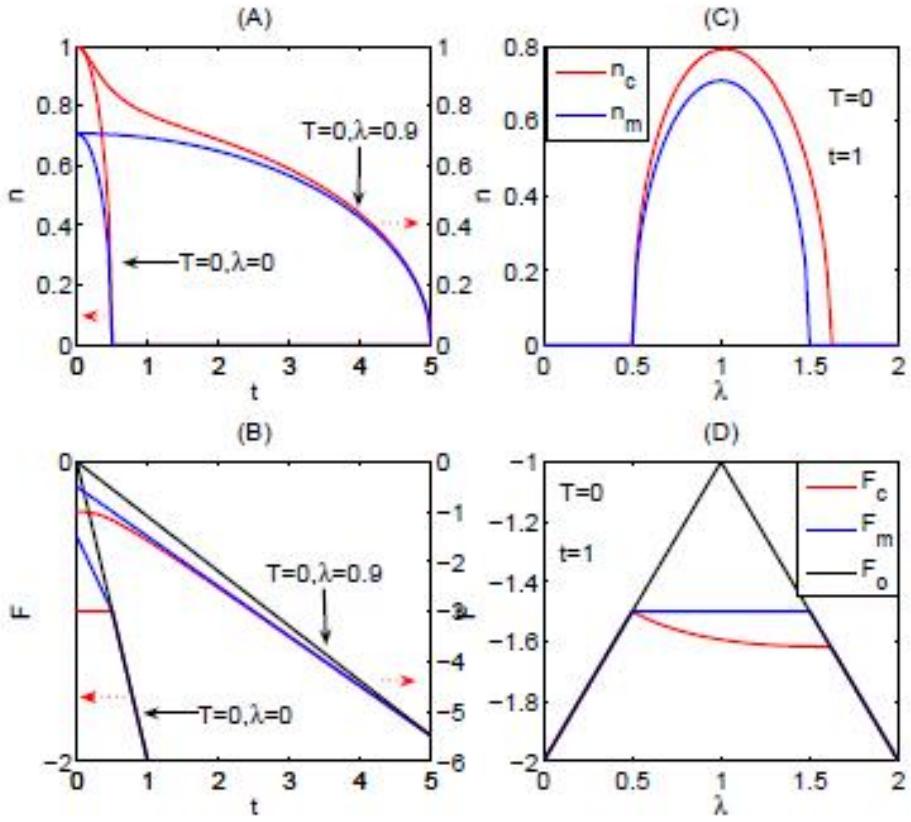

Figure 4.12: Numerical solutions at $T = 0$ of the MF equations of H_{4SM}. The c-type solution is written as $\langle \vec{n} \rangle_c = n_c(1,1)/\sqrt{2}$ and the m-type as $\langle \vec{n} \rangle_m = n_m(1,0)$. All energies are measured in units with $J(0) = 1$. (A) $n_{c,m}$ and (B) $F_{c,m}$ vs. t; (C) $n_{c,m}$ and (D) $F_{c,m}$ vs. λ. As predicted by eq.(4.26), two phase transitions are seen as λ is tuned. At $T = 0$ and $t = 1$, both transitions are discontinuous. In the text, this is explained assuming that the ordered phase is primarily the S-phase.

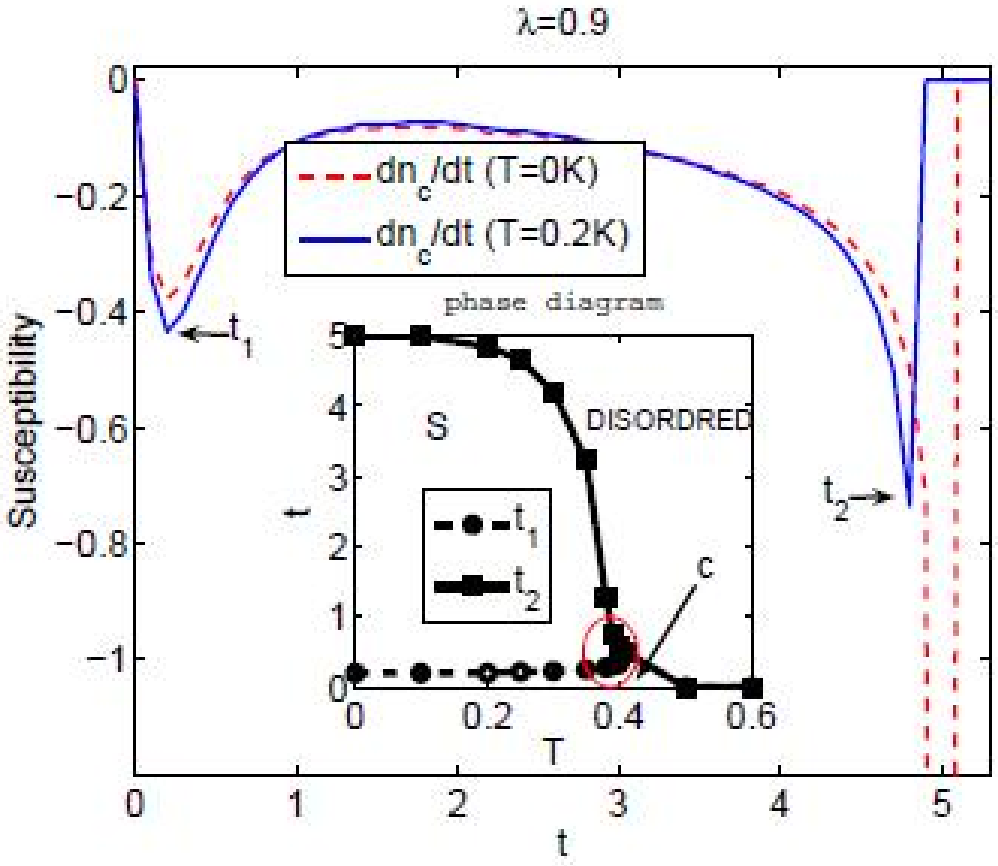

Figure 4.13: The susceptibility of the $n_{c,m}$ with respect to t for $\lambda = 0.9$ at $T = 0$ and $T = 0.2$. See text for the meanings of the peaks at t_1 and t_2, respectively. Inset: a schematic of the MF phase diagram of H_{4SM}, on which three phases are noted: the C-phase, the S-phase and the disordered phase. The dashed boundary, which is based on peak t_1, indicates the strong crossover between the C- and S-phase, while the solid line based on peak t_2 signifies the real transition between the S- and the disordered phase. These three phases meet at a single point, the pseudo-tri-critical point, as enclosed by the red ellipse.

4.5.3 Nambu-Goldstone Modes

After showing the legitimacy of ignoring the $|e\rangle$ and establising the recovery of the $SO(2)$ symmetry, we proceed to find out the NGB that must exist in the S-phase due to Nambu-Goldstone's theorem[143]. We at first construct explicitly the symmetry generator in terms of the orientation operators. Notice that, in the reduced Hilbert space which excludes $|e\rangle$, H_0 up to a constant can be written as $H_0 = -\Delta_2 \sum_i (\hat{n}_x^{i2} + \hat{n}_y^{i2})$. Then the entire Hamiltonian becomes

$$H = -\Delta_2 \sum_i \vec{\hat{n}}_i^2 - \sum_{<i,j>} \frac{J_{ij}}{2} \vec{\hat{n}}_i \cdot \vec{\hat{n}}_j \tag{4.27}$$

Under $SO(2)$ rotation by an angle θ, $\hat{n}_{x,y}$ are transformed to new vector $\hat{n}'_{x,y}$, which are related as

$$\begin{aligned} \hat{n}'_x &= \cos(\theta)\hat{n}_x + \sin(\theta)\hat{n}_y \\ \hat{n}'_y &= -\sin(\theta)\hat{n}_x + \cos(\theta)\hat{n}_y \end{aligned} \tag{4.28}$$

This transformation obviosuly leaves H invariant. On the other hand, one must also have $\vec{\hat{n}}' = U^\dagger(\theta)\vec{\hat{n}}U(\theta)$, where $U(\theta)$ is an element of $SO(2)$ group. Being a contiuous group, $U(\theta) = \exp(i\theta\hat{T})$, where $\hat{T}$ is hermitian and the generator of $SO(2)$. It is easy to find out $\hat{T}$ by looking at small θ, in which case one has

$$\begin{aligned} \hat{n}'_x &\approx \hat{n}_x + i\theta[\hat{n}_x, \hat{T}] \\ \hat{n}'_y &\approx \hat{n}_y + i\theta[\hat{n}_y, \hat{T}] \end{aligned} \tag{4.29}$$

Here [..., ...] indicates a commutator. By comparison with eq.4.28, we arrive at $i[\hat{n}_x, \hat{T}] = -\hat{n}_y$ and $i[\hat{n}_y, \hat{T}] = \hat{n}_x$, which can be satisfied with $\hat{T} = \frac{\hat{n}_m - \hat{n}_p}{\sqrt{2}i}$. Here $\hat{n}_p$ and $\hat{n}_m = \hat{n}_p^\dagger$ are defined by this algebra: (1) $[\hat{n}_x, \hat{n}_p] = \hat{n}_p$, (2) $[\hat{n}_x, \hat{n}_m] = -\hat{n}_m$, (3) $[\hat{n}_p, \hat{n}_m] = \hat{n}_x$ and (4) $\hat{n}_y = \frac{1}{\sqrt{2}}(\hat{n}_p + \hat{n}_m)$. The physical meanings of $\hat{n}_{p,m}$ turns clear once it is recognized that, this

algebra is also satisfied by the spin ladder operators $S_{\pm}$. Explicitely, we write $\hat{n}_p = |0\rangle\langle -| - \exp(i\phi)|+\rangle\langle 0|$, where $|0\rangle$, $|-\rangle$ and $\exp(i\phi)|+\rangle$ are the eigenstates of $\hat{n}_x$. Here $\exp(i\phi)$ is an arbitrary global phase that is usually taken to be 1. Note that, we have dropped the site index that are understood along with these quantities. The similarity between the H and the spin-1 XY model[144] suggested by the algebra is striking. Obviously, the inter-site term of H is basically identical to H_{XY}.

Denote the ground state of the S-phase by $|G\rangle$ and its energy by ε_G. NGB represent certain type of small fluctuations about $|G\rangle$. They are created by acting a local $SO(2)$ transformation, $U(\{\theta_i\})$, upon $|G\rangle$. Here $U(\{\theta_i\}) = \exp(i\sum_i \theta_i \hat{T}_i) = \prod_i U(\theta_i)$. Utilizing the translational symmetry, we write the NGB state as $|\vec{q}\rangle$, whose energy is denoted by $\varepsilon(\vec{q})$ relative to ε_G. The wave vector $\vec{q}$ plays role in that $\theta_i = \theta_{\vec{q}}\exp(i\vec{q}\cdot\vec{R}_i) + \theta^*_{\vec{q}}\exp(-i\vec{q}\cdot\vec{R}_i)$. Let's write H differently. Using that $2\vec{\hat{n}}_i\cdot\vec{\hat{n}}_j = \vec{\hat{n}}_i^2 + \vec{\hat{n}}_j^2 - (\vec{\hat{n}}_i - \vec{\hat{n}}_j)^2$, one finds

$$H = -(\Delta_2 + \frac{J(0)}{4})\sum_i \vec{\hat{n}}_i^2 + \frac{1}{4}\sum_{<i,j>} J_{i,j}(\vec{\hat{n}}_i - \vec{\hat{n}}_j)^2 \tag{4.30}$$

Now the NGB energy is calculated as $\varepsilon(\vec{q}) = \langle\vec{q}|H|\vec{q}\rangle - \varepsilon_G$. By the defintion of $|\vec{q}\rangle$, we have $\langle\vec{q}|H|\vec{q}\rangle = \langle G|H'|G\rangle$, where $H' = U^\dagger(\{\theta_i\})HU(\{\theta_i\})$. Evidently, the first term of H in eq.4.30 always commutes with $U(\{\theta_i\})$. And for small fluctuations, one has

$$U^\dagger(\vec{\hat{n}}_i - \vec{\hat{n}}_j)U \approx (\vec{\hat{n}}_i - \vec{\hat{n}}_j) + i\{\theta_i[\vec{\hat{n}}_i, \hat{T}_i] - \theta_j[\vec{\hat{n}}_j, \hat{T}_j]\} \tag{4.31}$$

Eventually, we obtain

$$\begin{aligned} H' &= H + linear - terms - in - \{\theta\} \\ &+ \frac{1}{4}\sum_{<i,j>} J_{i,j}\{\theta_i[\vec{\hat{n}}_i, i\hat{T}_i] - \theta_j[\vec{\hat{n}}_j, i\hat{T}_j]\}^2 \end{aligned} \tag{4.32}$$

Since ε_G is a saddle point in the energy of the system, the linear terms must vanish over

$|G\rangle$. Further, since we are considering an ordered phase in which long-range correlations exist, we may write $\langle G|[\vec{\hat{n}}_i, i\hat{T}_i]^2|G\rangle = \langle G|[\vec{\hat{n}}_j, i\hat{T}_j]^2|G\rangle = \langle G|[\vec{\hat{n}}_i, i\hat{T}_i][\vec{\hat{n}}_j, i\hat{T}_j]|G\rangle$. Finally,

$$\varepsilon(\vec{q}) \propto (i\vec{\nabla}\theta)^2 = \vec{q}^2 \tag{4.33}$$

where we have taken the long wavelength limit by replacing $(\theta_i - \theta_j)^2$ (divided by the lattice constant) with $(\vec{\nabla}\theta)^2$. Therefore, the NGB follow a quadratic dispersion, the same as in ferromagnets[143]. For their vanishing mass, the NGB must dominate the slow dynamics and the low temperature behaviors of the system. In particular, the specific heat should follow the power law, $C_v \propto T^\eta$, where the exponent is $\frac{3}{2}$ for quadratic dispersion[143].

In addition to the NGB, which are massless, there exist a spectrum of massive excitations (ME), if $\Delta_2 \neq 0$. To reveal them, we introduce a reference state, $|vac\rangle$, which has all sites in $|-\rangle$, i.e., $|vac\rangle = \prod_i |-\rangle_i$. Assume $|G\rangle$ lies much close to $|vac\rangle$, so that $\vec{\hat{n}}_x$ can be nearly regarded as a simple c-number in all the states under interest. Given this approximation, one has $[\hat{n}_p, \hat{n}_m] \approx -1$. Thus, we can carry out the Holstein-Primakoff transformation[146] to express every quantity in terms of bosonic annihilation and generation operators, a and $a^\dagger$. Specifically, we write $\hat{n}_p = a^\dagger$, $\hat{n}_m = a$, $\hat{n}_x = a^\dagger a - 1$ and $\hat{n}_y = \frac{1}{\sqrt{2}}(a + a^\dagger)$ as well as $\hat{T} = \frac{1}{\sqrt{2}i}(a - a^\dagger)$, from which we see that $\hat{n}_y$ and $\hat{T}$ are actually conjugates and that $U(\theta)$ displaces $\hat{n}_y$ by θ. The NGB would be revisited if the H_0 were treated as a constant as above. Relaxing this constraint, we get the ME. By substituting $\hat{n}_x^2 + \hat{n}_y^2 \approx \frac{1}{2}(a^{\dagger 2} + a^2) - a^\dagger a$ and $\hat{n}_x^i \hat{n}_x^j \approx -(a_i^\dagger a_i + a_j^\dagger a_j)$ as well as $\hat{n}_y^i \hat{n}_y^j = \frac{1}{2}(a_i^\dagger a_j^\dagger + a_i a_j + a_i^\dagger a_j + a_j^\dagger a_i)$ in eq.(4). Up to a constant and after a Fourier transform, we find $H \approx \sum_{\vec{q}}(\Delta_2 + \frac{J(0)}{2} - \frac{J(\vec{q})}{4})(a_{\vec{q}}^\dagger a_{\vec{q}} + a_{-\vec{q}} a_{-\vec{q}}^\dagger) + \frac{J(\vec{q}) - 2\Delta_2}{4}(a_{\vec{q}}^\dagger a_{-\vec{q}}^\dagger + a_{-\vec{q}} a_{\vec{q}})$. It can be diagonalized with a canonical transformation C, which acts upon $(a_{\vec{q}}, a_{-\vec{q}}^\dagger)^{tr}$. After C, one arrives at $H = \sum_{\vec{q}}\{\varepsilon_\beta \beta_{\vec{q}}^\dagger \beta_{\vec{q}} + \varepsilon_\alpha \alpha_{\vec{q}}^\dagger \alpha_{\vec{q}}\}$, where $(\alpha_{\vec{q}}, \beta_{\vec{q}}^\dagger)^{tr} = C(a_{\vec{q}}, a_{-\vec{q}}^\dagger)^{tr}$. Here tr takes care of the transpose. Notice that the ground state $|G\rangle$ is the vacumn of α- and β-type quasi-particles, whereas $|vac\rangle$ is the vacumn of

a-type ones, implying $|G\rangle \neq |vac\rangle$. Two branches result with energies $\varepsilon_\beta = \frac{\Delta_2 + J(0)}{2}$ and $\varepsilon_\alpha = \frac{3\Delta_2}{2} + \varepsilon(\vec{q})$, respectively, where $\varepsilon(\vec{q}) = \frac{J(0) - J(\vec{q})}{2}$ is simply the NGB energy.

4.5.4 Remarks

We add a few remarks to conclude this section. **(1)** In the Ising model, only massive excitations can exist. In the XY model, only NGB exist. But in H, both species are found. This unique feature comes from the H_0. As the NGB is associated with a continuous symmetry observed by H_0, the massive excitations are rooted at the elimination of $|e\rangle$, owed to which $\hat{\vec{n}}^2$ becomes a q-number. Despite the existence of ME, the low temperature description of H is evidently identical to that of the XY model, because only NGB are relevant in the low temperatre limit. **(2)** As emphasized, the SO(2) symmetry, though robust, is only approximate, which means the NGB should gain a very small mass[147]. In other words, they are virtually pseudo-NGB[148, 149, 150]. **(3)** The as-conducted analysis did not consider the effects of strains, which are expected to interact strongly with the massless modes in real materials; thus, more work need be done to see if the S-phase can occur in STO.

Chapter 5

IMPLICATIONS FOR LIGHTLY DOPED CUPRATE SUPERCONDUCTORS

5.1 Introduction

In this chapter, we employ the insights garnered from previous chapters to examine high temperature superconductors (HTC), whose representative is $La_{2-x}Sr_xCuO_4$ (LSCO). Here x denotes the doping level. These compounds host a bunch of myths that have engrossed enormous efforts since their discovery[151]. What brings them close to perovskites is the CuO_2 plane, which is a reminiscence of the BO_2 plane in a genuine perovskite ABO_3. We confine ourselfves to this particular issue: the influence of O phonon on the state of an excess hole in that plane. In some HTC models, the O vibrations are even supposed to be the main pairing channel[152, 153, 154].

Even in the insulating phase of HTC, the O vibrations can play an important role. Let x and T stand for the concentration of doped holes and temperature, respectively. At

low T and small x, these excess holes have been experimentally demonstrated to be randomly quenched and localized[155]. A plenty of work have been done to address problems regarding the nature of this localized state. No consensus has been reached, but such a state is likely to be underlying the pseudogap phase and therefore can be of fundamental importance in understanding the entire phase diagram of HTC[156]. In early works, an excess hole was thought to be confined exactly on an O site[157]. However, this picture does not respect the underlying lattice symmetry and disregards the formation of Zhang-Rice-Singlets. In Ref.[1], any localized hole was proposed to simultaneously take up two adjacent Zhang-Rice states[92] through tunneling. Such a complex state can be stable if the O sublattic is distorted locally. A very similar idea[158] had been forwarded to interpret the chekerboard pattern detected in the pseudogap phase[159].

Making use of the knowledge obtained in chapter 2 about O vibrations, we shall propose a polaron state for excess holes in the low concentration regime. Such state turns out to a mixture of Zhang-Rice singlet and O phonon. We state that, the V_O established in **sections 2.1 and 2.3** should equally apply to the O vibrations in CuO_2 plane. As is clear from the derivation of V_O, for it to be valid the only condition is the existence of an effective $3d_{x^2-y^2}$ and an effective $2p_x$, both partially filled and the former lying above the latter in energy. In $BaTiO_3$, these orbitals are no more than the usual $Ti3d_{x^2-y^2}$ and the $O2p_x$. Nonetheless, when talking of the Cu^{2+} in cuprate superconductors, one must take into account the Hubbard repulsion U. In case of large U, the $d_{x^2-y^2}$ splits into the upper and lower Hubbard orbitals. At half-filling, the lower orbital is nearly always fulfilled while the upper one is empty. In the level structure, one should have the upper Hubbard orbital lying at the highest, the lower Hubbard orbital the lowest while the O2p in between. Therefore, the relevant orbital entering eq. (2.21) are essentially the $O2p_x$ and the upper Hubbard orbital. Since the latter is empty and the corresponding Δ_{dp} is positive, the form of E_2 should still apply.

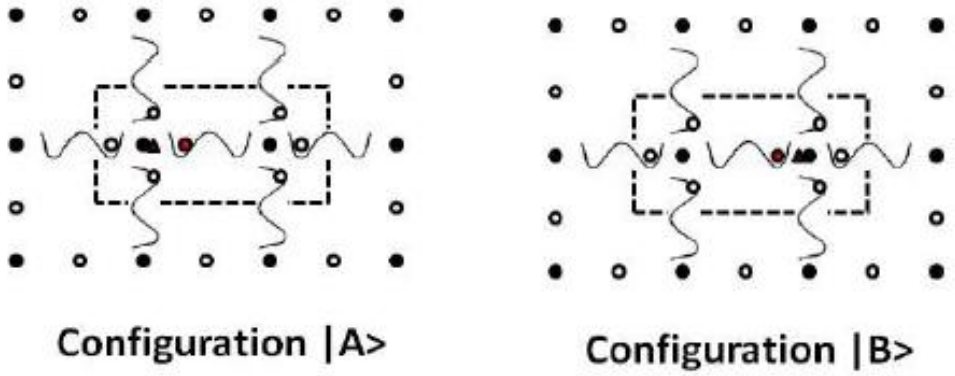

Figure 5.1: The polaron state as explained in the text. Solid circles denote the Cu sites, empty ones the O sites, and the triangle the doped hole. A plaquette is made of a Cu site and the O sites surrounding it. The dashed rectangle encloses the polaron, which is supposed to be in a combination of the two low energy states $|A\rangle$ and $|B\rangle$, respectively. Such states can be stable at low temperatures, as argued in text.

5.2 Assumptions

We shall consider a single CuO_2 sheet, which is widely believed to be responsible for the essential physics. A profound mystery lies with the pseudogap phase, which initiates with a glassy-like state resulting from quenched holes[160]. It is characterized by a $T^*(x)$ line on the lightly doped side in the $x-T$ phase diagram. Experimentally, the electronic excitations in this region were found extremely incoherent at small x prior to the onset of superconductivity and gradually gaining coherence at increasing x[156]. The incoherence is likely to originate from hole localization occuring at small x, as observed by STM probes[161]. The nature of this localized hole state was recently hypothesized to represent a compounded object comprising a doped hole, local magnons and local lattice distortion[1]. Here we elaborate on this picture and give a more quantitative analysis.

The undoped CuO_2 sheet is an antiferromagnet configured as $Cu3d^9O2p^6$. Each Cu site is furnished with a spin. Now we dope a very small number of holes into this sheet, which are supposed to be randomly quenched and populate Zhang-Rice states[1, 92]. Their

correlations may be ignored since their mean distance is large at small x. We therefore focus on a single hole and imagine it falls on a Zhang-Rice state $|1\rangle$. What will happen to it? First, it will interact strongly with the Cu spin $\vec{S}_1$ in the same plaquett, as first proved in Ref.[92]. Second, it will tunnel to another Zhang-Rice state $|2\rangle$ in proximity to minimize its kinetic energy[1]. Third, this tunneling allows it to interact also with Cu spin $\vec{S}_2$. Fourth, it will pull the O sites around to maximize its interactios with Cu spins, since the interaction strength K is sensitive to the overlap between the $d_{x^2-y^2}$ and p orbital, which in turn is a function of the $Cu-O$ bond length. As reasoned in Ref.[1], the localized state should be primarily determined by the interplay between the Zhang-Rice states $|i; i=1,2\rangle$, the Cu spins $\vec{S}_{1,2}$ and the O distortion. The situation has been sketched in FIG.1, where the dashed rectangle encloses the main part of the polaron under interest. To make progress, we assume the validity of V_O as expressed in eq.(2.54). This will considerably simplify the analysis. According to that equation, we may safely neglect the O vibrations perpendicular to the $Cu-O$ bonds, since they are energetically infavorable. As seen in FIG.5.1, there is an O atom (whose displacement along the bond will be denoted by x) that is shared by both plaquettes. Among the remaining O atoms, the left three form an aggregate to be referred as A1 while the right three form aggregate A2. For each aggregate, when restricted to bond-direction vibrations only three eigenmodes can exist and evidently, among them the one that couples most efficiently to the doped hole and the Cu spins should have all the constituting O atoms moving in phase. Let's denote the coordinate of this mode by $x_{i=1,2}$, where $i=1$ and $i=2$ correspond to A1 and A2, respectively. All other modes are irrelevant and then omitted hereafter.

Further, we assume $K_l < 0$, which is possible if the covalent bond and the O polarizability are strong enough. Thus, one ends up with a double-well potential. This allows us to reduce the O Hilbert space by including only states in the vicinity of the potential minima. In other words, merely two pairs of states need be considered: $|O_1\rangle$ and $|O_2\rangle$

for the shared O atom while $|Far, i\rangle$ and $|Near, i\rangle$ for the aggregates. Here Far and $Near$ are referring to the distance of the potential minima from the corresponding Cu site. Note that each of these states can approximately be regarded as the ground state of the corresponding harmonic oscillator. Thus, the low energy sector of the O subsystem is equivalent to a system of three pseudo-spins. The Hamiltonian can in general be couched as $H_O = \Omega \sum_{i=1,2}(|Far, i\rangle\langle Near, i| + h.c.) + \Omega'(|O1\rangle\langle O_2| + h.c.)$, where Ω and Ω' denote the tunneling energies and are expected to depend conversely on the well separation $2l_0 = \sqrt{\frac{2|\gamma|}{\alpha}}$. We also expect $\Omega' \gg \Omega$, because the aggregates are much heavier than a single O atom. The eigenstates of H_O are given by $|sgn_O\rangle \otimes |sgn_1\rangle \otimes |sgn_2\rangle$ with energy $\Omega(sgn_1 + sgn_2) + \Omega' sgn_O$, where $sgn_{O,1,2} = \pm 1$ and $|sgn_O\rangle = \frac{1}{\sqrt{2}}(|O1\rangle + sgn_O|O_2\rangle)$ as well as $|sgn_i\rangle = \frac{1}{\sqrt{2}}(|Far, i\rangle + sgn_i|Near, i\rangle)$. Note that x and x_i have vanishing average over these states.

5.3 The Variational Form of A Polaron State

We proceed to conceive an approximate ground state by physical arguments. Let's for the moment forget about the kinetic energy (i.e., tunneling effects) of the hole and the O atoms. We can then let the hole simply settle on, say, the left plaquette. The ground state would then be simply the Zhang-Rice singlet (denoted by $|ZRS1\rangle$) with all O atoms pulled into the potential wells closer to the Cu site, namely, $|ZRS1\rangle \otimes |Near, 1\rangle \otimes |O_1\rangle$. Now we relax the O atoms and render it tunnel. The O states are then expected to be admixed and the ground state needs be modified. In general, we may write it as $|A\rangle = |ZRS1\rangle \otimes |\lambda', Near_1\rangle \otimes |\lambda; 1\rangle$ where $|\lambda'; Near_1\rangle = \frac{1}{\sqrt{1+\lambda'^2}}(|Near, 1\rangle + \lambda'|Far, 1\rangle)$ and $|\lambda; 1\rangle = \frac{1}{\sqrt{1+\lambda^2}}(|O_1\rangle + \lambda|O_2\rangle)$, with λ' and λ being parameters that can be determined via variational methods. Similarly, if the hole settles on the right plaquette, the state should be $|B\rangle = |ZRS2\rangle \otimes |\lambda', Near_2\rangle \otimes |\lambda; 2\rangle$ with analogous definitions of $|\lambda'; Near_2\rangle$

and $|\lambda;2\rangle$. Finally, we allow the hole to tunnel at a rate of t_0. This will mix $|A\rangle$ and $|B\rangle$ to yield the desired polaron state,

$$|P\rangle = \frac{1}{\sqrt{2}}(|A\rangle + |B\rangle)$$

For comparison, we also write down the normal state as

$$\begin{aligned} |N\rangle &= \frac{1}{\sqrt{2}}(|ZRS1\rangle + |ZRS2\rangle) \\ &\otimes \ |sgn_O = -1\rangle \otimes |sgn_1 = -1\rangle \otimes |sgn_2 = -1\rangle \end{aligned}$$

in which no O lattice distortion is assumed. The polaron formation energy E_f is hence given by the difference between the energies of $|P\rangle$ and $|N\rangle$. In evaluating E_f, that $\lambda' \approx 0$ will be assumed. This is realistic considering $t_0 \gg \Omega' \gg \Omega$.

5.4 Polaron Formation Energy

To evaluate E_f, we need to build a Hamiltonian to model the polaron depicted in FIG.5.1. Presuming localization, we may generally write it as

$$\begin{aligned} H &= J'\vec{S}_1 \cdot \vec{S}_2 + \vec{s} \cdot [K(x_1, x)\vec{S}_1 + K(x_2, x)\vec{S}_2] \\ &- \ t_0(|1\rangle\langle 2| + h.c.) + H_O + H' \end{aligned} \tag{5.1}$$

where J' denotes the coupling between $\vec{S}_{1,2}$, $K(x_i, x)$ signifies the Zhang-Rice coupling between the hole spin $\vec{s}$ and the Cu spin $\vec{S}_i$ and t_0 represents the hole tunneling energy between the Zhang-Rice states $|i = 1, 2\rangle$. Tunneling out of the rectangle is disfavored because of the distorted O aggregates. In addition, H' stands for the interactions of $\vec{S}_{1,2}$ with all the rest Cu spins of the CuO_2 layer, namely, $H' = \sum_{<i,j>,i=1,2} J(x_i)\vec{S}_i \cdot \vec{S}_j$, with

the pair $< 1, 2 >$ excluded in the summation. In the presence of anti-ferromagnetic order, one may write $H' \approx \sum_{i=1,2} J(x_i) S_i^z \cdot (-1)^i M_0$, where M_0 is the average magnetization. The spin-phonon interactions are manifested in J and K. They can be expanded as $J(x_i) = J_0 - x_i^2 |\frac{\partial^2 J}{2\partial x_i^2}|$ and $K(x_i, x) = K_0 + (x_i + x)\frac{\partial K}{\partial x_i}$, where all derivatives are taken at $x = 0$ and $x_i = 0$, the linear term in $J(x_i)$ vanishes by virtue of symmetry and that $\frac{\partial K}{\partial x_i} = \frac{\partial K}{\partial x} > 0$ has been assumed. Notice that both H' and the J'-leading term vanish when averaging over either $|P\rangle$ or $|N\rangle$, since they vanish over $|ZRS\rangle$. The stability of Zhang-Rice singlets indicates the dominance of the K-leading term over others.

Now we evaluate E_f and assess the stability of the polaron state. By definition, we have $E_f = \langle P|H|P\rangle - \langle N|H|N\rangle$. It is useful to notice that both H' and the J'-leading terms vanish when averaging over $|P\rangle$ and $|N\rangle$, since they vanish over $|ZRS\rangle$. Making use of the fact that $x = l_0(|O_2\rangle\langle O_2| - |O_1\rangle\langle O_1|)$ and that $x_i = l_0(|Near_i\rangle\langle Near_i| - |Far_i\rangle\langle Far_i|)$ and after some algebra, we find

$$E_f = \Omega + (\Omega' + \frac{t_0}{2})\frac{(1-\lambda)^2}{1+\lambda^2} - \frac{3g}{4}\frac{1-\lambda^2}{1+\lambda^2} - \frac{9g}{4} \tag{5.2}$$

where $g = l_0\frac{\partial K}{\partial x}$. The first term in E_f is no more than the lattice energy cost of pulling the aggregates while the last one is the energy lowering of ZRS due to that pulling. The energy cost as expressed in the second term has two contributions: the increasing of the lattice energy of off-center shifting the shared O atom and the increasing of the hole's kinetic energy when the hopping is impeded by that off-center shift. Meanwhile this shift lowers the ZRS energy by the amount contained in the third term. Minimizing this expression, we arrive at

$$\lambda = \sqrt{1+\beta^2} - \beta, \quad \beta = \frac{3g}{4\Omega' + 2t_0}$$

Substituting it back, the E_f can be found. When $\beta \ll 1$, one has $\lambda \approx 1 - \beta$. In this case,

the stability condition that $E_f < 0$ translates into the following

$$\frac{\Omega}{g} < \frac{9}{4} \tag{5.3}$$

which is independent of β. While if $\beta \gg 1$, one has $\lambda \approx \frac{1}{2\beta}$ and the stability condition becomes

$$\frac{\Omega}{g} < 3 \tag{5.4}$$

For general values of β, we have plotted E_f vs. β in FIG.3, where it is exhibited that for $\Omega/g < 3$, that $E_f < 0$ is much likely to be gratified and the polaron picture is quite plausible. In addition, it is seen that the main energy to be circumvented is that of pulling the aggregates while the off-center shift always results in a lower total energy.

It is possible to make a realistic estimate. Notice that expression (4) involves four parameters: t_0, Ω', Ω and g. Let's look at t_0 and g first. From the expression of K as given in Ref.[1], we learn that $K \sim V^2[\frac{1}{\Delta} + \frac{1}{U-\Delta}]$, where V is the overlap between the Cu $d_{x^2-y^2}$ and O p orbital wave functions and U is the Hubbard repulsion on Cu sites whereas Δ is the charge transfer gap. Assuming an exponetial dependence of V on the Cu-O bond length variation δ, i.e., $V \approx V_0 \exp(\frac{\delta}{y_0})$, we obtain $g \approx V_0^2[\frac{1}{\Delta} + \frac{1}{U-\Delta}]\frac{2l_0}{y_0}$. Taking $V_0 \sim 1.3$eV, $U \sim 10.5$eV, $\Delta = 3.6$eV and $\frac{l_0}{y_0} \sim 0.1$, we would get $g \approx 100$meV. Here y_0 denotes the average Cu-O bond length. Similarly, we have $t_0 \sim V_0^2[\frac{1}{\Delta} - \frac{1}{U-\Delta}] \sim 0.2$eV. On the other hand, Ω' and Ω should be much smaller, since they are lattice vibration energies. Actually, in perovskite compounds they are often found less than 200cm^{-1}, amounting to about 20meV. Given such estimates, we obtain $\beta \sim 0.6$, $\frac{\Omega}{g} \sim 0.2$ and $E_f \approx -2g \sim -t_0$, which is a very large portion of energy. Although very rough, the estimate, which is indicated by the spot in FIG.3, shows that the polaron state can be very stable.

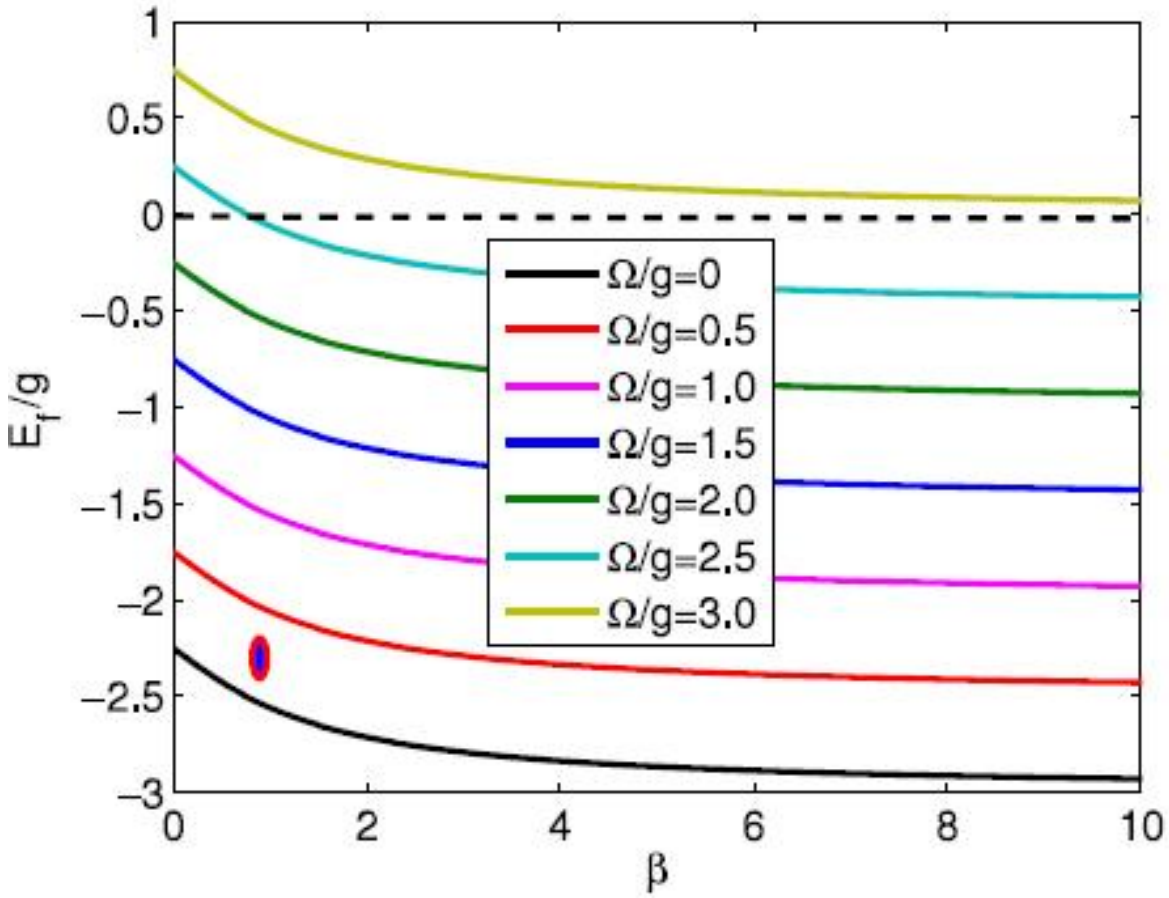

Figure 5.2: The polaron formation energy E_f as a function of β for various $\frac{\Omega}{g}$. The spot corresponds to an estimate given in the text.

5.5 Discussions

A direct corollary of the two-plaquette picture is the spatial Cu-O bond length variations at low dopings. According to this picture, a doped hole shall form a polaron with two Cu spins by attaching the O atoms nearby. As a result, three pairs of anomalous Cu-O bonds shall be created locally. With x being the doping level, we then anticipate that, the fraction of these anomalous bonds amounts to about $1.5x$. In Ref.[165], experiments aimed at detecting local lattice distortions were performed on $La_{0.75}Sr_{0.15}CuO_4$. The authors indeed found enlongated Cu-O bonds, whose fraction was about 20% and close to the expected value. Their experiments seemingly did not detect the shorter bonds, but this may be due to limited resolution.

Locally, the electronic density distribution associated with the polaron state should be bond-centered and look like a dipole, with the maxima occuring on the ends, thereby breaking the four-fold rotational symmetry. Interestingly, this type of symmetry breaking has already been discovered experimentally[162, 163]. In Ref.[163], the dipole pattern seems clearly detected in the pseudogap phase and the onset temperature of the latter seems tracking the pattern forming temperature.

The as-constructed polaron is magnetic in the sense that it carries a small but finite magnetic moment, which has been demonstrated in Ref[1]. Largely, it is due to an unusual double-exchange effect: the hole couples simultaneously via hopping to both Cu spins and therefore acts to align the spins, thence generating finite magnetism and breaking time-reversal symmetry. The moment for typical material parameters could be easily as large as $0.1\mu_B$[1]. This should be seeable by e.g. Kerr rotation and neutron scattering. Experiments have indeed observed unusual magnetic phenomena that are most pronounced in the pseudogap phase of very underdoped materials[166, 167].

In view of all these appealing features, it is appropriate to speculate on the connections of the polaron state with the pseudogap phase. As already said, they seem to have the

same symmetries broken locally and the pseudogap onset seemingly synchronizes with the appearance of these features. A more interesting evidence is discussed below.

Recently, simultaneous **r**- and **k**-space imaging techniques have revealed remarkable evolutions in the nature of the electronic excitations when the doping tends toward zero[156]. Such evolutions seem to place the polaron state (maybe its variants) as a strong candidate for the pseudogap state. As is well known, in underdoped samples two distinctive categories of electronic excitations can be seen at low energies and high energies, respectively. Utilizing the imaging technique, Kohsaka et al. observed two classes of excitations: one is well defined in k-space whereas the other localized in r-space[156]. The k-space excitations were proved to be simply the Bogoliubov quasi-particles generated out of the superconducting phase. On the other hand, the r-space excitations were found with higher energies and destroying aforementioned symmetries locally. They demonstrated that, these r-space excitations are just the pseudogap excitations. Very intriguingly, upon decreasing doping the phase volume occupied by the k-space excitations shrinks rapidly and the spectrual weight is transfered to the r-space states. In light of our reasoning, one may conjecture that, these r-space states could be intimately linked with the polaron states described above. If so, one should have $|E_f| \sim T^*$.

In the present work, we have focused on the single-polaron aspects. Future work are desired to investigate the inter-polaron correlations (which should be of importance to superconductivity) and the inter-relations between polarons and the antiferromagnetic background.

Chapter 6

SUMMARY

In summary, some intriguing problems that were found with two old perovskite compounds (BTO and STO) have been examined using an atomistic model. These two have similar crystal and electronic structures but show distinct lattice dynamics. The model was constructed in such a spirit: the relevant physics are primarily associated with the TiO_3 sub-lattice, while the A sub-lattice is only secondary. Evidences have been discussed to corroborate this spirit. The core of the model rests with the Ti sub-lattice, while the O one also proves indispensable. The Bersuker calculation for a single TiO_6 cluster has been generalized to a crystal and it was found that, the latter tends to strengthen the off-center shifts that would already exist in the former. As for the O vibrations, a strong anisotropy has been found as a result of the covalent Ti-O bonding that is responsible for the perovskite structure formation. This anisotropy states that, O vibrates much more easily along the Ti-O-Ti bond than in the perpendicular direction. In this model, a linear coupling has been assumed between adjacent Ti and O atoms. The coupling strengthes ($\beta_{l,t}$) also display anistropy and must be positive to be consistent with observations. The positiveness can not be warranted unless the O ion polarization effects are taken into account.

Competitions between Ti off-center shifts (u) and O cage tilting (φ) have been discussed by exploring electron-phonon interactions. The former mode tends to condense at zone center while the latter at zone boundary, which is why the former is a polar mode (to result in ferroelectricity) while the latter is non-polar. Although both were discovered many years ago, they have been considered largely independent till very recently. Except for the work by Yamanaka et al.[75] and Bussmann-Holder et al.[115], few have been attracted to such possible competitions. What was found in this thesis is that, these two types of modes actually germ out of the same electronic transitions between the $p_{O_\rho|\rho}$ orbital and t_{2g} d orbital. These transitions must be aided by phonons with proper symmetry, and these phonons can be of O or/and Ti character corresponding to O cage tilting and Ti off-center shifts, respectively. It turns out that, the amplitudes u and φ have to satisfy a simple relation that gives rise to competitions between these modes. In other words, they are adverse to each other. This finding should, at least partly, underlie the differences between BTO and STO. In BTO, u is large and therefore φ should be suppressed. In STO, the opposite takes place: the O cage tilting hinders ferroelectricity.

In light of the atomistic model, all observed dielectric modes (below $600cm^{-1}$) have been assigned according to their characters. The modes located around $180cm^{-1}$ and $510cm^{-1}$, which are very stable and insensitive to temperatures and survive all phases, are shown to stem from O vibrations along and perpendicular to the Ti-O-Ti bonds, respectively. These modes are essentially the same in both BTO and STO, with slight differences explicable by our model. In comparison with BTO, the $180cm^{-1}$-mode was found at a bit smaller frequency while the $510cm^{-1}$ at a little higher one in STO, in consistency with the fact that the covalent bonding in this compound is a little stronger. The remaining modes display characteristic temperature dependences and have been argued to originate from Ti motions. These motions are highly anharmoic, as expected from the form of the corresponding single-body potential. Every Ti ion has been subjected to a multi-valley

potential that is symmetric about the central position (crystallographic position). The profile of this potenial determines the dielectric behaviors.

For BTO, the potential wells are deep and intra-well motions can exist in addition to inter-well ones. However, since both modes are attached to the same coordinate, their spectural weights together must conserve. As temperature changes, a transfer between their weights is bound to happen. Qualitative arguements suggest that, the inter-well mode would absorb most weights when intra-well fluctuations become great and conversely, the intra-well mode would dominate. It is therefore expected that, at high temperatures the intra-well mode is invisible, which is the reason why in the cubic phase BTO shows only three modes[1]. Below the cubic-tetragonal transition, the compound enters a state with Ti ordering (together with other sequela) along one axial direction, and intra-well mode gradually gains weight. Therefore, in tetragonal phase, BTO exhibits four modes in the ordering direction. As it cools down from the transition temperature, the weight is gradually transfered from the inter-well mode (the lowest frequency mode) to the intra-well mode (at about $270cm^{-1}$). According to our study, the inter-well mode follows Debye's law and represents a relaxation involving the previliged and disfavored potential wells. One must see that, in the tetragonal phase, the Ti ordering is only partial. The motions normal to the spontaneous polarization are still disordered and no intra-well motions can be seen. That is why there are only three modes that have been found in ϵ_a. This idea has been employed to resolve two longstanding issues: (1) the big discrepancy between the magnitudes of ϵ_c and ϵ_a and (2) the one-mode-vs-two-mode puzzle as expounded in **sections 1.7.1, 1.7.5 and 3.3.1**.

For STO, the potential wells are shallow and no intra-well motions can exist. In such case, three modes show up, with the lowest frequency mode corresponding to Ti inter-well motions. Differing from the incoherent thermal agitation in BTO, Ti motions in STO are

[1]Due to nano-size ferroelectric precursor formation, a fourth mode can also exist that levels off around $60cm^{-1}$ as the transition is approached.

very coherent and hence represent a resonance, whose position varies with temperature. As aforementioned, the O cage tilting transition occuring at $105K$ should have discernible impacts on this resonance. Especially, one anticipates that, across the transition $105K$, the potential well should become shallower, which means stronger zero-point fluctuations that hinder ferroelectricity. Although Yamanaka et al.[75] had demonstrated such enhanced fluctuations, direct evidence remains elusive. By studying the behaviors of the quantum temperature T_1, a direct evidence has been found. It appears as a broad dip around $105K$ in the $T_1 - T$ curve. Clearly, were not for the dip, T_1 would vanish at low temperatures and ferroelectricity would occur. This dip shows the inadequacy of some models like the PSM and DWA. It requires the presence of the 8CM or the ARM. In this sense, the $T_1 - T$ shape can serve as a fingerprint of the model.

As regards the O substitution induced ferroelectricity in STO18, a new and novel idea has been forwarded. According to this idea, the effective Ti vibration frequency decreases after isotope exchange, that is, the zero-point fluctuations on Ti sites are reduced. This constitutes another advocate of the claim that O cage tilting impact Ti motions. Nevertheless, how such impacts operate is not elucidated in the present thesis and might be matter for future research. It is noted that, the idea contrasts those of other authors[83, 117, 164].

Bibliography

[1] Hai-Yao Deng, J Phys.Condens.Matt., 21:075702 (2009)

[2] Hai-Yao Deng, Kaige Hu, Chi Hang Lam and Haitao Huang, Solid State Communications, 152:112(2012)

[3] Hai-Yao Deng, Phys.Lett.A, 375:3100(2011)

[4] Hai-Yao Deng and Kaige Hu, Phy.Scr., 84:025011(2011)

[5] Hai-Yao Deng, Chi Hang Lam and Haitao Huang, Solid State Communications, 151:474(2011)

[6] Hai-Yao Deng, Journal of Applied Physics, 111:033706(2012)

[7] Hai-Yao Deng, Chi Hang Lam and Haitao Huang, Superconductor Science and Technology, 25:075003(2012)

[8] Hai-Yao Deng, Haitao Huang and Chi Hang Lam, European Physical Journal B (2012), doi:10.1140/epjb/e-2012-30069-3

[9] Hai-Yao Deng, Chi Hang Lam and Haitao Huang, Probable Realizations of Rotor Systems In SrTiO3 and PZT (in preparation)

[10] M.E.Lines and A.M.Glass, Principles and Applications of Ferroelectrics and Related Materials (Clarendon Press, Oxford, 1977)

[11] K.A.Muller and H.Burkard, Phys.Rev.B, 19:3593(1979)

[12] F. Zavaliche, S.Y. Yang, T. Zhao, Y.H. Chu, M. P. Cruz, C.B. Eom, and R. Ramesh, Phase Transitions, 79:991(2006)

[13] J.G.Bednorz and K.A.Muller, Z. Phys.B, 64:189(1986)

[14] http://wikis.lib.ncsu.edu/index.php/Perovskite

[15] R. D. Shannon, Acta Crystallogr. Sect. A 32, 751 (1976)

[16] M.Itoh et al., Phys.Rev.Lett., 82:3540 (1999)

[17] A.H. Kahn and A.J.Leyendecker, Phys.Rev., 135:A1321(1964)

[18] R. D. King-Smith and David Vanderbilt, Phys.Rev.B, 49:5828(1994)

[19] Narayani Choudhury, Eric J. Walter, Alexander I. Kolesnikov, and Chun-Keung Loong, Phys.Rev.B, 77:134111 (2008)

[20] M. Posternak, R. Resta and A. Baldereschi, Phys.Rev.B, 50:R8911 (1994)

[21] R.E.Cohen, Nature, 358:136(1992)

[22] I.B.Bersuker, Physics Letters, 20:589(1966)

[23] M.Born and K.Huang, Dynamical theory of Crystal Lattices (Oxford University Press, London, 1954)

[24] W.Cochran, Rep.Prog.Phys., 26:1(1963)

[25] A.D.B.Woods, W.Cochran and B.N.Brockhouse, Phys.Rev.119:980(1960)

[26] R.A.Cowley, Phys.Rev., 134:A981(1964)

[27] S.K.Sinha, Physical Review, 177:1256(1969)

[28] R.Migoni, H.Bilz and D.B$\acute{}$auerle, Phys.Rev.Lett.,37:1155(1976)

[29] H.Bilz, G.Benedek and A.Bussmann-Holder, Phys.Rev.B, 35:4840(1987)

[30] R.A.Cowley, Adv.Phys.,29:1(1980)

[31] W.Cochran, Adv.Phys., 9:387(1960)

[32] K.K.Kobayashi, J.Phys.Soc.Jpn, 24:497(1968)

[33] Ya.Girshberg and Y. Yacoby, Solid State Communications, 103:425(1997)

[34] Ya.Girshberg and Y. Yacoby, J.Phy.:Condens.Matter, 11:9807(1999)

[35] Ya.Girshberg and Y.Yacoby, J.Phy.Condens.Matter, 13:8817(2001)

[36] Y.Yacoby, Y.Girshberg, E.A.Stern and R.Clarke, Phys.Rev.B,74:104113(2006)

[37] J. Hlinka, J. Petzelt, S. Kamba, D. Noujni and T. Ostapchuk, Phase Transitions, 79: 41-78(2006)

[38] Hiromoto Uwe and Tunetaro Sakudo, Phys.Rev.B, 13:271(1976)

[39] H. Vogt, G.Rossbroich, Phys.Rev.B, 24:3086(1981)

[40] Takeshi Shigenari, Kohji Abe, Tomohiko Takemoto, Osamu Sanaka, Takashi Akaike,1 Yoshihide Sakai, Ruiping Wang, and Mitsuru Itoh, Phys. Rev.B, 74:174121(2006)

[41] R. Comés, M. Lambert and A. Guinier, Acta Crysallogr. A., 26:244(1970)

[42] G.V$\acute{}$olkel and K.A.M$\acute{}$uller, Phys.Rev.B, 76:094105(2007)

[43] Bostjan, Valentin V.Laguta and Robert Blinc, Phys.Rev.Lett., 90:037601(2003)

[44] T.Miyanaga, D.Diop. S.I.Ikeda and H. Kon, Ferroelectrics, 274:41(2002)

[45] R. H Lyddane, R. G. Sachs, and E. Teller, Phys. Rev. 59, 673 (1941)

[46] P.M.Chaikin and T.C.Lubensky, Principles of Condensed Matter Physics (Cambridge, 1995)

[47] http://www.phy.iitkgp.ernet.in/ptaccd2/ppt/GMukhopadhyay1.pdf

[48] W.Zhong, David Vanderbilt and K.M.Rabe, Phys.Rev.B, 52:6301(1995)

[49] J.A.Sanjurjo, R.S.Katiyar and S.P.S.Porto, Phys.Rev.B, 22:2396(1980)

[50] Y. Luspin, J.L.Servoin and F. Gervais, J.Phys.C:Solid St.Phys., 13:3761(1980)

[51] H.Vogt and J.A.Sanjurjo and G.Rossbroich, Phys.Rev.B, 26:5904(1982)

[52] G.Shirane, J.D.Axe and J.Harada, Phys.rev.B, 2:3651(1970)

[53] H.Presting, J.A.Sanjurjo and H.Vogt, Phys.Rev.B, 28:6097(1983)

[54] I.Ponomareva, L.Bellaiche, T.Ostapchuk, J.Hlinka and J.Petzelt, Phys.Rev.B, 77:012102(2008)

[55] A.Pinczuk, W.Taylor, E.Burstein and I. Lefkowitz, Solid State Communications, 5:429(1967)

[56] W.G.Spitzer, Robert C.Miller, D.A.Kleinman and L.E.Howarth, Phys. Rev., 126: 1710(1962)

[57] H. Vogt, Phys.Rev.B, 51:8046(1995)

[58] Gerald Burns and F.H.Dacol, Phys.Rev.B, 18:5750(1978)

[59] G.Burns, Phys.Letters, 43A:271(1973)

[60] J.Hlinka, T.Ostapchuk, D.Nuzhnyy, J.Petzelt, P.Kuzel, C.Kadlec, P.Vanek, I.Ponomareva and L.Bellaiche, Phys.Rev.Lett., 101:167402(2008)

[61] Bostjan Zalar, Andrila Lebar, Janez Seliger , Robert Blinc, Valentin V.Laguta and M.Itoh, Phys.Rev.B, 71:064107(2005)

[62] R.Comes, M.Lambert and A.Guinier, Solid State Communications, 6:715(1968)

[63] A.S.Chaves, F.C.S.Barreto, R.A.Nogurira and B.Zeks, Phys.Rev.B, 13:207(1976)

[64] J.C.Slater, Phys.Rev.78:748(950)

[65] E.A.Stern, Phys.Rev.Lett., 93:037601(2004)

[66] T.Schneider and E.Stoll, Phys.Rev.Lett., 35:296(1975);ibid, 31:1254(1973)

[67] T.Schneider and E.Stoll, Phys.Rev.B, 17:1302(1978)

[68] M.Stachiotti, A.Dobry, R.Migoni and A.Bussmann-Holder, Phys.Rev.B, 47:2473(1993)

[69] Z.Li, M.Grimsditch, C.M.Foster and S.-K. Chan, J.Phys.Chem.Solids, 57:1433(1996)

[70]

[71] K.A.Muller and H.Burkard, Phys.Rev.B, 19:3593(1979)

[72] W. Zhong and David Vanderbilt, Phys.Rev.B, 53:5047

[73] G.Shirane and Y.Yamada, Phys.Rev., 177:858(1969)

[74] E.Courtens, Phys.Rev.Lett.,29:1380(1972)

[75] A.Yamanaka, M.Kataoka, Y.Inaba, K. Inoue, B. Hehlen and E.Courtens, Europhys.Lett.,50:688(2000)

[76] Roberto L Moreira, Ricardo P S M Lobo, Ganesanpotti Subodh, Mailadil T Sebatian, Mohan V Jacob and Anderson Dias, J.Phys.D: Appl.Phys.42:075411(2009)

[77] J.H.Barret, Phys.Rev.86:118(1952)

[78] M.Yuan, C.L.Wang, Y.X.Wang, R.Ali, J.L.Zhang, Solid State Commun.127:419(2003)

[79] Manuel I. Marqués, Carmen Aragó and Julio A. Gonzalo, Phys.Rev.B, 72:092103(2005)

[80] K.A.Muller, W. Berlinger, E. Tosatti, Z. Phys. B, 84:277(1991)

[81] R. Viana, P. Lunkenheimer, J. Hemberger, R.Bohmer and A. Loidl, Phys. Rev. B, 50:601 (1994)

[82] L. Arzel, B. Hehlen, F. Denoyer, R. Currat, K.-D. Liss and E. Courtens, Europhys. Lett., 61: 653 (2003)

[83] Y.Yacoby and Y.Girshberg, Phys.Rev.B, 77:064116(2008)

[84] Takeshi Shigenari, Kohji Abe, Tomohiko Takemoto, Osamu Sanaka, Takashi Akaike, Yoshihide Sakai, Ruiping Wang and Mitsuru Itoh, Phys.Rev.B, Phys.Rev.B, 74: 174121 (2006)

[85] M. Takesada, MItoh and T. Yagi, Phys.Rev.Lett., 96, 227602(2006)

[86] H. Taniguchi, T. Yagi, M. Takesada and M. Itoh, Phys.Rev.B, 72: 064111(2005)

[87] H.Vogt, M.D.Fontanna and G.E.Kugel and P.Gunter, Phys.Rev.B, 34:410(1986)

[88] Yakov Girshberg and Yizhak Yacoby, J.Phys.:Condens.Matter, 13:8817(2001)

[89] I.-K. Jeong, J.K.Lee and R.H.Heffner, Appl.Phys.Lett., 92:172911(2008)

[90] Nicola A. Hill, Annu.Rev.Mater.Res., 32:1 (2002)

[91] P W Anderson, Phys. Rev., 115:2 (1959)

[92] F C Zhang and T M Rice, Phys.Rev.B, 37:3759 (1988)

[93] L.F.Mattheiss, Phys.Rev.B, 6: 4718(1972)

[94] D Khatib, R Migoni, G E Kugel and L Godefroy, J. Phys.: Condens. Matter, 1: 9811 (1989)

[95] I.B.Bersuker and B.G.Vekhter, Ferroelectrics, 19:137(1978)

[96] I.B Bersuker, Ferroelectrics, 164:75(1995)

[97] Issac B Bersuker, The Jahn-Teller Effects, Cambridge University Press (2006)

[98] http://galileo.phys.virginia.edu/classes/752.mf1i.spring03/PeierlsTrans.htm

[99] G. Rickayzen, Green's functions and Condensed Matter (Academic Press, 1980)

[100] J K Kjems, G. Shirane, K A Muller and H J Scheel, Phys.Rev.B, 8:1119(1973)

[101] J D Axe, Phys. Rev., 157: 429 (1967)

[102] Ph. Ghosez, J.-P. Michenaud and X. Gonze, Phys. Rev. B, 58: 6224 (1998)

[103] Eric W. Weisstein, Wigner 3j-Symbol, From MathWorld (http://mathworld.wolfram.com/Wigner3j-Symbol.html).

[104] G.J.Conduit and B.D.Simons, Phys. Rev.B, 81:024102(2010)

[105] L Palova, P. Chandra and P. Coleman, Phys.Rev.B, 79:075101(2009)

[106] Nabyendu Das and Suresh G.Mishra, Arxiv:0906.0944v4(2010)

[107] Thomas R Koehler, Phys.Rev.Lett., 17:89(1966)

[108] Laura Walizer, Sergey Lisenkov and L.Bellaiche, Phys.Rev.B, 73:144105(2006)

[109] Narayani Choudhury, Laura Walizer, Sergey Lisenkov and L.Bellaiche, Nature, 470:513(2011)

[110] J.A.Krumhansl and J.R.Schrieffer, Phys.Rev.B, 11:3535(1975)

[111] H.J.Bakker, Phys.Rev.B, 52:4093(1995)

[112] Annette Bussmann-Holder, Physica B, 263-264:408(1999)

[113] M G Stachiotti, R L Migoni and U T Hochli, J. Phys.:Condens Matter,3:3689(1991)

[114] A Bussmann-Holder and A R Bishop, Phys.Rev.B, 78:104117(2008)

[115] A Bussmann-Holder, H Buttiner and A R Bishop, Phys.Rev.Lett., 99:167603(2007)

[116] Annette Bussmann-Holder and A R Bishop, Phys.Rev.B, 68: 155104(2003)

[117] A Bussmann-Holder and A R Bishop, Europhys.Lett., 76:945(2006)

[118] A Bussmann-Holder, H Buttiner and A R Bishop, J.Phys.:Condens Matter, 12:L115(2000)

[119] Annette Bussmann-Holder and Helmut Buttiner, J Phys.:Condens.Matter, 14:7973(2002)

[120] K Kobayashi, Phys.Lett., 26A:55(1967)

[121] R.Pirc and R.Blinc, Phys.Rev.B, 70:134107(2004)

[122] K.H.Fischer and J.A.Hertz, Spin Glasses, (Cambridge University Press, 1991)

[123] M.Doi and S.F.Edwards, The Theory Of Polymer Dynamics, Oxford Scientific Publications, 1986

[124] G.A. Samara and B. Morosin, Phys. Rev. B, 8: 1256(1973);

[125] V.V. Lemanova, A.V. Sotnikova, E.P. Smirnovaa, M. Weihnachtb, R. Kunzeb, Solid State Communications 110:611(1999)

[126] K.Alex.Müller, W.Berlinger and E.Tosatti,Z.Phys.B, 84:277(1991)

[127] M.Fischer, A.Lahmar, M.Maglione, A.San Miguel, J.P.Itié and A.Polian and F.Baudelet, Phys.Rev.B, 49:12451(1994)

[128] Bernard Hehlen, Anne-Laure Pérou, Eric Courtens and René Vacher, Phys.Rev.Lett, 75:2416(1995)

[129] E.K.H.Salje, B.Wruck and H.Thomas, Z.Phys.B: Condens.Matter, 82:399(1991)

[130] E.K.H.Salje, B.Wruck and S.Marais, Ferroelectrics, 124:185(1991)

[131] W.Kleemann, J.Dec, and B.Westwanski, Phys.Rev.B, 58:8985(1998)

[132] Alexander K. Tagantsev, Eric Courtens and Ludovic Arzel, Phys. Rev. B 64, 224107 (2001)

[133] J.A.Krumhansl and J.R.Schriffer, Phys.Rev.B,11:3535(1975)

[134] T.R.Koehler and N.S. Gillis, Phys.Rev.B, 7:4980(1973)

[135] N.S. Gillis and T.R.Koehler, Phys.Rev.B, 9:3806(1974)

[136] R.A.Cowley, Adv.Phys., 12:421(1963)

[137] H.Vogt, Phys.Rev.B, 51:8046(1995)

[138] Ruiping Wang and Mitsuru Itoh, Phys.Rev.B, 64:174104(2001)

[139] Mitsuru Itoh and Ruiping Wang, Applied Phys. Lett., 76:221(2000)

[140] H.Taniguchi, M.Itoh and T.Yagi, Phys.Rev.Lett., 99:017602(2007)

[141] S.E. Rowley, L.J. Spalek, R.P. Smith, M.P.M. Dean, G.G. Lonzarich, J.F. Scott, S.S. Saxena, arXiv:0903.1445v1(2009)

[142] L.Palova, Pchandra and P.Coleman, Phys.Rev.B, 79:075101(2009)

[143] Gene F.Mazenko, Fluctuations, Order, And Defects, John Wiley and Sons, Inc., Hoboken, NJ(2003)

[144] D.D.Betts and M.H.Lee, Phys.Rev.lett., 20:1507(1968)

[145] Subir Sachdev, Quantum Phase Transitions, Cambridge University Press (1999)

[146] Alexander Altland and Ben Simons, Condensed Matter Field Theory, Cambridge University Press(2006)

[147] Steven Weinberg, Phys.Rev.Lett., 29:1698(1972)

[148] Andrzej RADOSZ, Phys.Lett.A, 127:319(1988)

[149] C.P. Burgess, arxiv: hep-th/9808176 (1998)

[150] R. Anglani, R. Gatto, N. D. Ippolito, G. Nardulli and M. Ruggieri, Phys.Rev.D, 76, 054007 (2007)

[151] J.G. Bednorz and K.A. Mueller, Z. Phys. B, 64: 189(1986)

[152] A.Bussmann-Holder and A.R.Bishop, Phys.Rev.B, 44:2853(1991)

[153] A. S. Alexandrov and N. F. Mott, Polarons and Bipolarons (World Scientific, Singapore, 1995)

[154] S. Johnston, F. Vernay, B. Moritz, Z.-X. Shen, N. Nagaosa, J. Zaanen, and T. P. Devereaux, arXiv, 1007:3451(2010)

[155] Takagi H, Ido T, Ishibashi S, Uota M, Uchita S and Tokura Y, Phys. Rev. B, 40:2254(1989)

[156] Y. Kohsaka, C. Taylor, P. Wahl, A. Schmidt, Jhinhwan Lee, K. Fujita, J. W. Alldredge, K. McElroy, Jinho Lee, H. Eisaki, S. Uchida, D.-H. Lee and J. C. Davis, Nature, 454:1072(2008)

[157] Aharony A, Birgeneau R J, Coniglio A, Kastner M A and Stanley H E, Phys. Rev. Lett., 60: 1330(1988)

[158] Guy Deutscher and Pierre-Gilles de Gennes, C. R. Physique, 8:937(2007)

[159] Vershinin M, Misra S, Ono S, Abe Y, Ando Y and Yazdani A, Science, 303:1995(2004)

[160] Kyle M. Shen and J.C. Seamus Davis, Materials Today, 11:14(2008)

[161] Y.Kohsaka, C.Taylor, K.Fujita, A.Schmidt, C.Lupien, T.Hanaguri, M.Azuma, M.Takano, H.Eisaki, H.Takagi, S.Uchida and J.C.Davis, Science, 315:1380(2007)

[162] R.Daou, J.Chang, David Leboeuf, Olivier Cyr-Choiniére, Francis Laliberté, Nicolas Doiron-Leyraud, B.J.Ramshaw, Ruixing Liang, D.A.Bonn, W.N.Hardy and Louis Taillefer, Nature, 463:519(2010)

[163] M. J. Lawler, K. Fujita, Jhinhwan Lee, A. R. Schmidt, Y. Kohsaka, Chung Koo Kim, H. Eisaki, S. Uchida, J. C. Davis, J. P. Sethna and Eun-Ah Kim, Nature, 466:347(2010)

[164] Y.Yamada, N.Todoroki and S.Miyashita, Phys.Rev.B, 69:024103(2004)

[165] A. Bianconi, N. L. Saini, A. Lanzara, M. Missori, T. Rossetti, H. Oyanagi, H. Yamaguchi, K. Oka and T. Ito, Phys.Rev.Lett., 76:3412(1996)

[166] Yuan Li, Victor Baledent, Neven Barisic, Yongchan Cho, Benoit Fauque, Yvan Sidis, Guichuan Yu, Xudong Zhao, Philippe Bourges, Martin Greven, Nature, 455:372(2008)

[167] Rui-Hua He, M. Hashimoto, H. Karapetyan, J D Koralek, J P Hinton, J P Testaud, V Nathan, Y Yoshida, Hong Yao, K Tanaka, W Meevasana, R G Moore, D H Lu, S.-K. Mo, M Ishikado, H Eisaki, Z Hussain, T P Devereaux, S A Kivelson, J Orenstein, A Kapitulnik and Z.-X. Shen, Science, 331:1579(2011)